Spring 2012

Combustion instabilities: an experimental investigation on the effects of hydrogen in a lean premixed combustor

Douglas W. Karkow
University of Iowa

COMBUSTION INSTABILITIES: AN EXPERIMENTAL INVESTIGATION ON THE EFFECTS OF HYDROGEN IN A LEAN PREMIXED COMBUSTOR

by

Douglas W. Karkow

A thesis submitted in partial fulfillment
of the requirements for the Master of
Science degree in Mechanical Engineering
in the Graduate College of
The University of Iowa

May 2012

Thesis Supervisor: Associate Professor Albert Ratner

Graduate College
The University of Iowa
Iowa City, Iowa

CERTIFICATE OF APPROVAL

_____

MASTER'S THESIS

_____

This is to certify that the Master's thesis of

Douglas W. Karkow

has been approved by the Examining Committee
for the thesis requirement for the Master of Science
degree in Mechanical Engineering at the May 2012 graduation.

Thesis Committee: _____
Albert Ratner, Thesis Supervisor

_____
James Buchholz

_____
Ching-Long Lin

To my wife, Julia,
and my parents, William & Louaine

ACKNOWLEDGMENTS

I would like to start by humbly stating that this work would not have been done without the help of many around me. First, I must express my sincerest appreciation to my superb advisor, Professor Albert Ratner, for his unparalleled patience, guidance, encouragement, and overall support.

I would like to thank the members of my thesis committee, Professor James Buchholz and Professor Ching-Long Lin. I have learned much from these professors through their courses and counseling. Each of them holds my utmost respect, and I wish only that I had more opportunities to learn from them.

All the members of Albert Ratner's lab who have contributed to this research also deserve my immensely emphasized gratefulness. In particular, I express my sincere thanks to PhD student, Majid Emadi, for his leadership, guidance, and motivation through our experiments and the writing of this thesis; he has taught me nearly everything. I also owe my gratitude to Taleb Salameh, Tim Gentry, Matt Burkhalter, Ameet Gohil, and Antonio Melendez for any and all of their help in the lab.

Special thanks must also go out to the remaining members of Professor Ratner's graduate student office; Yan Zhang, Yunye Shi, Mohsen Ghamari, Scott Salsbury, and former students James Ulstad, Xinhui Zhang, and Marta Muilenburg. All of them have provided an enjoyable work environment, lots of homework help, and innumerable laughs and friendly conversations.

Finally, I offer my infinite indebtedness to my wife, Julia Karkow, for her unfathomable patience, endless support, and frequent sacrifices.

TABLE OF CONTENTS

LIST OF TABLES

Table

LIST OF FIGURES

Figure

CHAPTER 1

INTRODUCTION

1.1 Background

The gas turbine industry has become an industry of rapid growth due to its versatile applications and benefits over other methods of power generation. Gas turbines utilize high temperature, high pressure gases exiting the combustor to spin the turbine blades which power the upstream rotating compressor. This energy output may come in the form of shaft power, thrust, or compressed air and can be used to power anything from generators to aircraft to trains to ships and even tanks.

The gas turbine, or combustion turbine, offers a promising mode of power generation for the needs of the future since it provides one of the highest efficiencies for combustion power generation technology along with very low emissions. Additionally, their quick installation and shorter lead-time make them attractive to customers. Gas turbines commonly operate with natural gas but their design may be altered in order to accommodate propane, kerosene, and other less common gases. Like many other power generation methods, gas turbine engines emit harmful pollutants such as nitrogen oxides (NO_x - a major contributor to acid rain), carbon monoxide (CO), and sometimes unburned hydrocarbons (UHCs).

NO_x reduction is a driving factor in the gas turbine industry due largely to the Clean Air Act of 1955, but has been amended as late as 1990. These strict regulations control the allowed limits of NO_x emission that are produced during the combustion of fossil fuels. Another challenge the gas turbine industry faces is in providing increased efficiencies. However, the attempts at NO_x reduction and ever-improving efficiencies are often conflicting goals. The efficiency is generally improved when using higher working fluid temperatures, while higher temperatures increase NO_x formation. A solution may be to decrease the available oxygen to slow the formation of NO_x; however, this may result

in incomplete combustion which produces increased carbon monoxide and hydrocarbon emissions. Finally, increasing the working fluid temperature also strains the limits of the combustor materials [U.S. DEO (2005)]. And even for mixtures that are lean enough to achieve the sub-ppm NO_x emission level requirements, the combustion process is extremely difficult to stabilize against global extinction due to the low blow-out limits. These demands for improved efficiencies and leaner modes of combustion continue to serve as focal points for ongoing research.

This has inspired the gas turbine industry to develop new concepts for combustion technology. Among the most notable new technologies are lean-premixed (LPM) combustion, rich-burn quick-quench lean-burn (RQL) combustion, and catalytic combustion [Lefebvre (1995), Correa (1998)].

RQL methods have been tested and even reduced emissions, however it is difficult to scale them to other engines with different flow rates, different fuels, etc., since each design would exhibit different flame characteristics thus making it difficult and expensive to model experimentally, therefore making them an unrealistic option. RQL methods also seem to suffer from soot formation and incomplete mixing between air and fuel-rich combustion products, while catalytic combustion methods are hindered by cost, safety, and durability.

Lean premixed combustion appears to be the most promising strategy of the three methods. Processes have been developed that use excess air in order to reduce the flame temperature and nearly eliminate thermal NO_x [Zeldovich (1946), Turns (2001)] by premixing the fuel and air before entering the combustion chamber. A handful of companies have already adopted these methods in order to meet regulations. Companies such as General Electric and Siemens-Westinghouse (Dry Low NO_x or DLN), Rolls-Royce (Dry Low Emissions or DLE), and Solar Turbine (SoLo NO_x) have implemented these processes into their systems.

These methods are able to meet emission reduction regulations, however, they are more susceptible to combustion-driven oscillations, thus resulting in a higher likelihood of flame instability.

1.2. Combustion Instabilities

The ‘singing flame’ phenomenon, discovered by Higgins in 1777, may be identified as the first step in the exploration of combustion instabilities and the resulting methodical study of flame dynamics. Later, Rijke made the observation that when a heated metal gauze was inserted into an open tube, sound was generated when the gauze was placed in specific locations within the tube. More time passed and eventually the Rayleigh criterion [Rayleigh (1945)] offered a definition to the coupling between the local pressure and heat release stating that energy is added to the acoustic field when heat is added (or removed) from the gas when the local pressure is above (or below) its mean value. Various mathematical formulations have been derived [Putnam (1964), Chu (1956), Zinn (1987)], however the principle remains consistent; the phase relation between the pressure fluctuation and the heat release fluctuation.

Combustion instabilities may have different properties when observed in different systems depending on the combustion system geometry, and these instabilities are not limited to gas turbine engines. However, they are one of the biggest consequences of lean premixed combustion techniques. Unsteady flow oscillations, which are typical of lean premixed combustors, may reach amplitudes that inhibit engine operation. These oscillations or instabilities constrain the operating conditions and the power output of the machine and may even lead to serious damage of components (combustor liners, transition pieces, and fuel nozzles). Damaged components may result in as little as machine downtime for small repairs, but may extend to expensive turbine component replacement, in which either situation results in temporary machine unavailability. These

repairs and replacements cost the industry $1 billion annually, and result in hundreds of millions of dollars in lost revenue due to the downtimes [Lieuwen (2005)].

The occurrence of instabilities are primarily attributed to two fundamental causes [Culick (1992), Culick (1995)]: the internal processes that attenuate unsteady motions are weak, and the energy required to drive these unsteady motions are only a small fraction of the heat released by combustion. Gas turbine engines are particularly susceptible to these issues since the energy intensity is rather high and usually only 0.1% of the energy released in chemical reactions is needed to produce pressure fluctuations that have peak amplitudes equal to the mean chamber pressure [Huang (2009)].

As a combustion system becomes more and more lean, the fuel efficiency improves and NO_x emissions are reduced at the cost of an increasing susceptibility to perturbations, or instabilities. Recent work has been done to show the effects of hydrogen addition [Jackson (2003), Halter (2007)] in premixed flames in an attempt for increased flame stability. If hydrogen addition improves the stability of the combustion system, then these systems may be allowed to operate at even leaner conditions which would further reduce the emission of harmful pollutants.

1.3 Thesis Objective

The topic of combustion instability is rather extensive, and as mentioned before, it has received a lot of attention recently in both the academic and industrial realms. Even with this push to discover the underlying phenomena of flame dynamics, only the surface has been scratched in understanding it fully. Because of this, there are still a wide variety of methods, fuels, combustor designs, etc. being implemented in experiments and even actual industrial combustors. The goal of this work is to contribute to the global understanding of flame dynamics, specifically in the effects that hydrogen has in combustion. Through an experimental study of hydrogen's effects in a lean premixed

combustion system, the intent is to characterize combustion conditions so they may be scaled and applied to large-scale engines. With these combustion characteristics, commercial gas turbine engines may be modified to run in even leaner operating conditions, thus further reducing NO_x and other pollutant emissions which is possibly the biggest factor that the gas turbine industry faces today.

1.4 Thesis Outline

Following this introduction is a review of relevant literature that has been presented in the field of combustion instabilities and their mechanisms, and later focuses specifically on the effects of hydrogen on flame dynamics. A brief review of the measurement techniques used in similar systems is also provided. Chapter 3 goes into detail on the experimental configuration employed for this work with accurate descriptions of the burner, mixer, swirler, and OH-PLIF laser system.

Chapter 4 delves into the various results obtained from the experiment and relates them to what other researchers have found. A foundation for comparison is found in a paper by Allison et al (2012) since their experiment attempts to investigate similar trends, albeit with a different burner and chamber configuration and different fuel mixtures. The intent is to compare the results of the present work with the work done by Allison et al in order to determine which property trends remain consistent regardless of these differences. This work also includes new and additional information since the effects of pressurization and increased bulk flow velocities may be studied.

Chapter 5 offers various concluding remarks on the results presented and how they fit in with the results of similar experiments. Finally, a suggestion of future work that may increase our understanding of flame dynamics and the phenomena of combustion instabilities is presented.

CHAPTER 2

LITERATURE REVIEW

The topic of combustion instability has received a lot of attention in recent years with more and more research being undertaken and journal papers being published. The role hydrogen plays within the realm of combustion instabilities is only a subset of the broader topic, however, it too has seen its share of recent work. This chapter offers a summary of the research done in these fields and will help set up the scope of this present work and the work needed in the future. The review begins with the broad topic of combustion instability; the physical mechanism driving the damaging oscillations and the theoretical methods to predict and possibly control them. The summary then goes into more detail on the specific research done to determine the effects hydrogen has on flame dynamics, followed by an examination of this present work's measurement technique and choice of burner as compared to those employed in similar experiments.

2.1 Combustion Instabilities and Their Amplification

As mentioned in the previous chapter, the physical process that results in what is known as a "combustion instability" deals with the relationship between pressure fluctuations and heat release fluctuations. Either (or both) of these fluctuations may be responsible for driving this potentially catastrophic phenomenon. Pressure oscillations may arise from various properties such as chamber noise, the chamber acoustics, fluctuations from the injection system, or a combination of many other properties. Heat release instabilities, for premixed systems such as in the present work, are generally controlled by the mass flow rate, equivalence ratio, and instantaneous local pressure and temperature.

The Rijke tube is one of the oldest and simplest examples of an instability, specifically an instability caused by the acoustic properties of the tube. The experiment

consists of a simple open tube which houses gauze that is locally heated. This generates sound at a frequency corresponding to the tube's half-wave mode. Similarly, a tube closed at one end and open at the other produces a frequency corresponding to the quarter-wave mode of the tube [Swift (2002)]. Systems such as the dump combustors tend to generate oscillations similar to the latter situation.

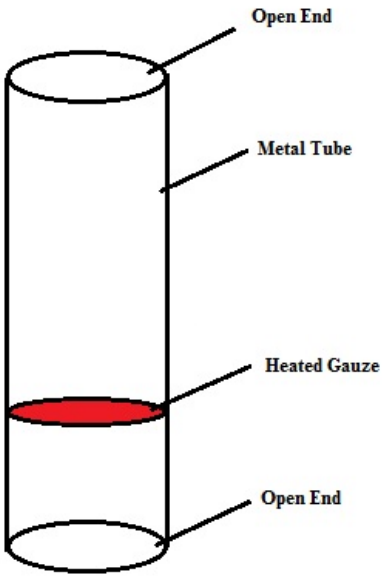

Figure 2.1 Rijke tube

An effort has been made to reduce system oscillations by chamber acoustic property analysis [Culick (2001), Dowling (2005), Bellows (2006)]. The goal is to dissipate the acoustic waves enough to eliminate the acoustic oscillations. This may be done by using perforated plates, Helmholtz resonators, or similar devices that will dampen the waves within the combustor.

2.2 Modeling Combustion Instabilities

Combustion instabilities are often a consequence of multiple driving mechanisms rather than a single, easily identifiable instability mechanism. Therefore, a single model has yet to be developed that may adequately describe this combination of instability mechanisms. Instead, independent models have been formed and employed with the knowledge that other phenomena may also be occurring simultaneously. This section gives an introduction to the developed models relating to the thermo-acoustic instability mechanism.

2.2.1 Lord Rayleigh's Criterion

In 1945, Lord Rayleigh described the conditions in which the acoustic field is amplified or dampened. The summary of Lord Rayleigh's statement is given in the previous chapter and describes how energy is added to the acoustic field when pressure and heat release fluctuations are in phase. Putnam [(1964)] is responsible for the mathematical formulation of this criterion, known as the Rayleigh integral:

$$\frac{1}{T}\int_0^T p'q'dt \succ 0 \qquad (2.1)$$

where p' denotes pressure fluctuations, q' represents heat release oscillations, and T signifies time.

The acoustic energy equation was derived by Chu (1956) including the effect of boundary condition and is shown below (2.2). The right hand side of the equation may be qualitatively described as energy gains minus energy losses, respectively, across the boundaries during combustion. Therefore if the gains exceed the losses, the result is an increase in magnitude of the acoustic instabilities. The additional variables are defined as follows: u is the velocity fluctuation, s is the area, and V is the volume, γ is a ratio of specific heats, and c is the sound speed.

$$\frac{\partial}{\partial t}\int_V \left(\frac{1}{2}\bar{\rho}u^2 + \frac{1}{2}\frac{p'^2}{\overline{\rho c}}\right)dV = \int_V \frac{(\gamma-1)p'q}{\overline{\rho c}^2}dV - \int_S p'u dS \tag{2.2}$$

Equation 2.3 is a generalization of the Rayleigh criterion where the left hand side is generally identified as the Rayleigh Index (discussed further in section 2.4.1).

$$\int_V \frac{(\gamma-1)p'q}{\overline{\rho c}^2}dV \succ \int_S p'u dS \tag{2.3}$$

Pressure oscillations may be evaluated simply by using a pressure transducer whereas heat release measurements require a more complex method. For experiments similar to the present research, often chemiluminescence and laser induced fluorescence (used for this work) techniques are employed and the latter will be described in more detail in the ensuing chapter.

2.3 Addition of Swirl

Swirl burners are used in engines other than just the gas turbine engines, such as in coal combustors and internal combustion engines. Swirl flames create a central recirculation zone and enhance mixing in the combustion region, thereby aiding in flame stabilization. This addition of swirl allows experimentation over a wider range of operating conditions while maintaining flame stability [Gupta (1984)]. Varying the swirl number and configuration has resulted in drastic combustion characteristic observation [Durbin and Ballal (1994), Syred and Beer (1972), and Syred (2006)]. The aforementioned central recirculation zone is created when the swirl number becomes large enough, and in this created zone heat and chemical species are circulated towards the flame base.

Typically, swirl is developed in one of two ways: an air-jet swirler injects air tangentially into the combustor, thus creating swirl and allowing air to mix with the fuel, or tangential blades may be installed [Roux et al (2005)] so when air or fuel flows past the blades, swirl is once again created. A swirl burner, or combustor, may have a naturally occurring driving frequency, whether it's proportional to the acoustic speed or if this frequency is scaled with the flow velocity. Even geometrically simple swirl flames are subject to thermoacoustic instabilities and often, several types of combustion instabilities are occurring simultaneously. The basic concepts of these mechanisms are offered by Zinn et al (2005) and Decruix et al (2003).

As will be described more in the subsequent chapter, the low swirl burner used in this work was designed by Cheng and coworkers (2000). This new burner has been designed as 1" (inner diameter) and 1.5" models, with this experimental configuration using the latter. Premixed air and fuel flow through vanes at the bottom of the swirler before being ignited in the combustion chamber. These vanes create the swirl that stabilizes the flame via flow divergence and the swirl number (the ratio of the vertical component of the velocity to the horizontal component) is adjustable while typically remaining below 0.6, identifying the design as a low swirl burner. This low swirl burner is less expensive and less complex geometrically than the aforementioned air-jet swirler. In addition to these advantages comes the report by Cheng et al (2006) that it emits less that 2 ppm in NO_x emissions. This astounding result has earned the new design a lot of attention, especially from gas turbine manufacturers.

2.4 Addition of Hydrogen

Once again, the global problem that gas industries face is to use lean fuel mixtures that decrease the combustion temperatures, henceforth reducing NO_x emissions as described the thermal NO_x generation mechanism. Leaner fuel mixtures eventually reach

flammability limits which results in unstable flames and possibly flame extinction. A solution has been presented reporting that the addition of hydrogen into the fuel mixture increases flame stability [Yamaoka (1992), Wierzba (2000), and Jackson (2003)].

Adding hydrogen to the premixed fuel stream has also been an approach to stabilizing global extinction and lean blow-out limits. Experimental studies [Littlejohn (2007), Cheng (2009)] demonstrate the feasibility of this strategy for a range of fuels in atmospheric and elevated pressure environments, in terms of improved extinction limits and emissions reduction.

A common concern may be to wonder how adding hydrogen to the fuel stream affects the quantification of the OH concentration, which is a common indicator of heat release. Katoh et al [(2006)] attempted to validate this assumption of a quasi-steady of the flame using planar laser induce fluorescence spectroscopy to observe the production of OH radicals from the combustion of both premixed hydrogen and methane flames and concluded that the assumption was reasonable and applicable for hybrid fuels. Another question arises concerning system operability when varying the fuel composition. Lieuwen et al (2008) investigated the impact that fuel composition had on lean premixed systems by assessing multi-species mixtures. Their results show that hydrogen addition has the greatest impact on turbulent flame speed and ignition delay time, however, their experiment did not include tests examining acoustic forcing and how the acoustic response changes due to the addition of hydrogen.

Many experiments have also been conducted to determine the effects of hydrogen addition on flame stability, reactivity, and emissions of hydrogen-methane-air flames [Mandilas (2007), Halter (2007), Lawn (2006), Strakey (2007), Kim HS (2008), Fairweather (2009), Day (2010)] . One result that was agreed upon after several experiments [Scholte (1959), Milton (1984), Yu (1986), Halter (2005), Ilbas (2006)] was that hydrogen addition resulted in an increase in the local burning rate throughout the flame surface, thus an increase in the global flame reactivity.

Halter et al (2005) concluded that adding hydrogen to the fuel mixture resulted in an increase in the laminar burning velocity and a reduction in the dependence of the laminar burning velocity of the flame against stretch. As for turbulent studies, they also concluded [Halter (2007)] that the addition of hydrogen reduces the flame front thickness due to a reduction in the flame turbulent length and the decrease in the laminar flame front thickness.

Similar results were obtained by others. Ilbas et al (2006) measured laminar flame velocities of hydrogen-air and hydrogen-methane-air mixtures and found that the flame speeds increase along with hydrogen concentration, thus increasing the burning velocities. Hu et al (2009) expanded upon these results to more realistic conditions by investigating the same trends at elevated pressures. Jackson et al (2003) obtained experimental and numerical results also indicating that increasing hydrogen content significantly increases the flame speeds and thus the extinction strain rates.

Ghoniem et al (2005) used a backward-facing step in their studies of lean premixed combustion with a propane-air mixture. Adding hydrogen to the propane mixture improved the flame stability over the entire air jet mass flow range while reducing pressure oscillations. Schefer et al (2003) showed that hydrogen addition increased the stable operating range of a swirl flame by enabling flame anchoring while this result was experimentally confirmed by Choudhuri and Gollahalli (2003).

Emadi et al (2012) reported that hydrogen-enriched methane-air flames caused blow-out limits to occur at lower equivalence ratios, which indicates a broadened range of stability. Also reported was an increase in flame area and flame front wrinkling with hydrogen enrichment due to contributions from a decrease in Lewis number, an increase in the local and overall burning rates of fuel (because of hydrogen's faster reaction rate), and interactions of turbulent small scales with the flame surface.

2.4.1 Rayleigh Index Maps

The Rayleigh Index refers to the left hand side of equations 2.1 or 2.3 above and may be determined experimentally if the pressure oscillation and heat release distribution are known. The calculation method is described in detail by Pun et al (2003). A Rayleigh Index greater than zero represents an amplification of the flame while indices less than zero correspond to thermo-acoustic dampening of the flame. The Rayleigh Index is therefore minimized when the heat release oscillations are 180 degrees out of phase with the pressure oscillations at the same frequency. Although these index maps are not offered in the present work, their use is widespread [Allison et al (2012), Huang (2008), Kang et al (2007), etc.] and offers valuable information as to the coupling between the pressure and heat release.

2.5 Numerical Theory and the Wave Equation

A derivation of the wave equation for reacting flows is offered by Poinsot and Veynante (2005) by working with the logarithm of pressure, a convenient method for this complex task. Using the Navier-Stokes equations in tensor form along with two assumptions, zero volume forces and zero volume heat sources, the equation (2.4) for ln(p) is extracted from the energy equation and the equation of state:

$$\frac{1}{\gamma}\frac{Dln(p)}{Dt} + \nabla \cdot \vec{u} = \frac{1}{\rho C_p T}\left[\dot{\omega}'_T + \tau : \nabla\vec{u} - \left(\rho \sum_{k=1}^{N} C_{p,k} Y_k \vec{V}_k\right) \cdot \nabla T\right] + \frac{1}{r}\frac{Dr}{Dt} \qquad (2.4)$$

Adding the divergence of the momentum equation as well as two additional assumptions, a low-speed mean flow and identical molecular weights for all species, produces a simple wave equation for ln(p) in reacting flows with a low Mach-number.

The text offers an order of magnitude analysis that further simplifies the equation, resulting in equation 2.5:

$$\nabla \cdot \left(c_0^2 \nabla \ln(p)\right) - \frac{\partial^2}{\partial t^2} ln(p) = -\frac{\partial}{\partial t}\left(\frac{1}{\rho C_v T}\dot{\omega}_T\right) - \gamma \nabla \vec{u} : \nabla \vec{u} \tag{2.5}$$

Linearizing this equation by defining the pressure as $p = p_0 + p_1$ (depicting an acoustic disturbance) with $p_1/p_0 << 1$ so that ln(p) is approximated by p_1/p_0 produces an equation for the pressure changes p_1:

$$\nabla \cdot (c_0^2 \nabla p_1) - \frac{\partial^2}{\partial t^2} p_1 = -(\gamma - 1)\frac{\partial \dot{\omega}_T}{\partial t} - \gamma p_0 \nabla \vec{u} : \nabla \vec{u} \tag{2.6}$$

As mentioned previously, the wave equation above is for a reacting flow. Combustion brings the complexity of a variable sound speed c_0 which must be kept in the ∇ operator, as well as the additional source term (first term on RHS) for the pressure equation with combustion that's absent for non-reacting flows. This term designates combustion noise and instabilities. As described by Poinsot and Veynante, the linearized form of equation 2.6 captures the growth of unstable modes, however, the non-linear effects observed in many limit-cycles demand non-linear extensions of the equation.

CHAPTER 3

EXPERIMENTAL CONFIGURATION AND TECHNIQUES

This experiment contains many system parts and measurement techniques, therefore, each section details only a subsystem in order to make it easier to keep track of what's actually going on. To begin, the experimental system and its components will be described so that its features may be disentangled from those of similar experiments. The second section offers an explanation of the measurement technique used, OH-PLIF, as the main data collection tool. Finally, the experimental procedure itself is visited in detail and the methodology for the subsequent data analysis is given.

3.1 Experimental System

The investigation of flame dynamics and combustion instabilities requires a complex system with many components and hardware pieces. Shown in Figure 3.1 below is a simple schematic of the intricate system used. The combustion chamber is made of segments of stainless steel pipes with internal diameters of 30 cm and lengths of 185 cm. Exiting at the top of the combustion chamber is the exhaust, which features a trio of adjustable valves which allow the pressurization of the experiment.

Housed within, at the base of the chamber, is a 1.5" low swirl burner, designed and built at the Lawrence Berkeley National Laboratory by Cheng et al (2000). The low swirl burner has been shown to take advantage of the propagating nature of the premixed flame while not relying on flow recirculation to anchor it, even under extremely turbulent conditions nearing the flammability limit. Therefore, the low-swirl burner offers a stable, freely propagating flame, however, basic system scaling needs to be performed in order to optimize the system efficiency and reduce NO_x emissions.

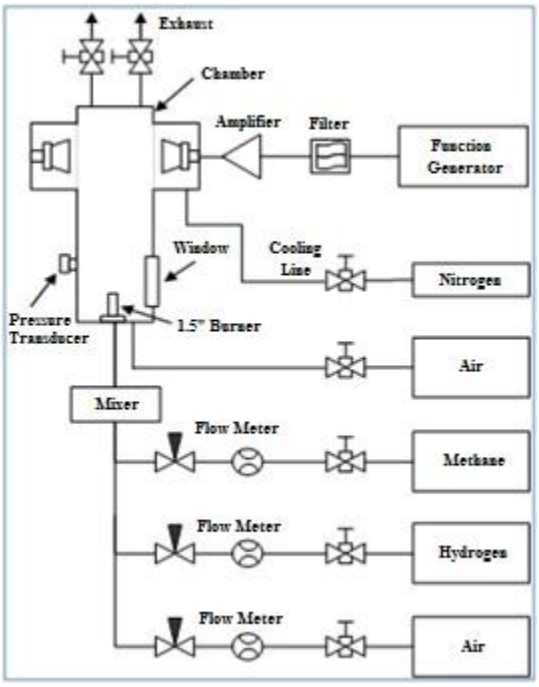

3.1. Gas Flow Schematic

This stable flame permits the quantification of various modifiable parameters. Various fuels and mixtures have been tested utilizing the designed low swirl burner, including methane- and hydrogen-based mixtures [Huang (2008), Yilmaz (2010), etc.]. The chamber itself also benefits from several advantages over other systems used for combustion instability research. It may function at elevated pressure conditions, which is typical of most practical combustion systems since operating conditions of much higher than one atmosphere are often needed. Second, the chamber dimensions are much larger than the dimensions of the burner and flame which eliminates any flame interactions with the chamber walls. As a precaution, nitrogen co-flow keeps the flame isolated and the chamber walls at a reasonable temperature. Lastly, the speakers are located downstream from the chamber and, therefore, the flame. This eradicates the risk of acoustic perturbations affecting the fuel supply and mixing process when the acoustics are located

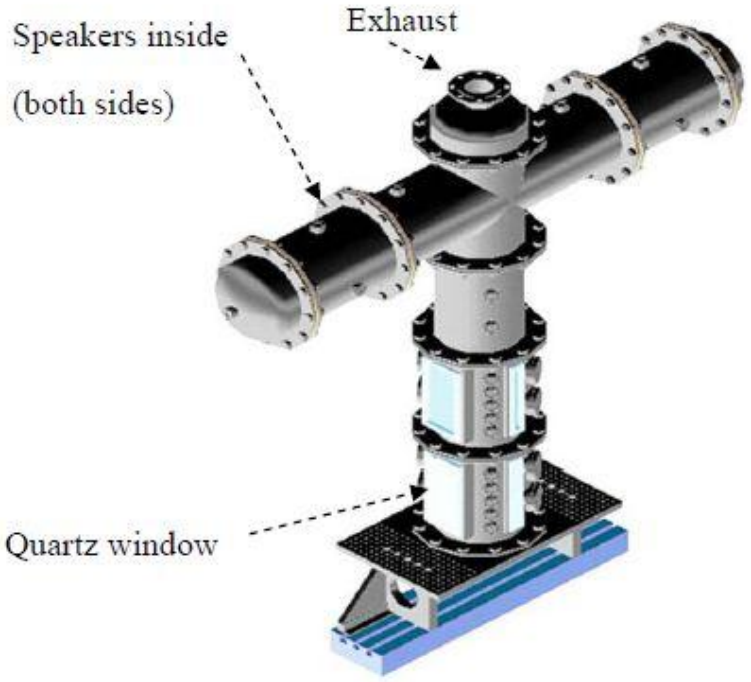

Figure 3.2 Acoustic chamber

Source: Huang, 2008

upstream of the system, as seen in many similar experiments. Here, four speakers are employed relatively far downstream and are driven in phase, thus creating the acoustic perturbation.

Located in the lower section of the combustion chamber are four quartz windows which allow optical access to the flame as well as an entrance for the laser sheet. Flow meters registered and controlled the flow rates of the oxidizer (via a Hastings HFC-D-307 instrument) while they also measured and controlled the fuel flow rate (via a Hastings HFC-D-303 instrument). A piezoelectric pressure transducer, located on the side of the chamber as shown in Figure 3.1, monitored the chamber pressure oscillations where the pressure wave may be assumed to be nearly uniform over the extent of the flame [Huang (2008)].

3.1.1 Low-Swirl Burner and Mixer

As mentioned previously, the constructed low-swirl burner by Littlejohn and coworkers (2007) is utilized in the present experiments. With an inner diameter of 3.81 cm, the burner is only slightly smaller than the 6.35 cm burners commonly found in the gas turbine industry. As shown in Figure 3.3 below, a swirler is contained within the burner consisting of 16 vanes, where the vane angle may be adjusted during the design process to offer varying swirl intensities. Also at the base of the burner is a mesh of 25 holes that aid in premixing the fuel before combustion.

To reiterate the point made previously, the low swirl burner stabilizes the flame via flow divergence, as opposed to recirculation, thus producing a more stable flame [Cheng et al. (2000)]. To supplement this, tests have already been performed using this low swirl burner model and have produced results indicating reduced NO_x emissions [Littlejohn et al (2007)].

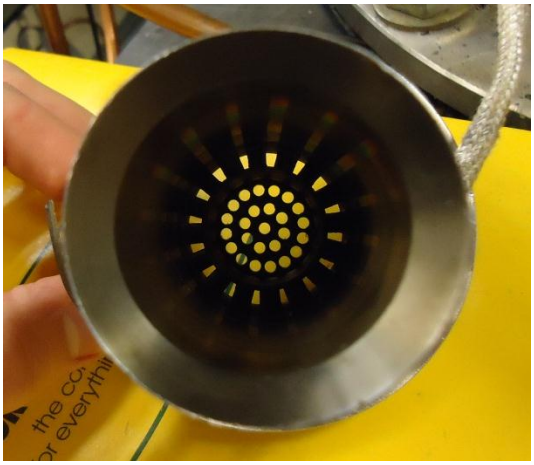

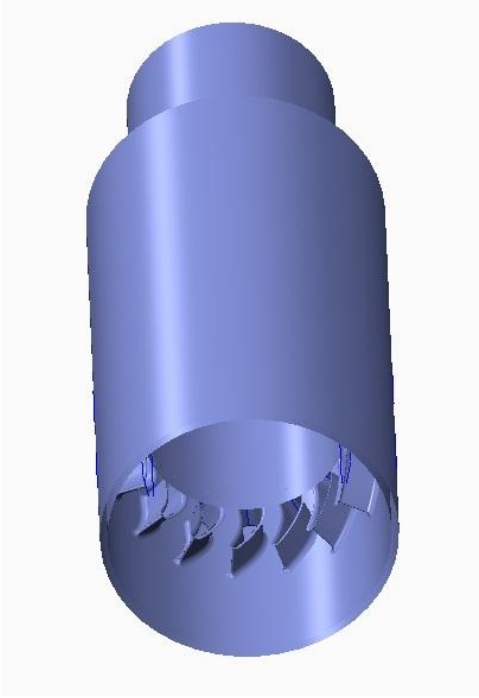

Figure 3.3 Swirler

For premixing purposes, a mixer was designed and implemented upstream of the burner and swirler. The premixer is a tube housing a section of marbles that does most of the premixing. The fuel passes through the marbles which break down any large vortical structures present and then the fuel passes through a mesh net before entering the swirler and burner as a “fully premixed” and fully developed flow.

3.1.2 PLIF Laser System

The combustion chamber flame is excited by a pulsed laser signal which features a high powered Nd:YAG pump laser, a tunable dye laser, and an optical frequency doubler. The Nd:YAG laser produces a pulsed laser signal which provides a higher peak power than continuous signal lasers, and is also useful for temporal resolution. The signal is a popular choice for planar laser induced fluorescence (PLIF) imaging and particle image velocimetry (PIV) experiments and can produce laser beams ranging from 532 nm to 1064 nm wavelengths. The 532 nm wavelength is used for PLIF imaging purposes as described later and appears visually as a green beam.

The Nd:YAG laser pulse enters the tunable dye laser, which contains a Rodamine 590-based solution. This chemical is a slightly toxic dye, therefore careful precautions are taken when making the solution; and the resultant dye solution is used to shift the laser wavelength from a 532 nm beam to a 564 nm wavelength beam. The tuned pulsed laser signal then enters the frequency doubler, cutting the wavelength in half to a 282 nm beam.

The beam consists of a few low frequency residuals which are separated from the UV light and absorbed by a Pellin-Broca prism. The filtered UV light (a purple beam) is then directed towards the optics configuration which optimizes the position, strength and uniformity of the laser sheet entering the combustion chamber. The frequency doubled laser signal then excites the hydroxyl ($^{+}$OH) radical used for PLIF imaging techniques.

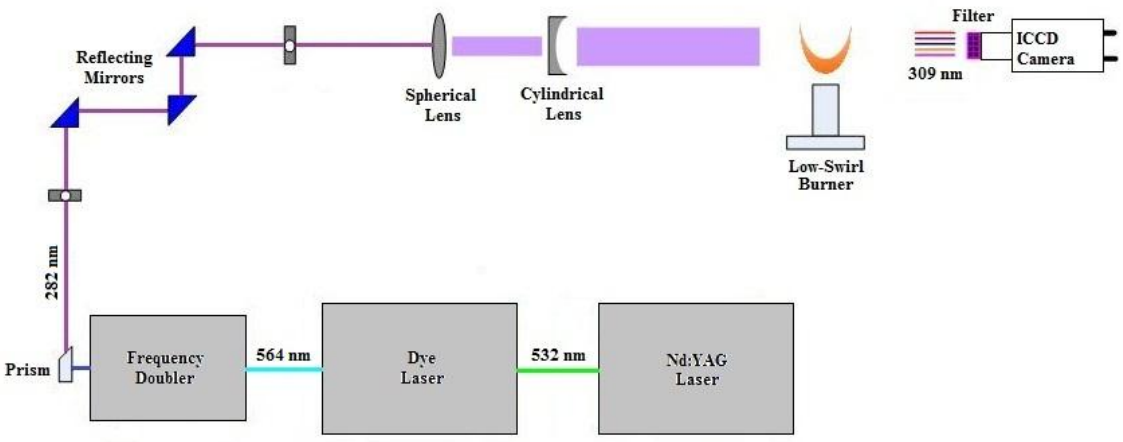

Figure 3.4 PLIF measurement system

Perpendicular to the laser sheet that enters the combustion chamber is the detection system consisting of an intensified charge-coupled device (ICCD) camera with a band pass filter (to remove any scattered light) and an ultraviolet lens. The triggering mechanism allows synchronization between the Nd:YAG laser's timing electronics and the ICCD camera's image acquisition via a delay circuit. In this manner, the laser pulses may be tracked with precise timing and the delay circuit sends the information to the camera in order to capture the appropriate images.

3.2. Planar Laser Induced Fluorescence (PLIF) Imaging

Laser-induced fluorescence imaging is a species-specific imaging technique that holds several significant advantages over line-of-sight imaging methods such as laser tomography or spontaneous emission imaging. PLIF imaging has the advantage of being able to identify the spatial structure of reaction zones by imaging the chemical species that are known to be abundant in these regions [McManus et al (1995)]. Other species-specific imaging techniques are available, such as Rayleigh or Raman techniques, however these techniques typically produce weaker signals.

The principal behind the laser-induced fluorescence technique is that laser radiation can excite a specific chemical species of interest to a higher energy state during the laser absorption process [Eckbreth (1996) and Hassel (2000)]. After the species is excited it reverts, or decays, back to its lower energy level which results in the spontaneous emission of a photon. This spontaneous emission is also known as fluorescence. The emitted radiation is then collected by the ICCD camera and the processed images may be used to obtain a variety of flow properties of interest.

3.2.1 Advantages of PLIF Imaging

The PLIF imaging technique used in this experiment offers many advantages over other combustion imaging methods. It offers an abundance of qualitative data and has been used to investigate reacting shear layer structures, to examine the interaction between a laminar flame and a vortex pair, and in the analysis of turbulent diffusion flames. It has been reported that PLIF images offer a better temporal resolution over time-resolved emission images due to its reduced time exposure. In addition to this, the signal-to-noise ratio was improved since it is controlled by laser intensity, and the spatial resolution with the PLIF technique also increased since the signal comes from a sheet as compared to a line-of-sight integration utilized in emission imaging [McManus (1995)].

A more comparable and somewhat recent technological technique is that of chemiluminescence, a common method used in similar research [Kim D (2010), Kim KT (2010), Lee (2007)]. Ratner et al (2002) reported that chemiluminescence is generally easier and less expensive to implement due to equipment costs, however, it tends to highlight only the exterior flame boundaries while interior structures become indistinguishable. In contrast, PLIF imaging is an ideal technique for examining the internal structure of the flame since it only images the spatial regions illuminated by the laser sheet. They concluded that chemiluminescence is best used to capture flame

oscillatory movement and to determine the impact on resonance of flame flow-field or chemical-field modifications. As a low cost and easily implemented method, it is useful for both industrial and research use. PLIF provides information on the flame chemical structure motion and is useful for examining internal flame structures, especially when considering acoustic forcing. Therefore, it is a useful method for physical flame processes and in designing burners where susceptibility to an acoustic field must be considered.

CHAPTER 4

RESULTS

This chapter expands on the material presented in chapter 2 with the intent of providing some experimental data and insight into the behavior of combustion flame dynamics. While experimenting with methane-air and methane-hydrogen-air fuel mixtures, the focus is on the effects of hydrogen fuel enrichment while parameters such as the equivalence ratio, driving frequencies, pressure fluctuations, and bulk velocities are varied. The goal is to then explore how each of these individual parameters affects the flame dynamics. The tables below offer the various operating conditions explored. Due to a large number of data and their subsequent graphs, only choice plots are offered in this chapter while the remainders are included in the Appendices.

Table 4.1 Operating Conditions: 0% H_2, 100% CH_4

Pressure (atm)	1	2	3	4
Equiv. Ratio	0.700 – 0.800	0.675 – 0.800	0.650 – 0.800	0.650 – 0.800
Bulk Vel. (m/s)	10 – 30	5 – 15	3.33 – 10	2.5 – 7.5

Table 4.2 Operating Conditions: 20% H_2, 80% CH_4

Pressure (atm)	1	2	3	4
Equiv. Ratio	0.675 – 0.750	0.600 – 0.725	0.600 – 0.725	0.625 – 0.725
Bulk Vel. (m/s)	10 – 30	5 – 15	3.33 – 10	2.5 – 7.5

Several of the graphed results that were obtained in this experiment were also explored by Allison et al (2012) which will be used as a cornerstone for this work's results and comparisons. Their configuration also housed a low-swirl burner and their experiments varied a similar set of parameters, although the chamber geometry, fuel mixtures, and imaging techniques employed were different. The advantage then of these

comparisons is that global trends may be distinguished from those that are dependent upon the experimental configuration. The additional information this work contributes are pressurization trends and increased bulk velocity trends, while adding data from a completely different burner and chamber geometry to the "data pool."

4.1 Acoustic Modes

Every chamber and burner configuration will have its own naturally occurring resonant frequencies. Some may be weak enough to be hidden in the noise, while others may cause significant effects on flame dynamics. When performing an experiment and trying to examine flame dynamics under varying conditions that you hope to apply to industrial sized chambers, one may counter these frequencies via active control methods and then drive selectable frequencies that match those of an industrial combustor. This allows experimentation easily scalable to the larger combustor since the frequencies will match and the flame dynamics at those frequencies may be examined on a smaller laboratory model.

The dominant acoustic modes for this burner and chamber geometry appear to fall within the three frequency ranges listed below. A range is listed, as opposed to a single value, since the natural frequencies shift when varying certain parameters, but the ranges remain rather concise.

Table 4.3 Dominant Acoustic Modes

1st Mode	85 – 100 Hz
2nd Mode	140 – 170 Hz
3rd Mode	260 – 300 Hz

Other excitation frequencies were reported, above and below the frequency ranges listed above, however they were not analyzed due to their inconsistency, lower intensity signals, and differences in the underlying flame dynamics at those frequencies. The strengths of these acoustic modes are shown in Figure 4.1. It is apparent that the strengths decrease from one mode to the next, seemingly without any influence of changing pressure although the values are consistently lower at 1 atm. The first mode is the strongest, with a power spectrum density (PSD) strength ranging from approximately 60 – 100 dB/Hz. The second mode ranges in strength from 40 – 80 dB/Hz, and the third mode reduces further yet to roughly 30 – 50 dB/Hz.

These acoustic modes are natural resonant frequencies based on the burner and the chamber geometry. Huang (2008) reported no natural acoustic resonance, but this was due to the smaller 1" burner and a smaller fuel flow rate. Since the area in the current configuration has increased and is coupled with an increase in the flow rate, the effective increase in power is much larger than that of Huang's acoustic signal. Therefore, even though the chamber was identical, the acoustic frequencies were drowned out in the noise due to a much lower signal. The lack of strong, naturally occurring frequencies allowed Huang to select and force any frequencies necessary using speakers located downstream of the combustion chamber.

The same idea holds for Yilmaz et al (2010) who performed similar experiments with the slightly smaller, 1 inch, low swirl burner in the same combustion chamber and reported four forcing frequencies of 85, 125, 222, and 399 Hz. The differences in burner geometries are largely the cause of the altered excitation frequencies; however the operating conditions were also different focusing on hydrogen fractions of 7%, 20%, and 30%, all at a pressure of 1 atm and equivalence ratio of 0.5.

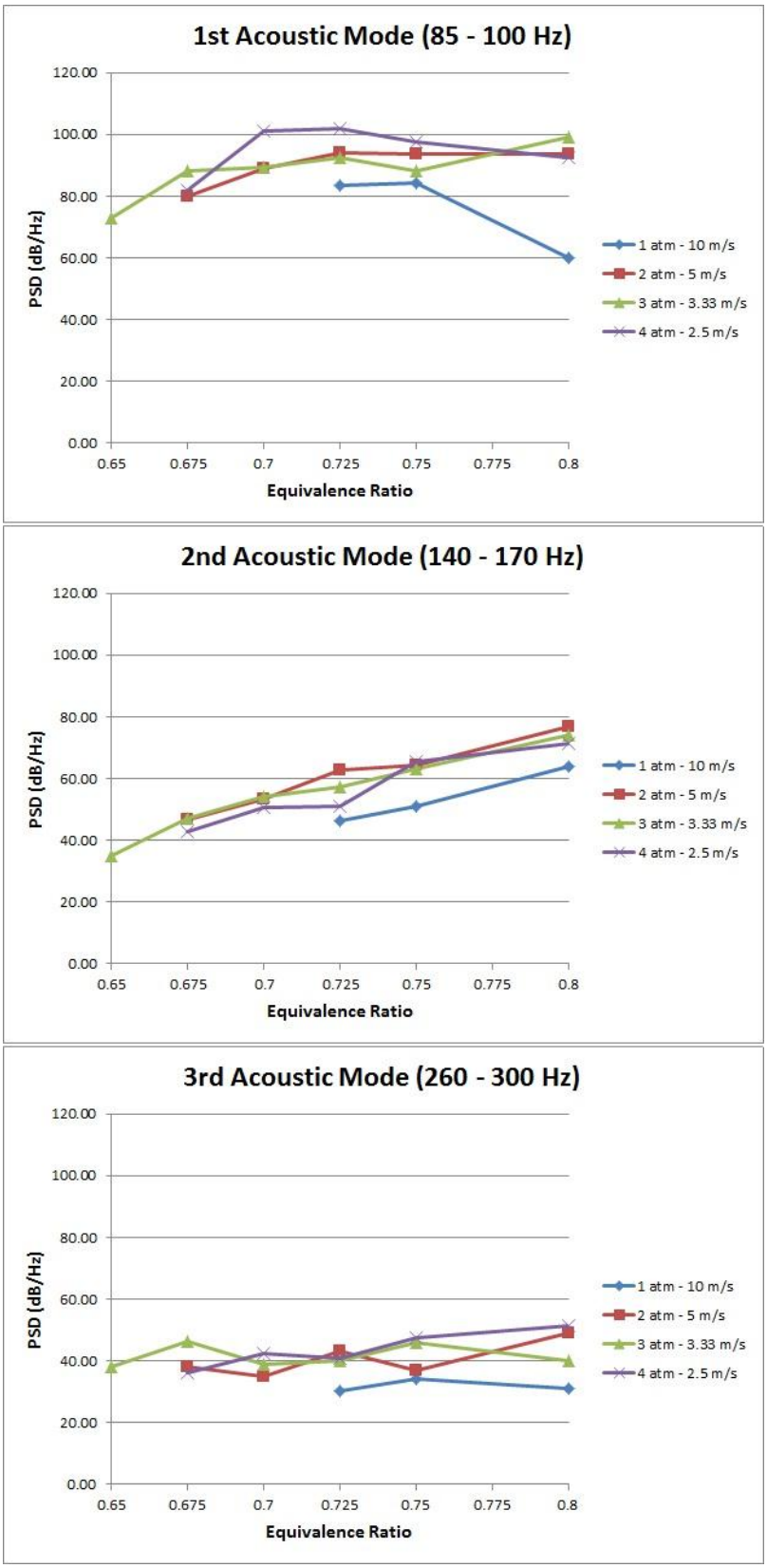

Figure 4.1 Acoustic mode strengths (methane)

4.2 Pressure Fluctuations

The pressure to velocity relationship may be explained in terms of momentum conservation or in terms of a constant level of heat release. When doubling the pressure, the mass doubles, therefore the momentum doubles unless the velocity is halved (i.e. 1 atm at 10 m/s = 2 atm at 5 m/s). The idea is similar for constant heat release. When you increase the pressure, you increase the heat release. Reducing the flow velocity balances this so keeping a constant heat release requires halving the velocity when doubling the pressure.

As mentioned in Chapter 3, a pressure transducer measures the fluctuations present in the combustion chamber. With these measurements, frequency and amplitude responses are extracted and used for analysis. A sample of the pressure data showing the acoustic modes and their respective amplitudes is shown in Figure 4.2. This plot was extracted using a MATLAB code designed to determine the FFT of the pressure data, and subsequently take the logarithm of that FFT. The three peaks are easily identifiable and represent the three natural acoustic modes of the burner/chamber configuration.

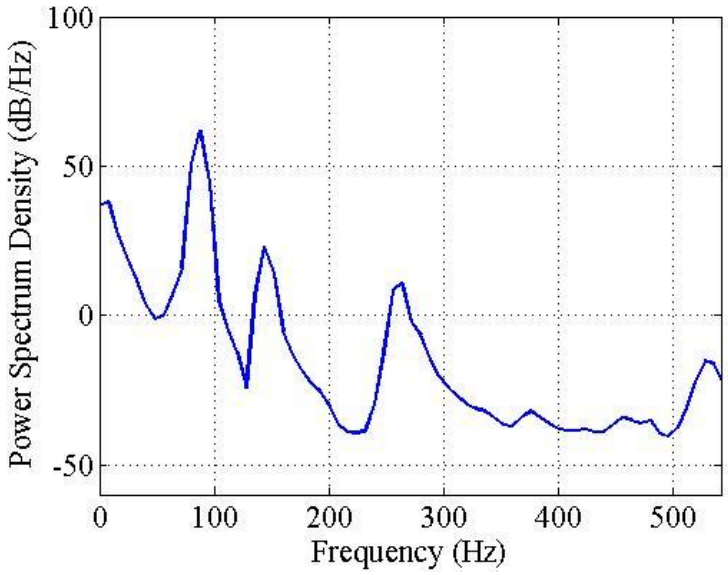

Figure 4.2 Sample power spectrum density plot

For each case, this pressure data is recorded and the PSD and frequencies were extracted. This allows analysis of any relationship between fuel concentrations, equivalence ratio, chamber pressure, bulk velocity, PSD, and the acoustic modes. As a first step in the analysis, the PSD versus equivalence ratio trend was examined for both the 100% CH_4 (0% H_2) and 80% CH_4 (20% H_2) cases. Plots of this trend were constructed for each pressure and fuel flow rate tested during those cases. The amplitude behavior showed varying trends for both fuels employed, but generally displayed a slight decrease in PSD strength when decreasing the equivalence ratio. A pair of samples is offered below in Figure 4.3 while the remainders are provided in the Appendices.

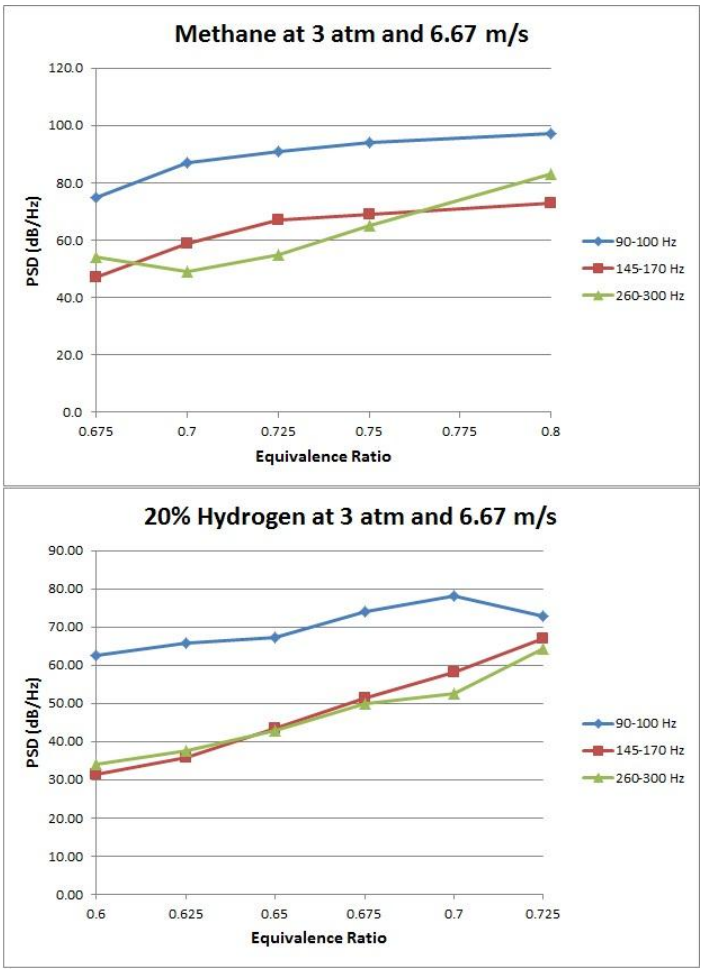

Figure 4.3 Sample PSD vs. Equivalence Ratio trend

Allison et al (2012) also displayed results of the amplitude behavior showing varying trends with changing equivalence ratios for each fuel and concluded that these amplitude behaviors are not consistently scaled with the increase in global heat release.

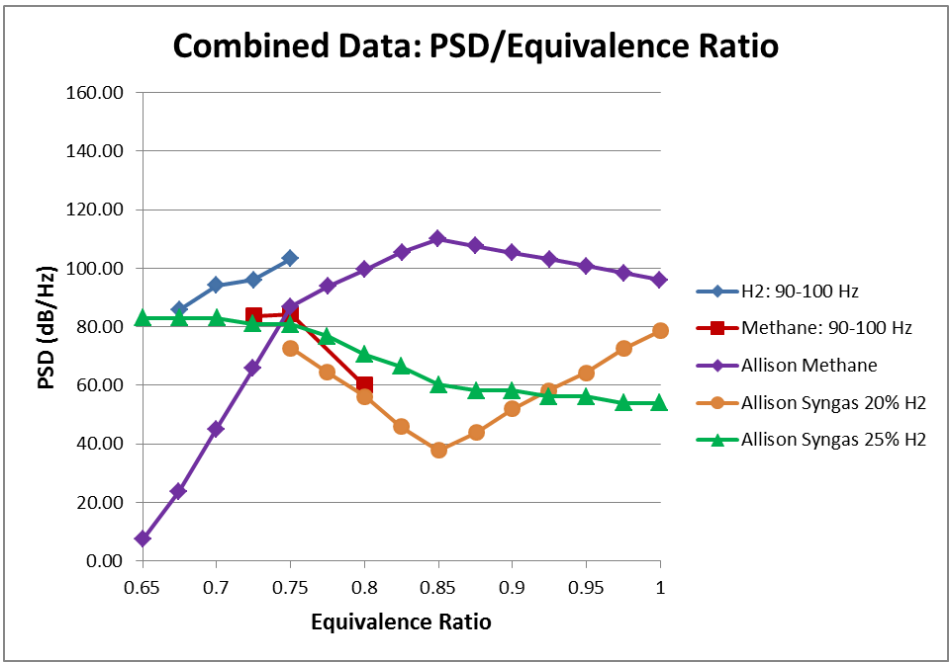

Figure 4.4 PSD response compared to Allison et al (2012) data

Figure 4.4 above shows the trends reported by Allison et al (2012), represented by the three lines that reach an equivalence ratio of 1, along with the trends depicted by the 0% and 20% H_2 concentrations examined in this work. The data from Allison et al shows inconsistent trends for each of the three mixtures used here. Their methane mixture's PSD strength continually increases until an equivalence ratio of about 0.85, while their syngas mixture of 20% H_2 shows an almost completely opposite behavior, decreasing until 0.85 and then gradually increasing thereafter. The third mixture, syngas with 25% H_2, also follows a different trend by gradually decreasing over the entire range of equivalence ratios.

For the current work, where only the first acoustic mode is shown due to its stronger signal, the trends are opposite those of Allison et al. The methane data show a decreasing trend with increasing equivalence ratio, while the 20% hydrogen data increases over the range of equivalence ratios tested. This methane trend only reflects the data obtained at a chamber pressure of 1 atm, a bulk velocity of 10 m/s, and the first acoustic mode. This case was chosen as it contains the most similarities with the data obtained by Allison et al: atmospheric pressure, lowest bulk velocity, and strongest acoustic mode. In general, the methane data increased slightly with an increase in equivalence ratio, similar to the 20% H_2 trend, as can be seen in Appendix A. The differences between these experimental configurations are many, such as the burner, chamber geometry, combustion fuels, flow rate, and range of equivalence ratios tested, and therefore, very few consistent conclusions may be drawn from this comparison.

4.3 Equivalence Ratio

Figure 4.5 shows the frequency response to changing equivalence ratio, in this instance a comparison between chamber pressures of 1 and 4 atmospheres concerning the 20% H_2, 80% CH_4 mixture. Similar plots (available in the Appendices) were constructed over the ranges listed in Tables 1 and 2 above and the results depicted parallel trends.

It can be seen in Figure 4.5a that when increasing the equivalence ratio, the dominant acoustic modes increase slightly and Figure 4.5c shows that the trend holds for elevated pressures. These shifts in the acoustic modes may be seen in more detail in the plots shown on the right (Figure 4.5b&d). When constructing these specific plots, the frequency associated with the lowest equivalence ratio was taken as the reference point for each dominant mode, therefore the zero frequency shift at these points (and each of the analogous plots in the Appendices) offer little information unless provided with data from an even lower equivalence ratio. It is plain to see that regardless of pressure, the

frequencies of these modes increase with increasing equivalence ratio, and further, these shifts are more dramatic for the higher frequency modes.

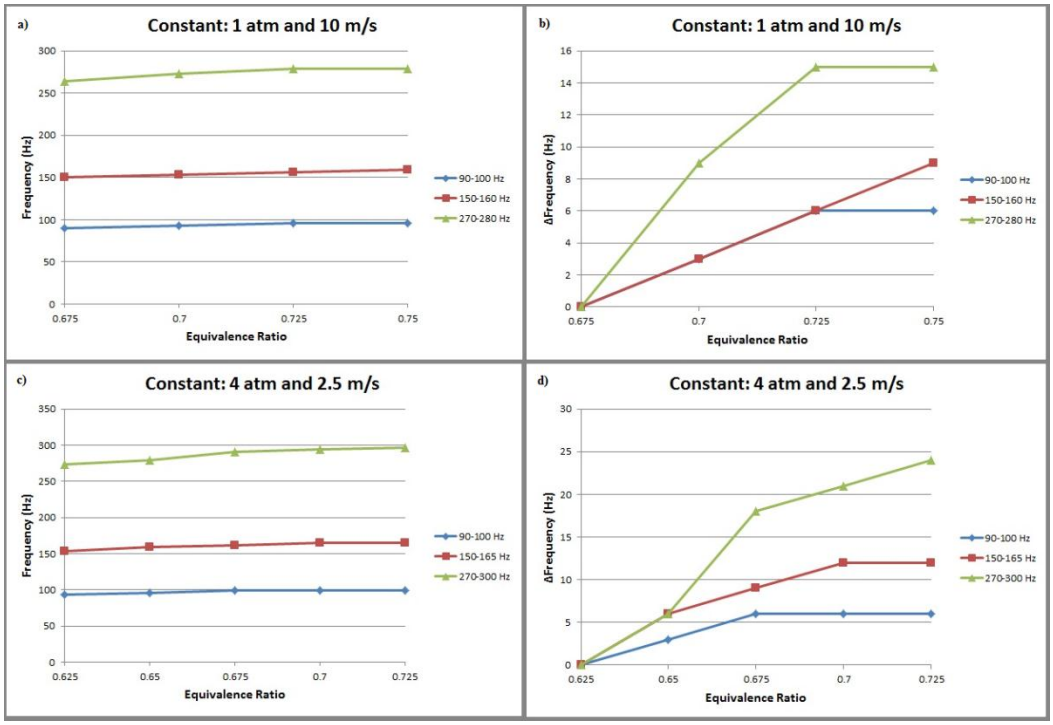

Figure 4.5 Frequency vs. Equivalence Ratio trend (20% H_2)

Allison et al (2012) also found that the frequency response generally increases with equivalence ratio. Figure 4.6 combines data from this work with some selected inlet fuel data from Allison et al (2012). The data represent the measured frequency of the pressure oscillation as a function of the equivalence ratio. The two lower lines correspond to frequencies of the first acoustic mode of this work (at 0% H_2 and 20% H_2), which were chosen due to their relatively high signal strength when compared to the second and third modes. The upper lines represent the relevant data from Allison et al, which contained three fuel mixtures: pure methane, syngas mixture of 20% H_2, and another syngas mixture of 25% H_2. These latter trend lines have been truncated for closer comparison

since fuel-rich mixtures (equivalence ratios great than 1) behave very differently than the fuel-lean mixtures examined here.

Unlike the combined PSD trends shown in the previous section, both sets of data seem to be in agreement in regard to the frequency response when varying the equivalence ratio (with a possible exception of the 25% H_2 syngas mixture between 0.75-0.85), regardless of the vast differences in burner and chamber configurations. The increasing frequency response with increasing equivalence ratio is suggestive of flame speed scaling, however Allison et al found that the frequencies for matched fuels were not similar, noting that their fuel-rich ethylene data did not match up with the 20% syngas data even though they have the same flame speed. This indicates that the flame speed is not the dominating factor but just a parameter that may be coupled with other parameters that control the acoustic performance.

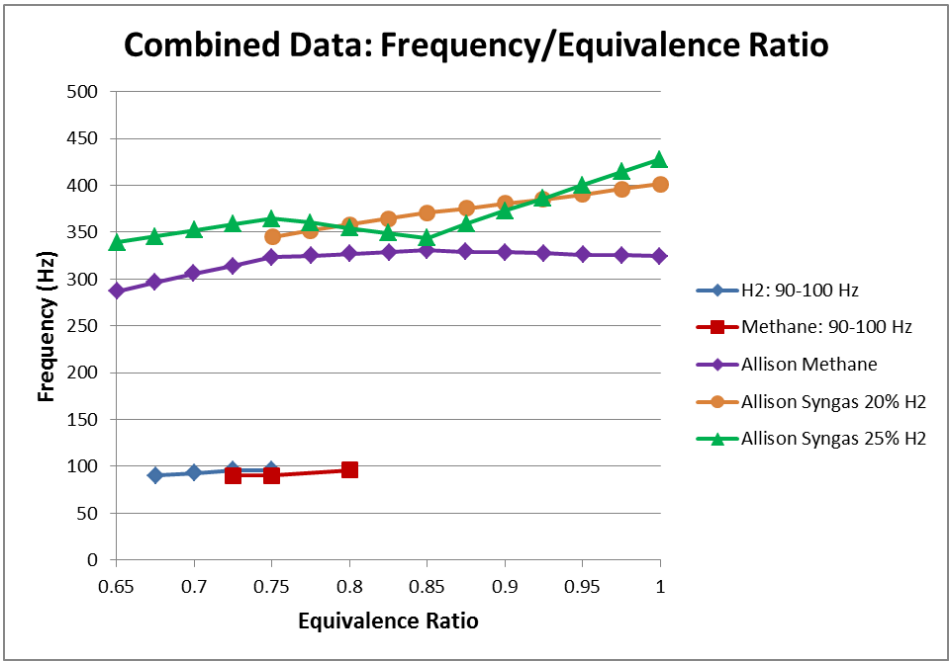

Figure 4.6 Frequency response compared to Allison et al (2012) data

Despite the many differences in experimental configurations, the conclusion may be drawn that the acoustic frequency decreases when the combustion mixture becomes more and more fuel-lean.

4.4 Effects of the Bulk Flow Velocity

Another variable parameter examined was the inlet gas velocity, or inlet bulk flow velocity. Figures A.10-12 in Appendix A show the trends for chamber pressures from 1-4 atm using the methane-air mixture. This trend is nearly independent of frequency for the first acoustic mode, while the trend is more apparent for each subsequent acoustic mode as seen in the frequency shifts presented in Figures A.13-15. Figure 4.7 below shows the frequency and PSD trends for the strongest acoustic mode of this work next to those reported by Allison et al (2012). Each result corresponds to a chamber pressure of 1 atm, while Allison et al tested at an equivalence ratio of 1, while the maximum equivalence ratios used in this work were 0.800 (100% methane, 0% hydrogen) and 0.725 (80% methane, 20% hydrogen). The figure below as well as those included in the appendices show that for this work the frequency decreases very slightly with increasing bulk velocity (or air mass flow rate), contradictory to the results reported by Allison et al. The interesting note here is that in each case, there is an upward shift in frequency when initially increasing the flow rate followed by decreasing trends thereafter. This phenomenon was even noticed physically during testing since the chamber itself would exhibit small vibrations.

For the 20% hydrogen mixture, similar trends are observed. The first acoustic mode varies minimally with increasing bulk flow velocity, especially at higher pressures, while the third mode shows a more significant variation. The hydrogen-enriched fuel was examined at even lower equivalence ratios than the pure methane mixture and the trend remains valid across this leaner regime.

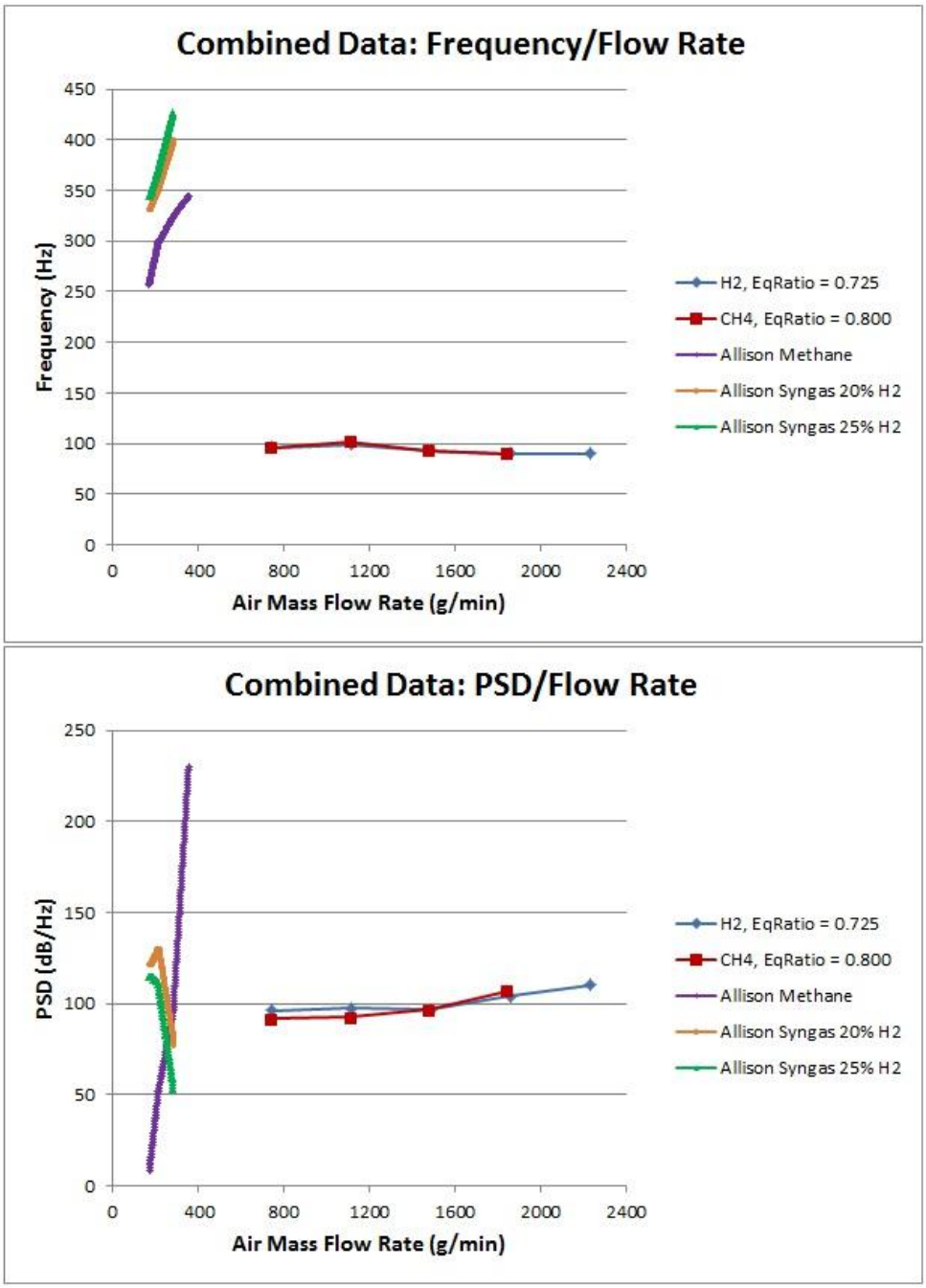

Figure 4.7 Air Mass Flow Rate response compared to Allison et al (2012) data

Allison et al (2012) discusses how convective-acoustic instabilities typically display a frequency that varies with the gas velocity, as opposed to those that are of the Helmholtz type of instability. Investigating the effects of varying the bulk flow velocity may shed some light onto which types of instabilities are being seen here. As mentioned previously, Allison et al found that the frequency of the instability increases with an increase in the mass flow rate, which suggests that the instability depends on a Strouhal number and has a convective-acoustic component. Syngas (with 25% H_2) and ethylene, which have the same flame speeds, show very similar frequency data.

Also seen above in Figure 4.7 are the PSD trends obtained here, along with Allison et al. The apparent trend of this work for both mixtures is deceptive since it only portrays one acoustic mode at one equivalence ratio and atmospheric pressure. The plots in the appendices display a wide variety of trends when varying either the equivalence ratio or the elevating the pressure, and the trends even vary from one acoustic mode to the next within the same set of parameters. This was also observed by Allison et al where the amplitude data displayed an assortment of varying trends for the various fuels observed. Both syngas mixtures dropped in amplitude strength whereas thermoacoustic instabilities of methane (and other hydrocarbons) were amplified at higher flow rates.

4.5 Changes in Chamber Pressure

One of the advantages of the present experimental configuration is its ability to test at elevated pressures. Since commercial combustors operate at pressures exceeding 20 atmospheres, elevated pressure trends are worth investigating in order to better understand the effects they may play on flame behavior.

Figure 4.8 below shows four graphs displaying PSD and frequency trends when adjusting the chamber pressure for 0% H_2 and 20% H_2 mixtures and a variety of equivalence ratios. Figures 4.8a-b examine the frequency trends of these mixtures, and

the results appear to be similar for each case. For the methane mixture, elevating the pressure slightly increases the frequencies but otherwise has no significant effect. As for the 20% hydrogen mixture, there appears to be a more direct and consistent increase in the frequencies when increasing the chamber pressure. From the figures, it is easy to see that the equivalence ratio plays a stronger role in altering the instability frequencies, where the frequencies drop when reducing the equivalence ratio.

Figures 4.8c-d below depict the PSD trends for higher pressures. As with the majority of the other PSD trends, it is difficult to extract any consistent behavior once again. Both mixtures show sporadic relationships between pressure fluctuations and pressure elevation. Similar to the frequency trends, it is easy to see that the equivalence ratio plays a more significant role since both mixtures drop in frequency when the equivalence ratio is lowered.

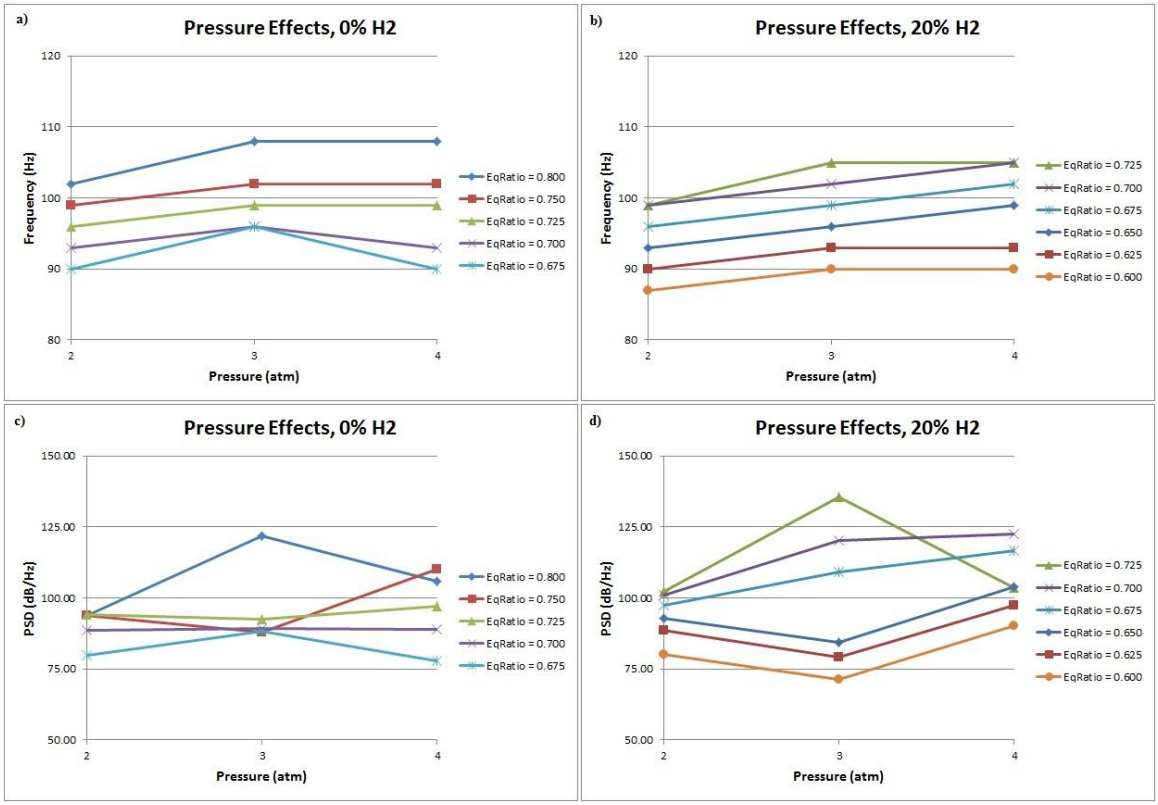

Figure 4.8 Pressure effects for various equivalence ratios and mixtures

4.6 Hydrogen Composition Variation

Over the range of tests performed, the methane-air data and the hydrogen-methane-air data were analyzed side-by-side in order to determine trends that may be directly contributed to the addition of hydrogen. In comparing the Frequency Shift vs. Equivalence Ratio trends shown in sections A.2 and B.2, it is noted that the 20% H_2 case showed consistently lower shifts in frequencies as compared to the pure methane mixture, however, these data were also taken at a lower range of equivalence ratios.

The PSD vs. Equivalence Ratio plots in sections A.3 and B.3 didn't offer any significant information due to the addition of hydrogen since the trends varied widely for either fuel mixture. The trends for the 20% H_2 mixture at lower chamber pressures (1-2 atm) displayed less randomness than the methane mixture, however, further hydrogen addition tests would be needed to further explore this trend.

Finally, the Frequency Shift vs. Bulk Velocity trends shown in sections A.5 and B.5 exhibit some notable trends at the higher pressures (3-4 atm). At these pressures, the frequency shifts for the hydrogen mixture are nearly all positive, while mostly negative for the methane mixture. This corresponds to frequencies that are shifted upwards when increasing the fuel flow rate for the hydrogen mixture, while shifting the frequencies downward at elevated bulk velocities for the methane mixture. Further hydrogen-enrichment would help in validating this trend. As in most of the previous Frequency Shift plots, the trends seem to be best portrayed in the third acoustic mode where more significant fluctuations are observed.

Allison et al (2012) found that the frequency at a given equivalence ratio is nearly independent of the hydrogen concentration. Instead, the increase in hydrogen results in an increase in the flame speed until a cutoff is reached and the instability is no longer active and the flame becomes non-resonating. This cutoff appears to be mainly equivalence ratio dependent, however the limit is extended for increasingly (hydrogen) enriched flames.

CHAPTER 5

CONCLUSIONS

The gas turbine industry faces more and more strict regulations each decade and therefore accurate laboratory experimentation has received plenty of focus in order to understand flame behavior and predict the instabilities that hinder lower emissions and increased efficiencies. An in-depth analysis has been presented in the previous chapter investigating how various parameters effect combustion dynamics considering two mixtures that are commonly used. A consistent comparison with Allison et al (2012) was offered in order to detect global effects versus geometry-dependent effects.

For either of these mixtures, the dominant acoustic modes increase when increasing the equivalence ratio, and portray higher shifts at higher modes. These results are in agreement with Allison et al even with a different low swirl burner and different chamber geometry. It is concluded that this is a global behavior and thus may be considered a significant result when scaling the dimensions to an industrial-sized gas turbine engine.

The pressure fluctuations, or power spectrum density, plots showed sporadic and widely varying trends which was also noted by Allison et al. Therefore, no significant conclusions were able to be drawn that could shed some light on PSD effects or how their values may be predicted. As for elevating the chamber pressure, the hydrogen mixture showed slight increases in frequencies at increasing pressures. This trend was less significant for the pure methane mixture.

Next, the effects of equivalence ratio changes were examined. The results of this work seemed to be in agreement with those of Allison et al. Both burner and chamber configurations saw an increase in frequency when increasing the equivalence ratio over the entire lean combustion regime.

Commercial engines operate at bulk fuel velocities much greater than those obtainable in laboratory testing; however, identifying similar trends between the lower flow rates used by Allison et al with those in the present work were used to offer some insight into the effects of higher inlet fuel velocities. It was shown that increasing the bulk velocity has little effect on the primary acoustic mode, however the frequencies did slowly decrease over the range of bulk velocities tested. This trend is contradictory to what was reported by Allison et al who found that increasing the bulk velocity also increased the instability frequencies, therefore it is hypothesized that there are other effects that contribute to these patterns such as the different burners and combustion chambers.

5.1 Future Work

It would be advantageous to investigate further the effects of hydrogen addition by increasing the fuel ratio to, say, 40-60%. Also investigating active control methods in order to examine the effects of acoustic forcing could offer more information on the dynamics of the instabilities often seen by large-scale engines.

A closer examination on the effects of elevated chamber pressures would be the next appropriate step in attempting to scale instability phenomena that occur within commercial engines. Specifically, experimenting at pressures exceeding the 4 atm that this work's configuration is limited to would be greatly beneficial. Along the same train of thought would be to push the limits of the fuel flow rates in order to get closer to what a full scale model operates at since, ultimately, this is a main goal in experimentation.

Finally, observing flame dynamics at the blow-out limits by operating at even leaner equivalence ratios would offer valuable research for the future since there is an increasingly demanding push for leaner and leaner emissions.

REFERENCES

Allison PM, Driscoll JF, Ihme M. Acoustic Behavior of a Partially-Premixed Gas Turbine Model Combustor. AIAA Aerospace Sciences Meeting, Nashville, TN. 2012.

Bellows BD, Neumeier Y, Lieuwen T. Forced Response of a Swirling, Premixed Flame to Flow Disturbances. Journal of Propulsion and Power. Vol. 22, Issue 5, 2006.

Cheng RK, Littlejohn D, Nazeer N, Smith KO. Laboratory studies of the flow field characteristics of low-swirl injectors for adaptation to fuel-flexible turbines. 2006 ASME Turbo Expo, GT2006-90878. 2006.

Cheng RK, Littlejohn D, Strakey PA, Sidwell T. Laboratory investigations of a low-swirl injector with H_2 and CH_4 at gas turbine conditions. Proceedings of the Combustion Institute. Vol. 32, 2009, pp. 3001-3009.

Cheng RK, Yegian DT, Miyasato MM, Samuelsen GS, Benson CE, Pellizzari R, Loftus P. Scaling and development of low-swirl burners for low-emission furnaces and boilers. Proceedings of the Combustion Institute. Vol. 28, Issue 1, 2000, pp. 1305-1313.

Choudhuri AR, Gollahalli SR. Stability of hydrogen/hydrocarbon blended fuel flames. Journal of Propulsion and Power. Vol. 19, Issue 2, 2003, pp. 220-225.

Chu BT. Mechanism of generation of pressure waves at flame fronts. National Advisory Committee for Aeronautics – Technical Notes, 1956, pp. 20.

Correa S.M. Power generation and aeropropulsion gas turbines: From combustion science to combustion technology. Symposium (International) on Combustion, Vol. 27, Issue 2, 1998, pp. 1793-1807.

Culick FEC. Dynamics of combustion systems: fundamentals, acoustics, and control. A short course of lectures. 2001.

Culick FEC, Yang V. Overview of combustion instabilities in liquid-propellant rocket engines. Liquid Rocket Engine Combustion Instability, Vol. 169. Progress in Astronautics and Aeronautics, AIAA, Washington, DC, USA, 1995.

Culick FEC, Yang V. Prediction of the stability of unsteady motions in solid-propellant rocket motors. Chapter 18, DeLuca L, Summerfield M (Eds.). Progress in Astronautics and Aeronautics. Vol. 143, 1992, pp. 719-779.

Day MS, Gao X, Bell JB. Properties of lean turbulent methane-air flames with significant hydrogen addition. Proceedings of the Combustion Institute. Vol. 33, Issue 1, 2011, pp. 1601-1608.

Decruix S, Schuller T, Durox D, Candel S. Combustion dynamics and instabilities: elementary coupling and driving mechanisms. Journal of Propulsion and Power. Vol. 19, Issue 5, 2003, pp. 722-734.

Dowling AP, Morgan AS. Feedback control of combustion oscillations. Annual Review of Fluid Mechanics. Vol. 37, 2005, pp. 151-182.

Durbin MD, Ballal DR. Optimizing the performance of a step swirl combustor. Proceedings of the 29th Intersociety Energy Conversion Engineering Conference – IECEC '94, AIAA, Monterey, CA, USA. Vol. 2, 1994, pp. 631-635.

Eckbreth AC. Laser diagnostics for combustion temperature and species. Gordon and Breach Publishers. 1996.

Emadi M, Karkow D, Salameh T, Gohil A, Ratner A. Flame Structure Changes Resulting from Hydrogen-Enrichment and Pressurization for Low-Swirl Premixed Methane-Air Flames. In Press. 2012.

Fairweather M, Ormsby MP, Sheppard CGW, Woolley R. Turbulent burning rates of methane and methane-hydrogen mixtures. Combustion and Flame. Vol. 156, Issue 4, 2009, pp. 780-790.

Ghoniem AF, Annaswamy A, Park S, and Sobhani ZC. Stability and emissions control using air injection and H_2 addition in premixed combustion. Proceedings of the Combustion Institute. Vol. 30, 2005, pp. 1765-1773.

Gupta AK, Lilley DG, Syred N. Swirl Flows. Abacus Press. 1984.

Halter F, Chauveau C, Djebaili-Chaumeix N, Gokalp I. Characterization of the effects of pressure and hydrogen concentration on laminar burning velocities of methane-hydrogen-air mixtures. Proceedings of the Combustion Institute. Vol. 30, 2005, pp. 201-208.

Halter F, Chauveau C, Gokalp I. Characterization of the effects of hydrogen addition in premixed methane/air flames. International Journal of Hydrogen Energy, Vol. 32, Issue 13, 2007, pp. 2585-2592.

Hassel EP, Linow S. Laser diagnostics for studies of turbulent combustion. Measurement Science and Technology. Vol. 11, 2000, pp. 37-57.

Hu E, Huang Z, He J, Zheng J, Miao H. Measurements of laminar burning velocities and onset of cellular instabilities of methane-hydrogen-air flames at elevated pressures and temperatures. International Journal of Hydrogen Energy. Vol. 34, 2009, pp. 5574-5584.

Huang Y. Combustion Dynamics of Swirl-Stabilized Lean Premixed Flames in an Acoustically-Driven Environment. PhD Thesis. University of Iowa. 2008.

Huang Y, Yang V. Dynamics and stability of lean-premixed swirl-stabilized combustion. Progress in Energy and Combustion Science. Vol. 35, Issue 4, 2009, pp. 293-364.

Ilbas M, Crayford AP, Yilmaz I, Bowen PJ, Syred N. Laminar-burning velocities of hydrogen-air and hydrogen-methane-air mixtures: an experimental study. International Journal of Hydrogen Energy. Vol. 31, 2006, pp. 1768-1779.

Jackson GS, Sai R, Plaia JM, Boggs CM, Kiger KT. Influence of H_2 on the response of lean premixed CH_4 flames to high strained flows. Combustion and Flame. Vol. 132, 2003, pp. 503-511.

Kang DM, Culick FEC, Ratner A. Combustion dynamics of a low-swirl combustor. Combustion and Flame. Vol. 151, Issue 3, 2007, pp. 412-425.

Kang DM, Fernandez V, Ratner A, Culick FEC. Measurements of fuel mixture fraction oscillations of a turbulent jet non-premixed flame. Combustion and Flame. Vol. 156, 2009, pp. 214-220.

Katoh A, Oyama H, Kitagawa K, Gupta AK. Visualization of OH radical distribution in a methane-hydrogen mixture flame by isotope shift/planar laser induced fluorescence spectroscopy. Combustion Science and Technology. Vol. 178, Issue 12, 2006, pp. 2061-2074.

Kim D, Park SW. Effects of hydrogen addition on flame structure and forced flame response to velocity modulation in a turbulent lean premixed combustor. Fuel. Vol. 89, Issue 11, 2010, pp. 3475-3481.

Kim HS, Arghode VK, Gupta AK. Flame characteristics of hydrogen-enriched methane-air premixed swirl flames. International Journal of Hydrogen Energy. Vol. 34, Issue 2, 2008, pp. 1063-1073.

Kim KT, Lee JG, Quay BD, Santavicca DA. Response of partially premixed flames to acoustic velocity and equivalence ratio perturbations. Combustion and Flame. Vol. 157, Issue 9, 2010, pp. 1731-1744.

Lawn CJ, Schefer RW. Scaling of premixed turbulent flames in the corrugated regime. Combustion and Flame. Vol. 146, 2006, pp. 180-199.

Lee JG, Kim K, Santavicca DA. Measurement of equivalence ratio fluctuation and its effect on heat release during unstable combustion. Proceedings of the Combustion Institute. Vol. 28, Issue 1, 2000, pp. 415-421.

Lefebvre AH. The Role of Fuel Preparation in Low-Emission Combustion. Journal of Engineering for Gas Turbines and Power. Vol. 117. 1995, pp. 617-654.

Lieuwen T, McDonell V, Petersen E, Santavicca D. Fuel flexibility influences on premixed combustor blowout, flashback, autoignition, and stability. Journal of Engineering for Gas Turbines and Power. Vol. 130, 2008, pp. 1-10.

Lieuwen T, Yang V, editors. Combustion Instabilities in Gas Turbine Engines: Operational Experience, Fundamental Mechanisms, and Modeling. AIAA Progress in Astronautics and Aeronautics, Vol. 210, 2005, 657 pages.

Littlejohn D, Cheng RK. Fuel effects on a low-swirl injector for lean premixed gas turbines. Proceedings of the Combustion Institute. Vol. 31, 2007, pp. 3155-3162.

Mandilas C, Ormsby MP, Sheppard CGW, Woolley R. Effects of hydrogen addition on laminar and turbulent premixed methane and iso-octane-air flames. Proceedings of the Combustion Institute. Vol. 31, 2007, pp. 1443-1450.

Markstein GH, Guenoche H, Putnam AA. Nonsteady flame propagation. AGARDograph 75, 1964, pp. 328.

McManus KR, Poinsot T, Candel S. A review of active control of combustion instabilities. Progress in Energy and Combustion Science. Vol. 19, Issue 1. 1993, pp. 1-29.

Milton BE, Keck JC. Laminar Burning Velocities in Stoichiometric Hydrogen and Hydrogen-Hydrocarbon Gas Mixtures. Combustion and Flame. Vol. 58, 1984, pp. 13-22.

Poinsot T, Veynante D, editors. Theoretical and Numerical Combustion (2nd Edition). R.T. Edwards, Inc., 2005, 522 pages.

Pun W, Palm SL, Culick FEC. Combustion dynamics of an acoustically forced flame. Combustion Science and Technology. Vol. 175, 2003, pp. 499-521.

Ratner A, Pun W, Palm SL, Culick FEC. Comparison of Chemiluminescence, OH PLIF, and NO PLIF for Determination of Flame Response to Acoustics Waves. Western States Section Meeting of the Combustion Institute. 2002.

Rayleigh JWS. The Theory of Sound. Dover Publications. Vol. 2, 1945, 504 pages.

Roux S, Lartigue G, Poinsot T, Meier U, Berat C. Studies of mean and unsteady flow in a swirled combustor using experiments, acoustic analysis, and large eddy simulations. Combustion and Flame. Vol. 141, 2005, pp. 40-54.

Schefer W, Wicksall DM, Agrawal AK. Combustion of hydrogen-enriched methane in a lean premixed swirl-stabilized burner. Proceedings of the Combustion Institute. Vol. 29, 2003, pp. 843-851.

Scholte TG, Vaags PB. Burning Velocities of Mixtures of Hydrogen, Carbon Monoxide and Methane with Air. Combustion and Flame. Vol. 3, 1959, pp. 511-524.

Strakey P, Sidwell T, Ontko J. Investigation of the effects of hydrogen addition on lean extinction in a swirl stabilized combustor. Proceedings of the Combustion Institute. Vol. 31, Issue 2, 2007, pp. 3173-3180.

Swift GW. Thermoacoustics: a unifying perspective for some engines and refrigerators. Acoustical Society of America. 2002.

Syred N. A review of oscillation mechanisms and the role of the precessing vortex core (PVC) in swirl combustion systems. Progress in Energy and Combustion Science. Vol. 32, Issue 2, 2006, pp. 93-161.

Syred N, Beer JM. The damping of precessing vortex cores by combustion in swirl generators. Proceedings of the 3rd Colloquium on Gasdynamics of Explosions and Reactive Systems, Marseille, France. Vol. 17, 1972, pp. 783-801.

Turns SR. An Introduction to Combustion. McGraw Hill. 2000.

U.S. Department of Energy Office of Fossil Energy. Enabling Near-Zero Emission Coal-Based Power Generation. NETL: Turbine Program. 2005.

Wierzba I, Kilchyk V. Rich flammability limits of fuel mixtures involving hydrogen at elevated temperatures. International Journal of Hydrogen Energy. Vol. 25, Issue 1, 2000, pp. 75-80.

Yamaoka I, Tsuji H. An anomalous behavior of methane-air and methane-hydrogen-air flames diluted with nitrogen in a stagnation flow. Symposium (International) on Combustion. Vol. 25, Issue 1, 1992, pp. 145-152.

Yilmaz I, Ratner A, Ilbas M, Huang Y. Experimental investigation of thermoacoustic coupling using blended hydrogen-methane fuels in a low swirl burner. International Journal of Hydrogen Energy. Vol. 35, Issue 1, 2010, pp. 329-336.

Yu G, Law CK, Wu CK. Laminar Flame Speeds of Hydrocarbon + Air Mixtures with Hydrogen Addition. Combustion and Flame. Vol. 63, 1986, pp. 339-347.

Zeldovich J. The Oxidation of Nitrogen Combustion and Explosions. Acta Physiochimica URSS. Vol. 21, Issue 4, 1946, pp. 577-628.

Zinn BT, Lieuwen T. Combustion instability: basic concepts. Combustion Instabilities in Gas Turbine Engines. AIAA. 2005.

Zinn BT. Combustion instabilities: problems, solutions, and research needs. Chemical and Physical Processes in Combustion: 1986 Fall Technical Meeting. Combustion Institute, Pittsburgh, PA, USA, San Juan Bautista, PR. 1987, pp. 1-12.

APPENDIX A – 0% HYDROGEN (100% METHANE) DATA

A.1 Frequency vs. Equivalence Ratio

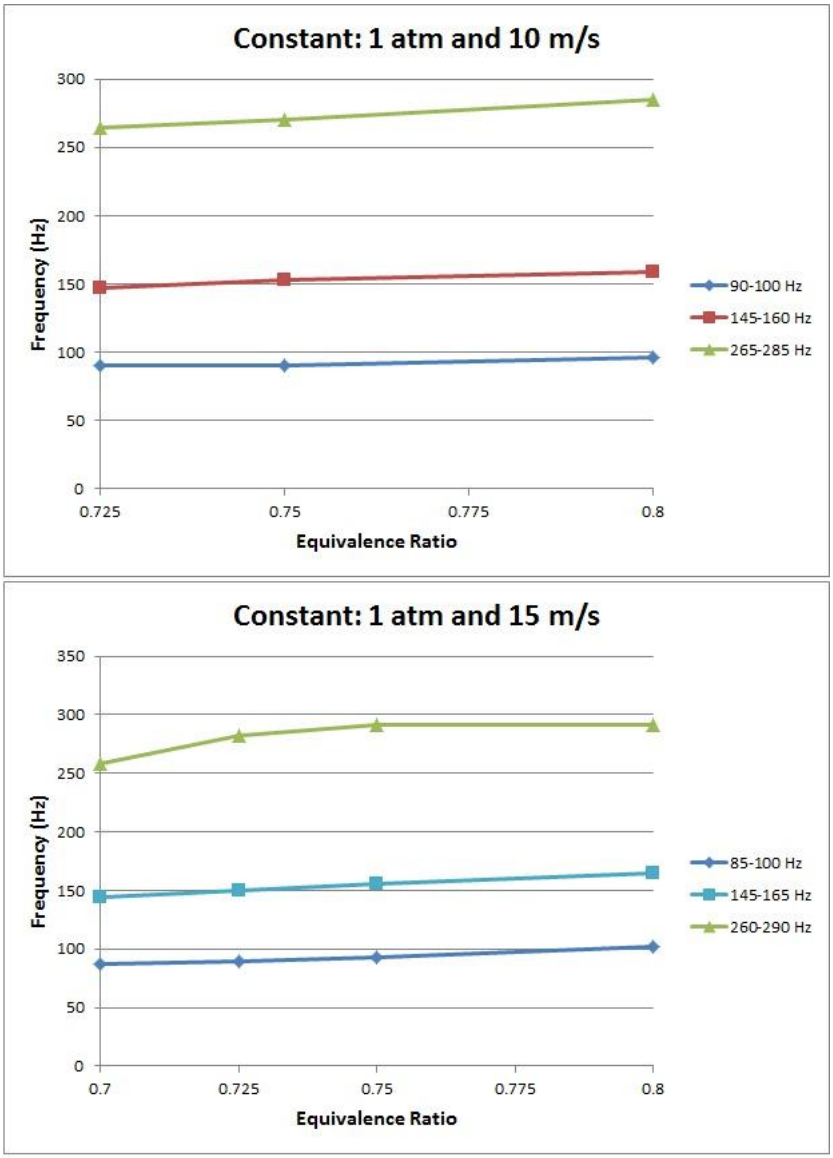

Figure A.1 Frequency vs. Equivalence Ratio at 1 atm

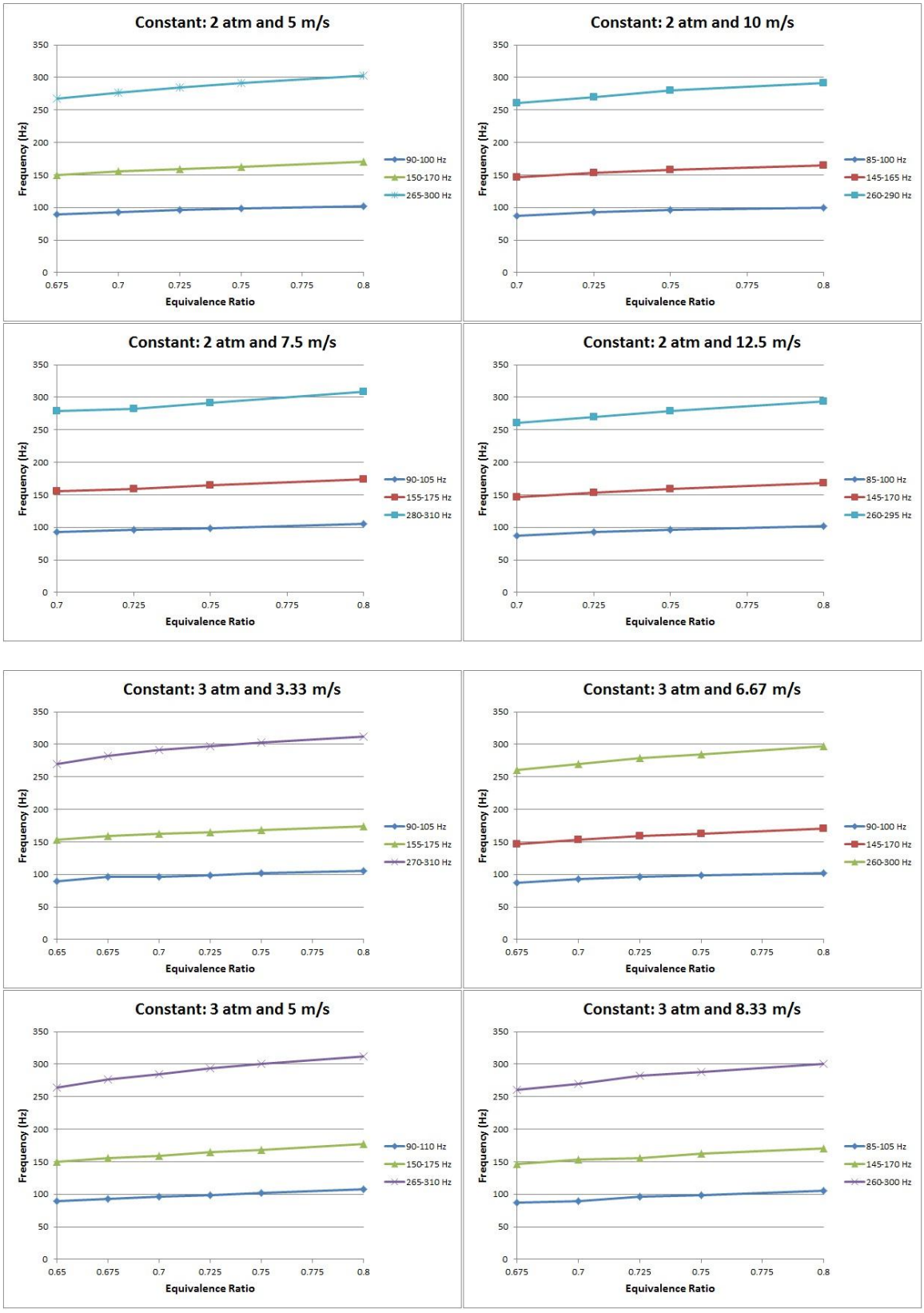

Figure A.2 Frequency vs. Equivalence Ratio at 2 and 3 atm

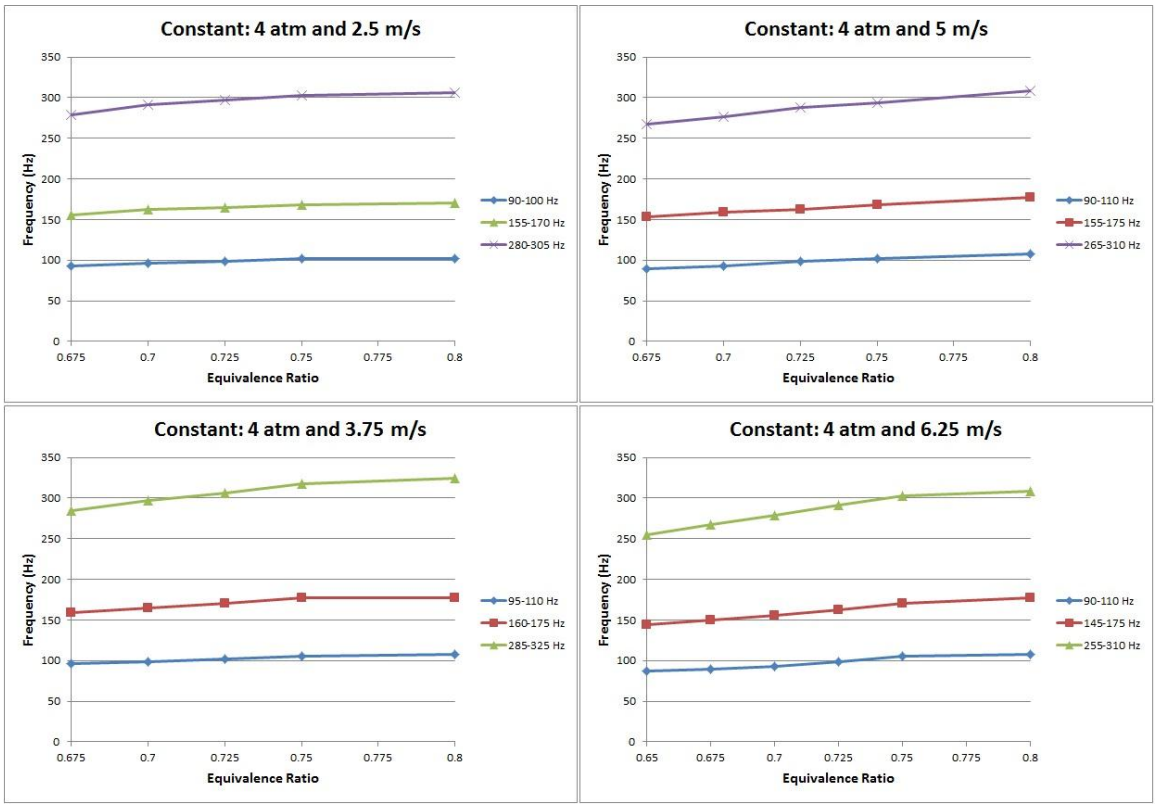

Figure A.3 Frequency vs. Equivalence Ratio at 4 atm

A.2 Frequency Shift vs. Equivalence Ratio

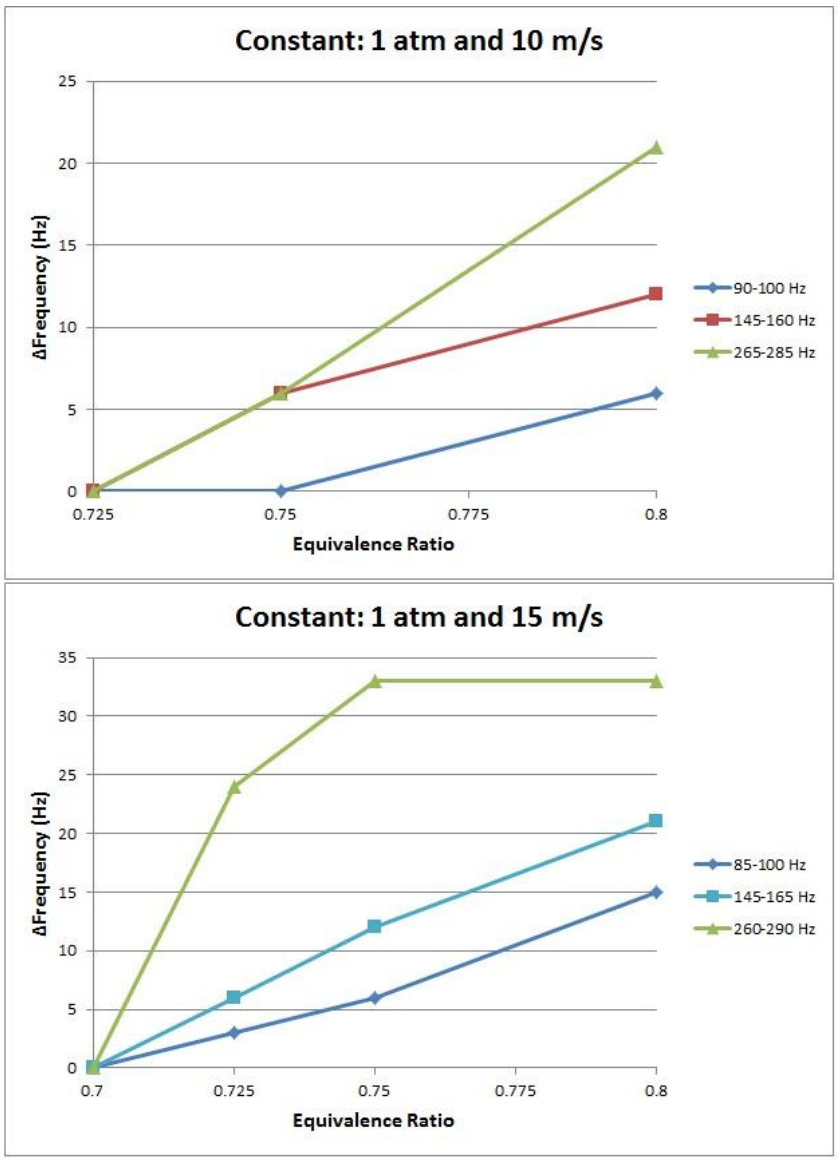

Figure A.4 Frequency Shift vs. Equivalence Ratio at 1 atm

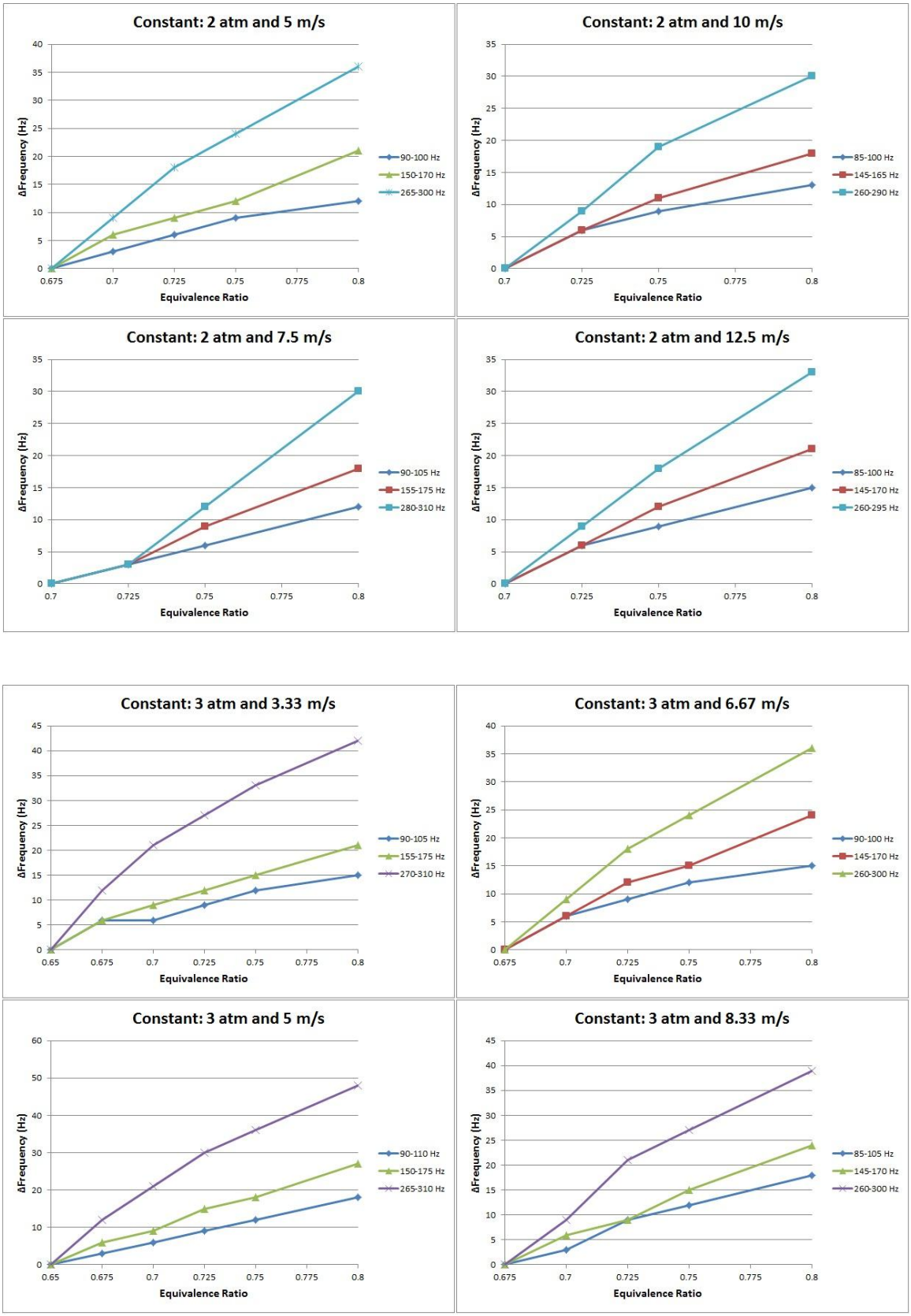

Figure A.5 Frequency Shift vs. Equivalence Ratio at 2 and 3 atm

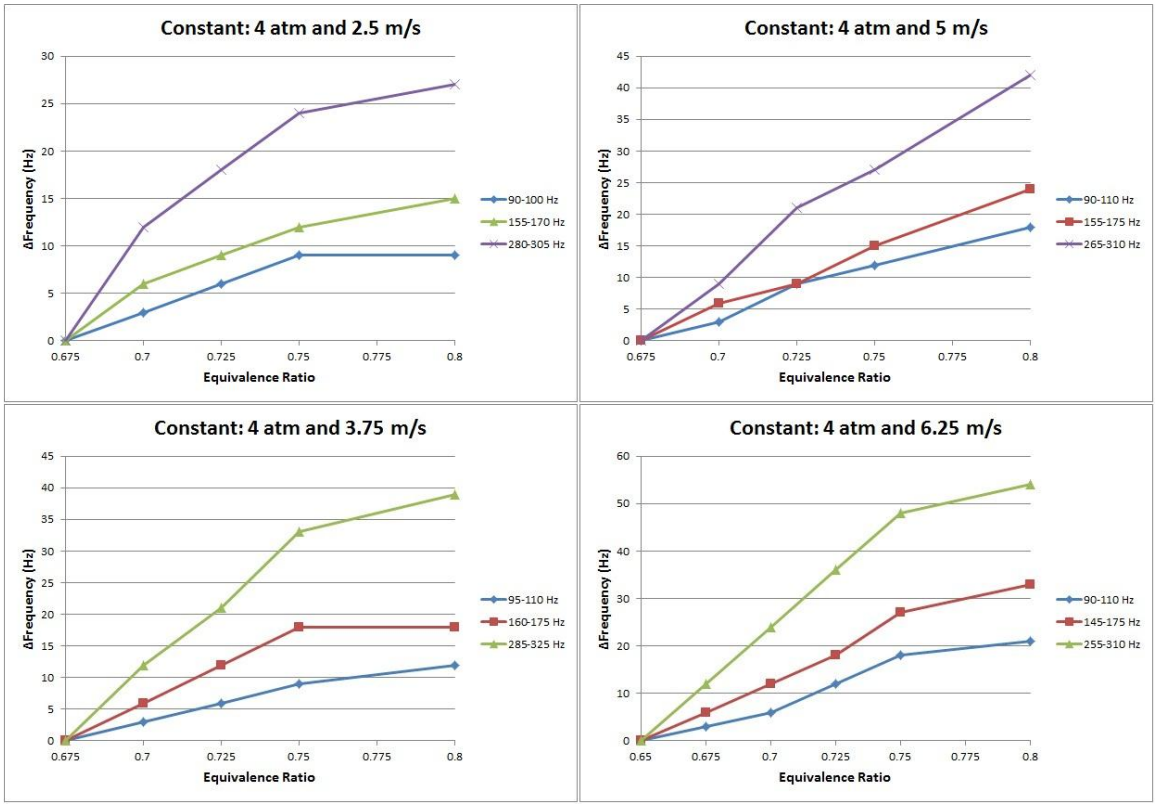

Figure A.6 Frequency Shift vs. Equivalence Ratio at 4 atm

A.3 PSD vs. Equivalence Ratio

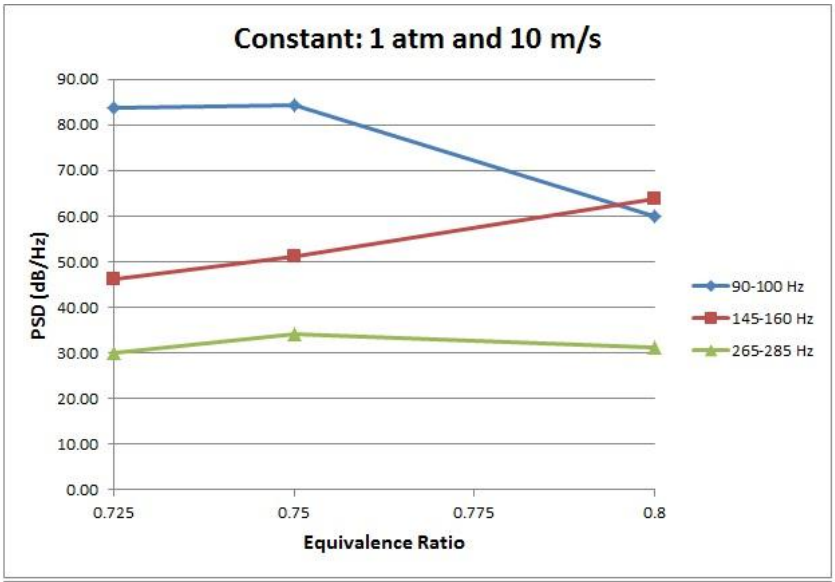

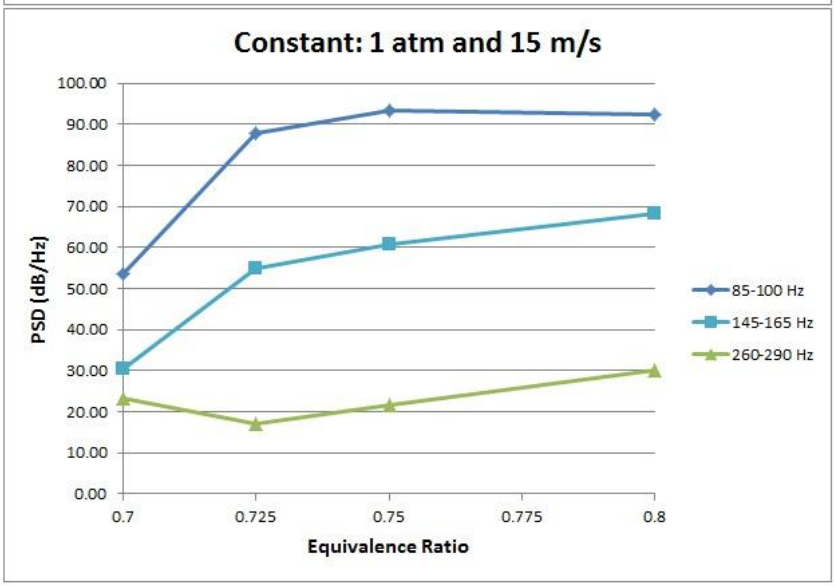

Figure A.7 PSD vs. Equivalence Ratio at 1 atm

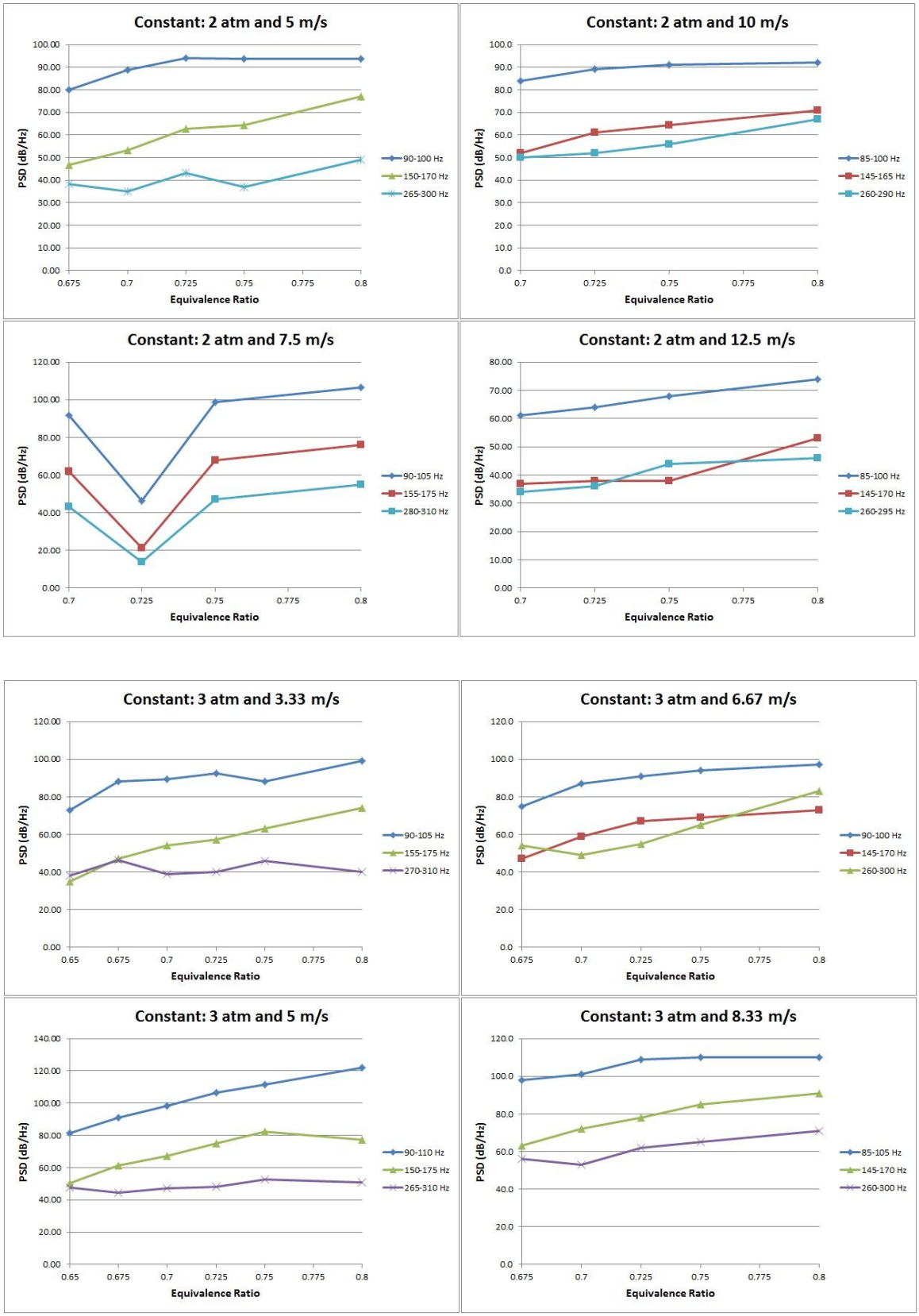

Figure A.8 PSD vs. Equivalence Ratio at 2 and 3 atm

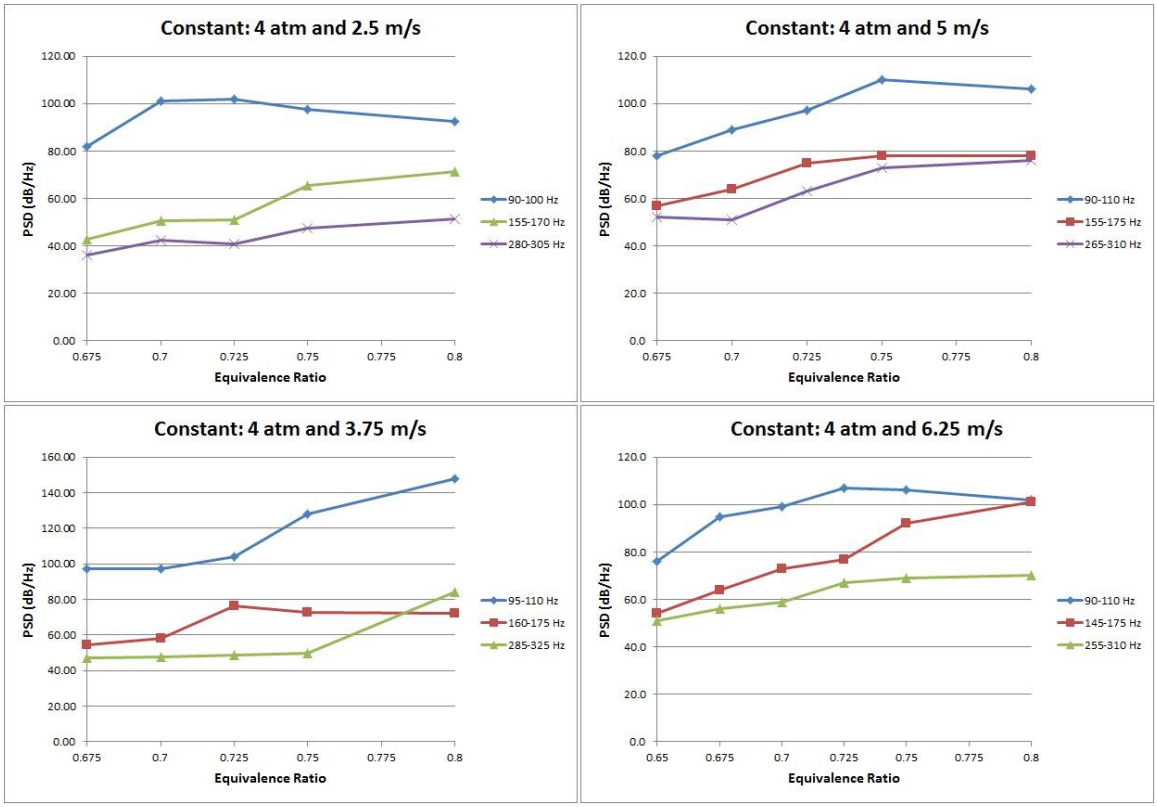

Figure A.9 PSD vs. Equivalence Ratio at 4 atm

A.4 Frequency vs. Bulk Velocity

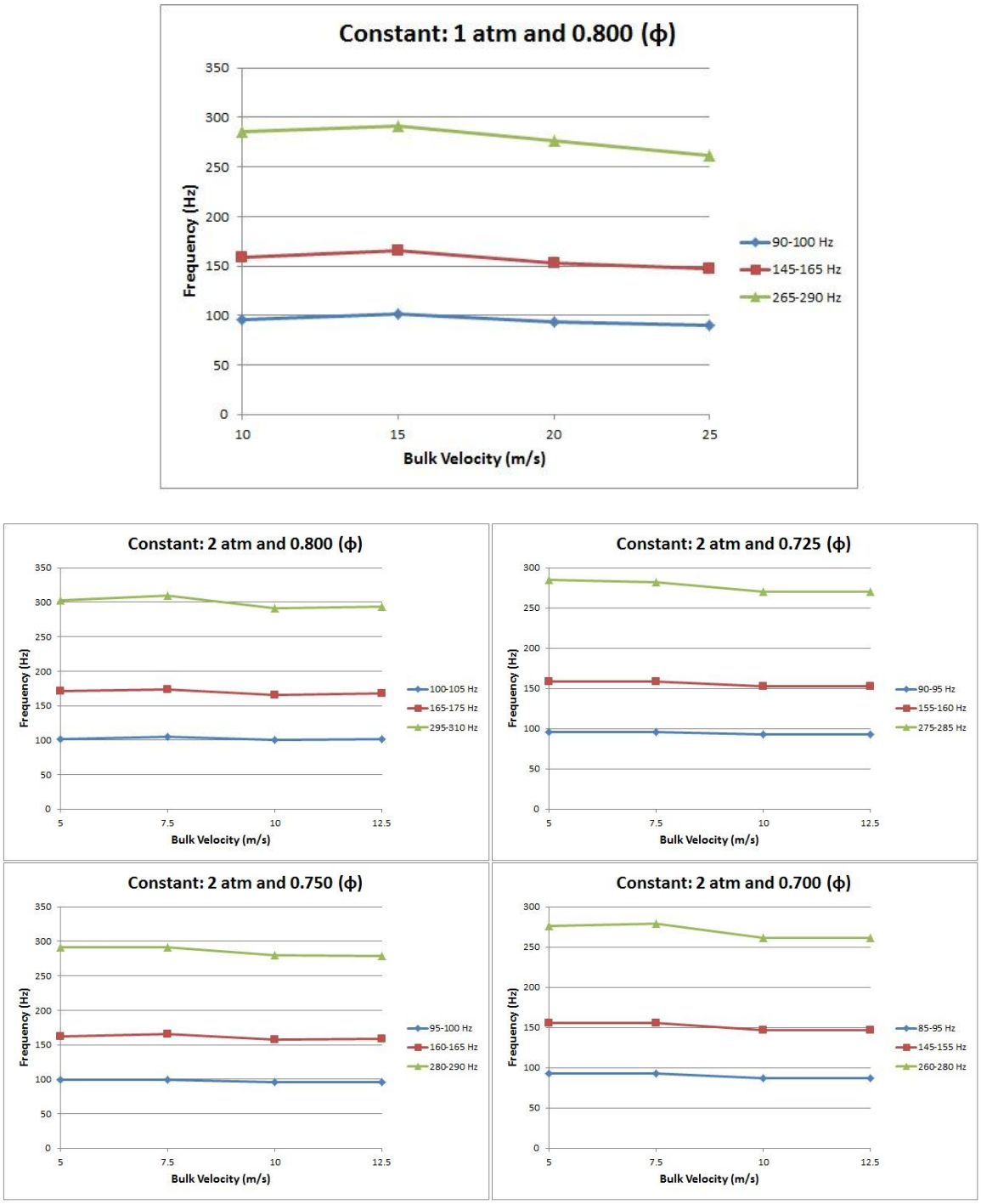

Figure A.10 Frequency vs. Bulk Velocity at 1 and 2 atm

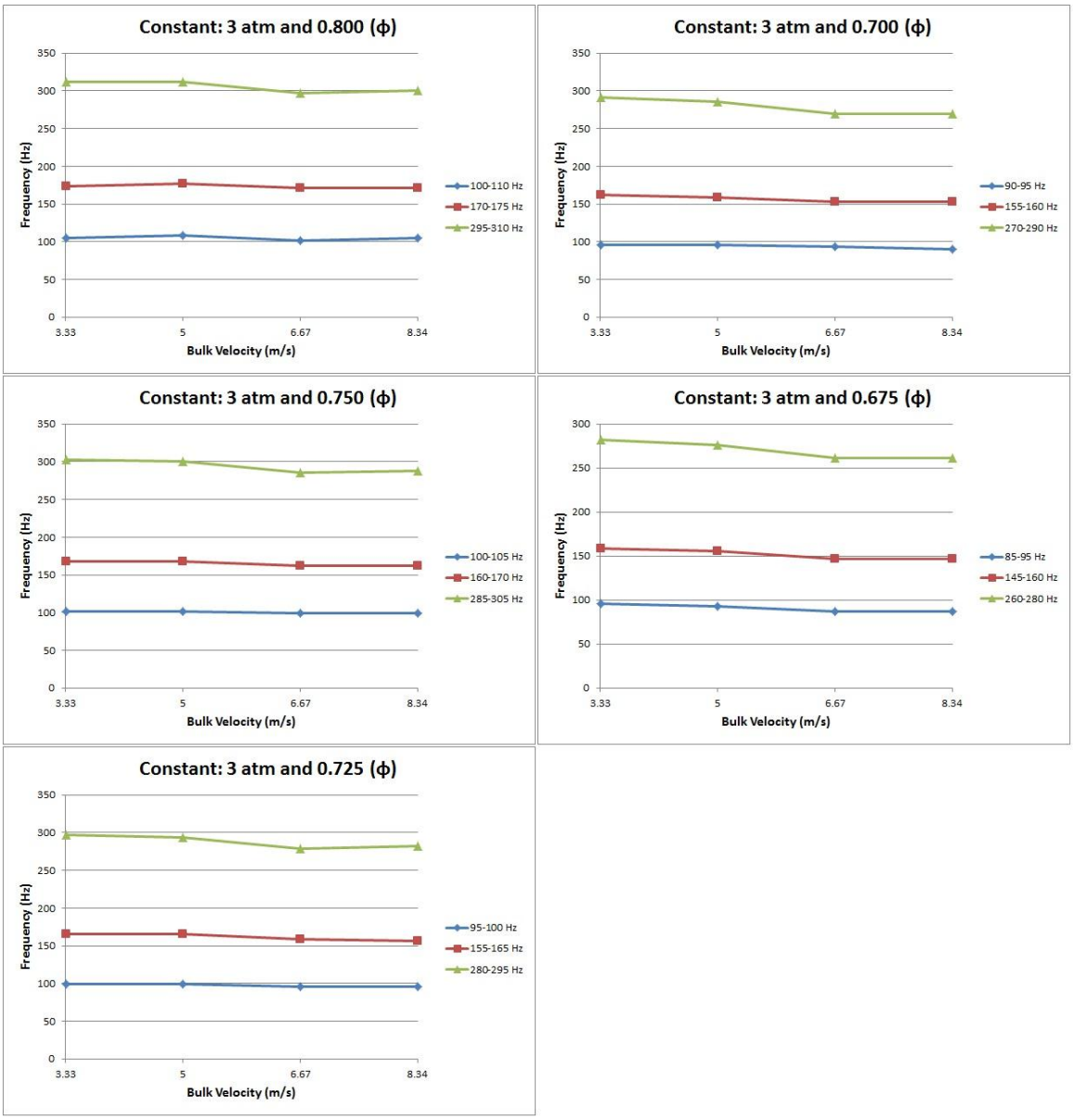

Figure A.11 Frequency vs. Bulk Velocity at 3 atm

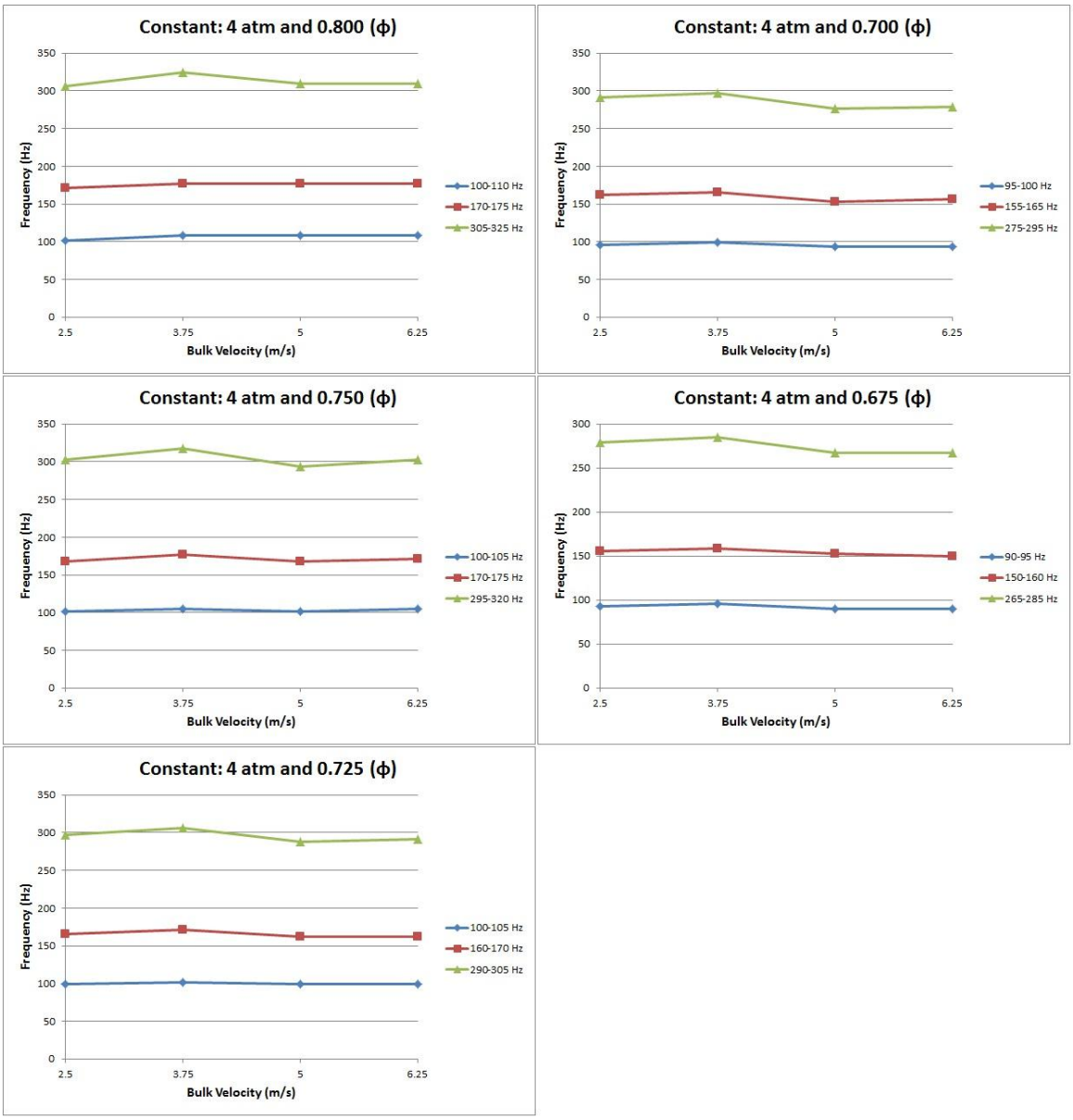

Figure A.12 Frequency vs. Bulk Velocity at 4 atm

A.5 Frequency Shift vs. Bulk Velocity

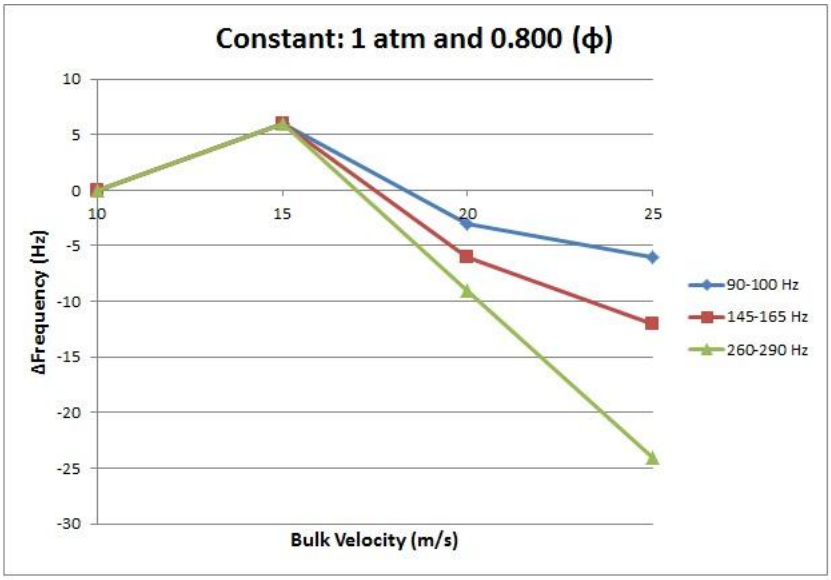

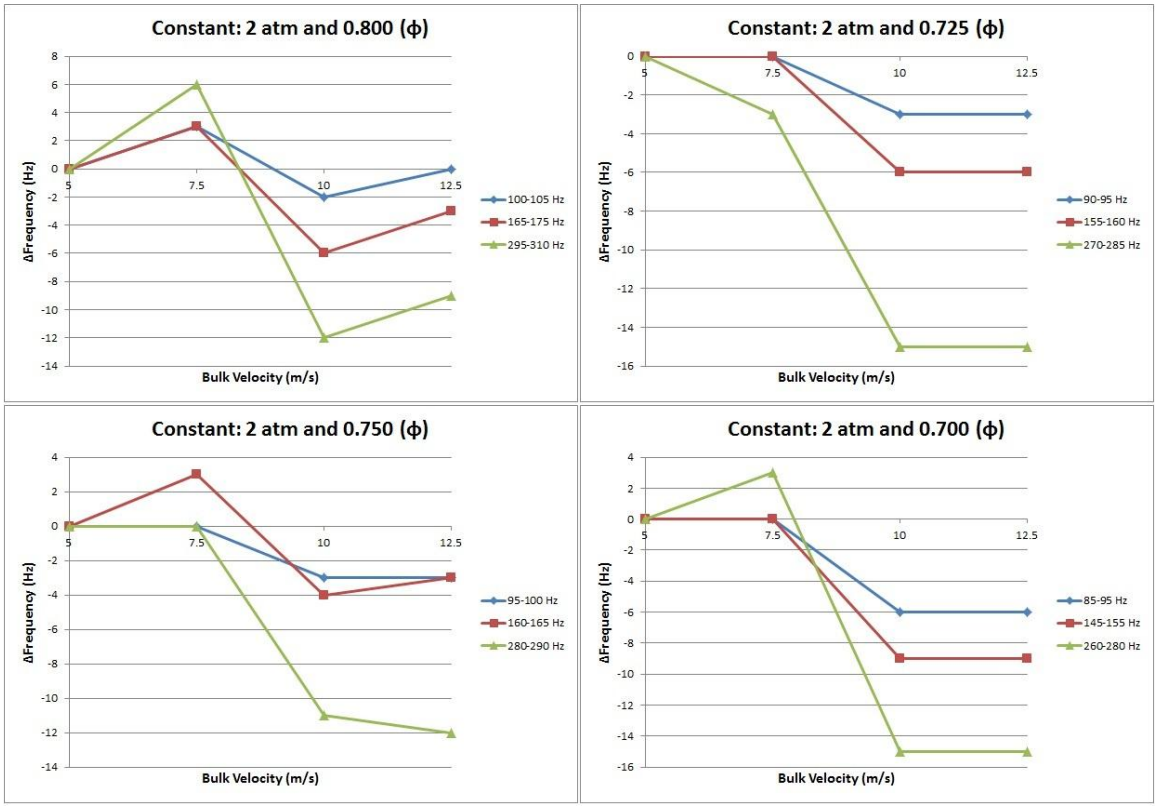

Figure A.13 Frequency Shift vs. Bulk Velocity at 1 and 2 atm

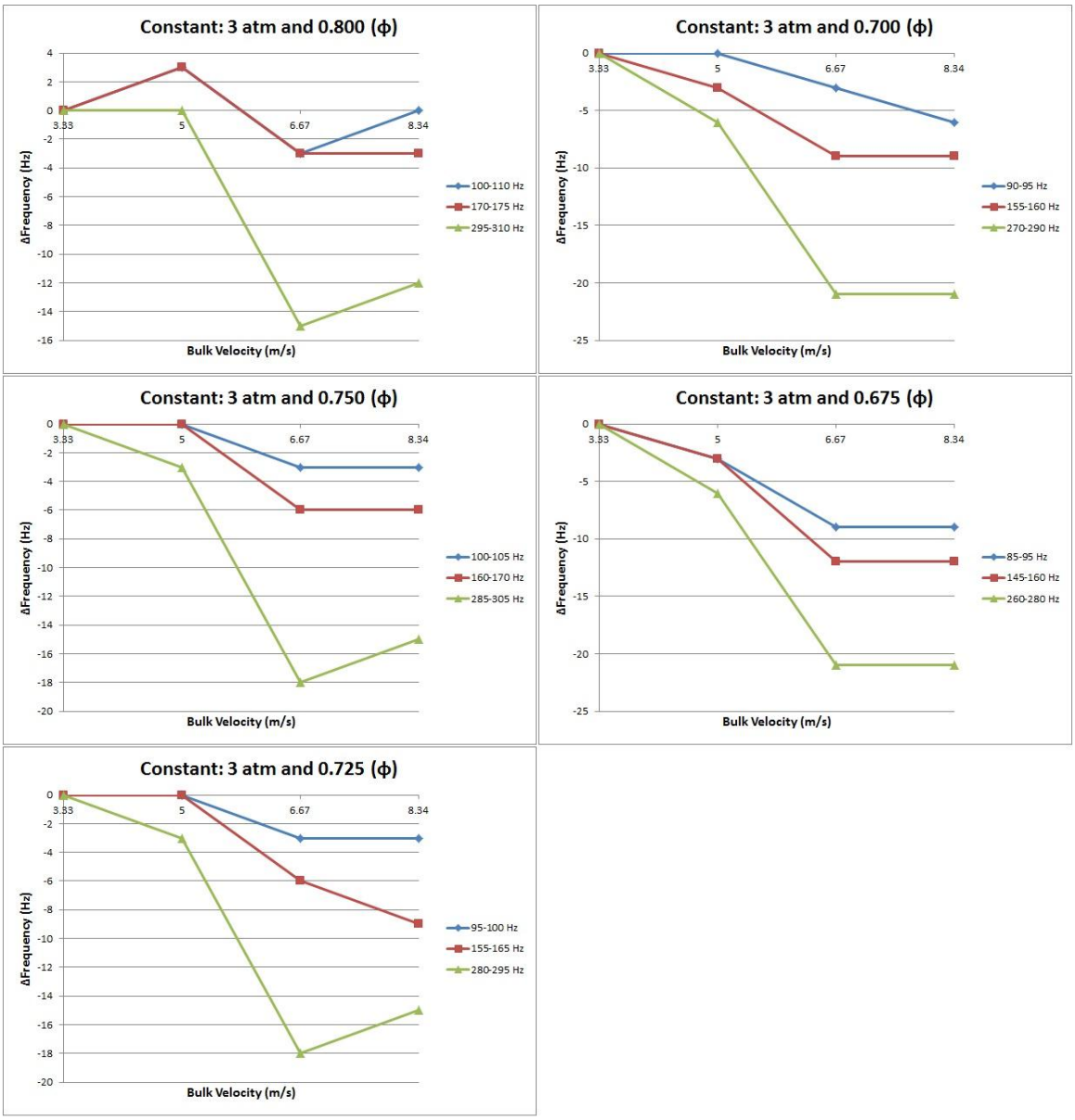

Figure A.14 Frequency Shift vs. Bulk Velocity at 3 atm

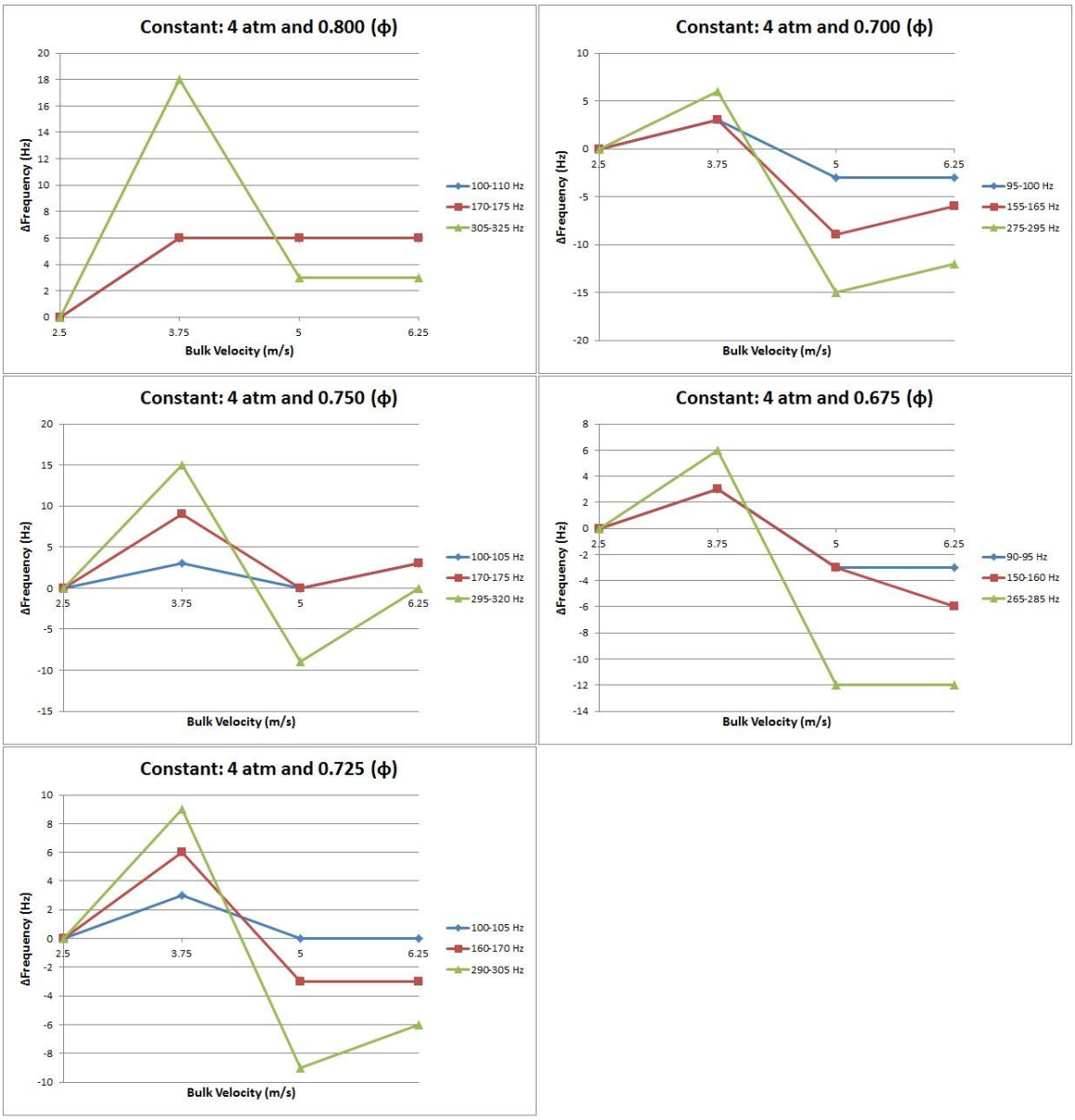

Figure A.15 Frequency Shift vs. Bulk Velocity at 4 atm

A.6 PSD vs. Bulk Velocity

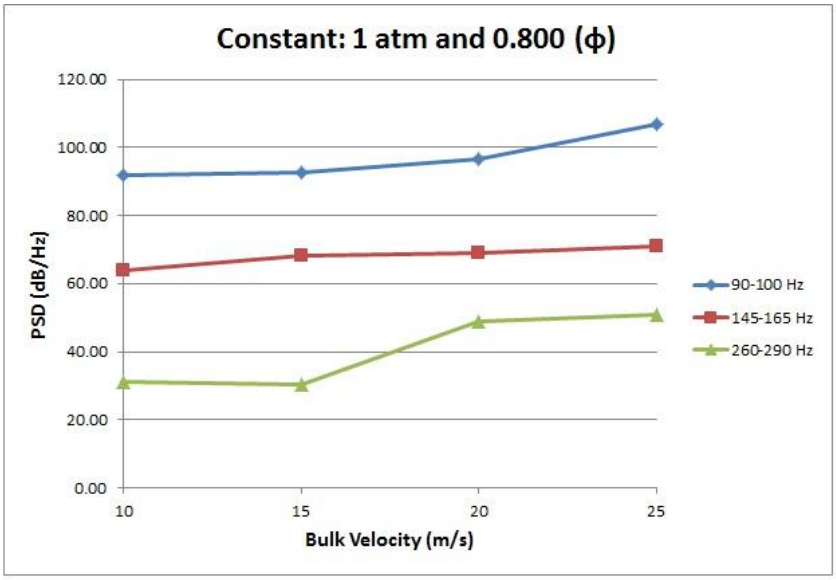

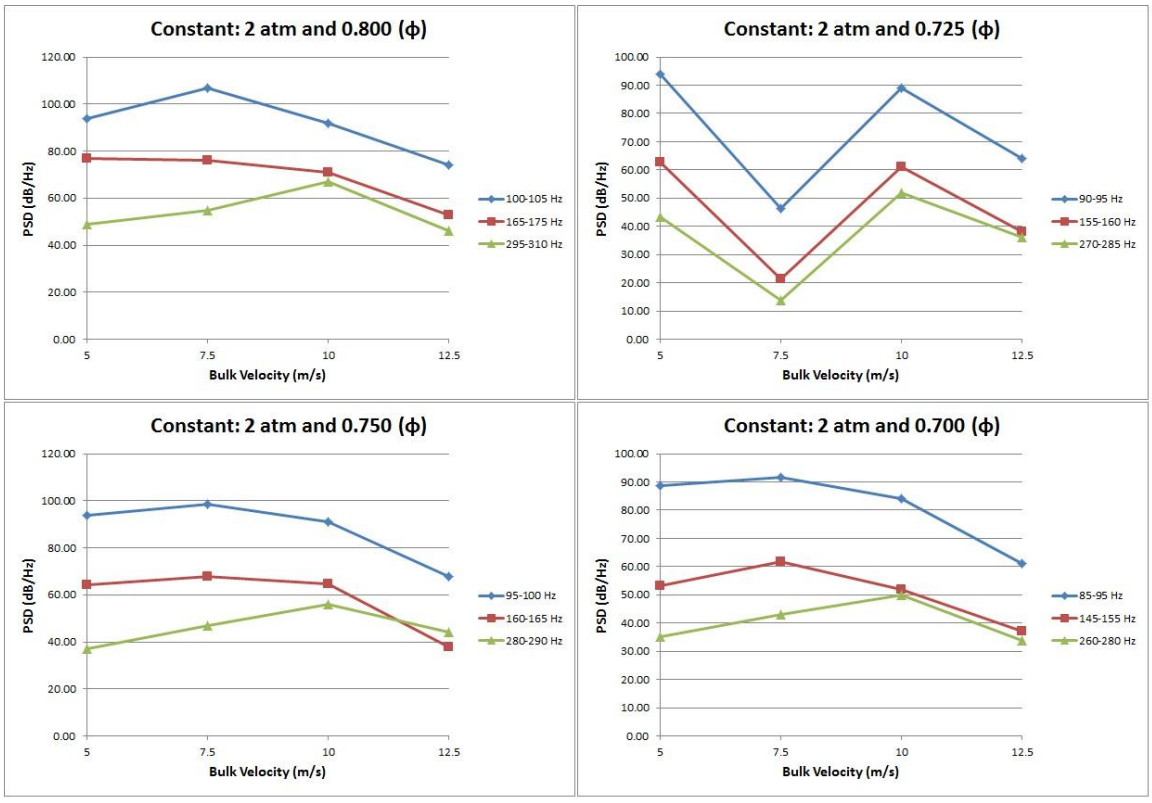

Figure A.16 PSD vs. Bulk Velocity at 1 and 2 atm

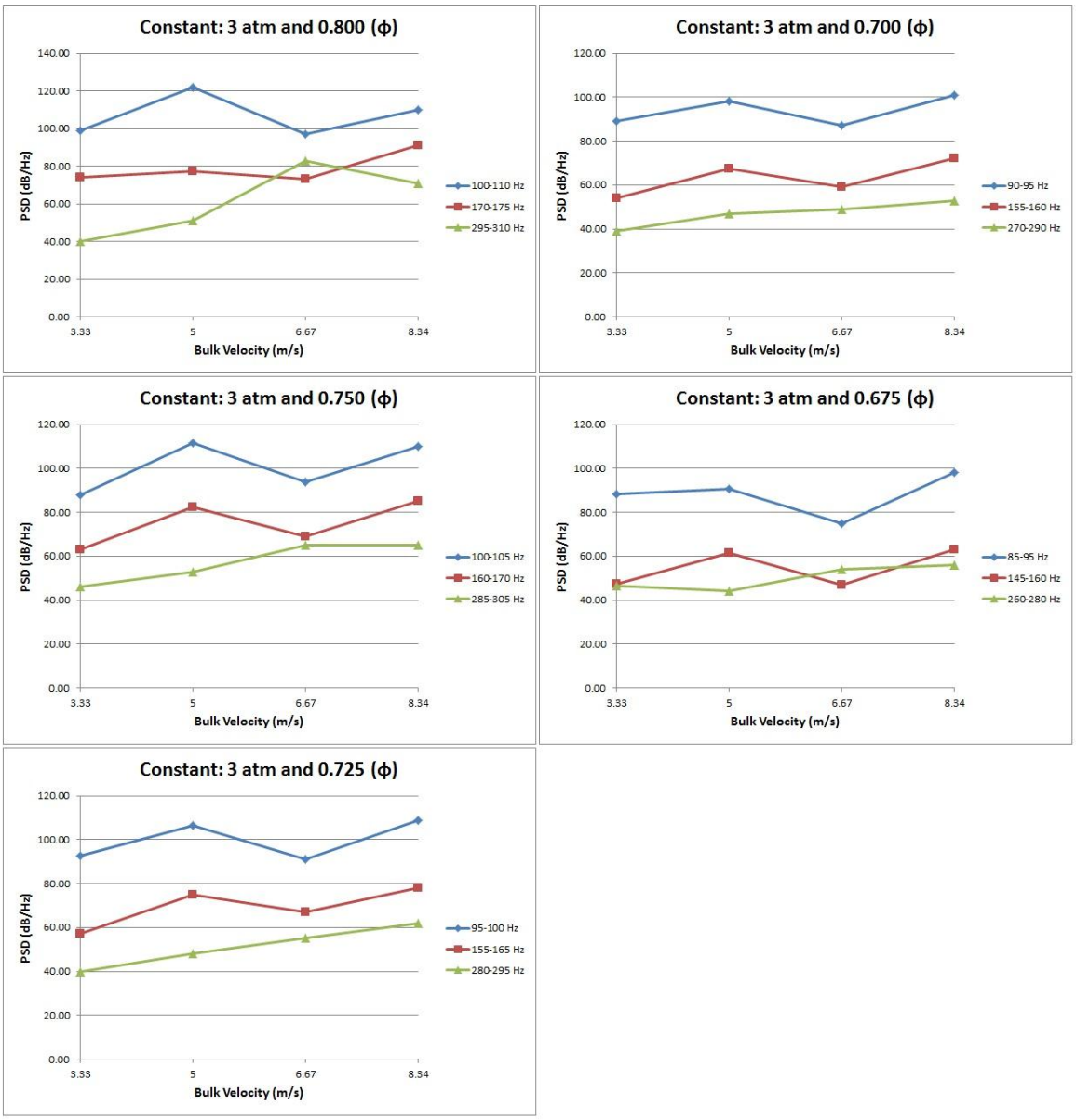

Figure A.17 PSD vs. Bulk Velocity at 3 atm

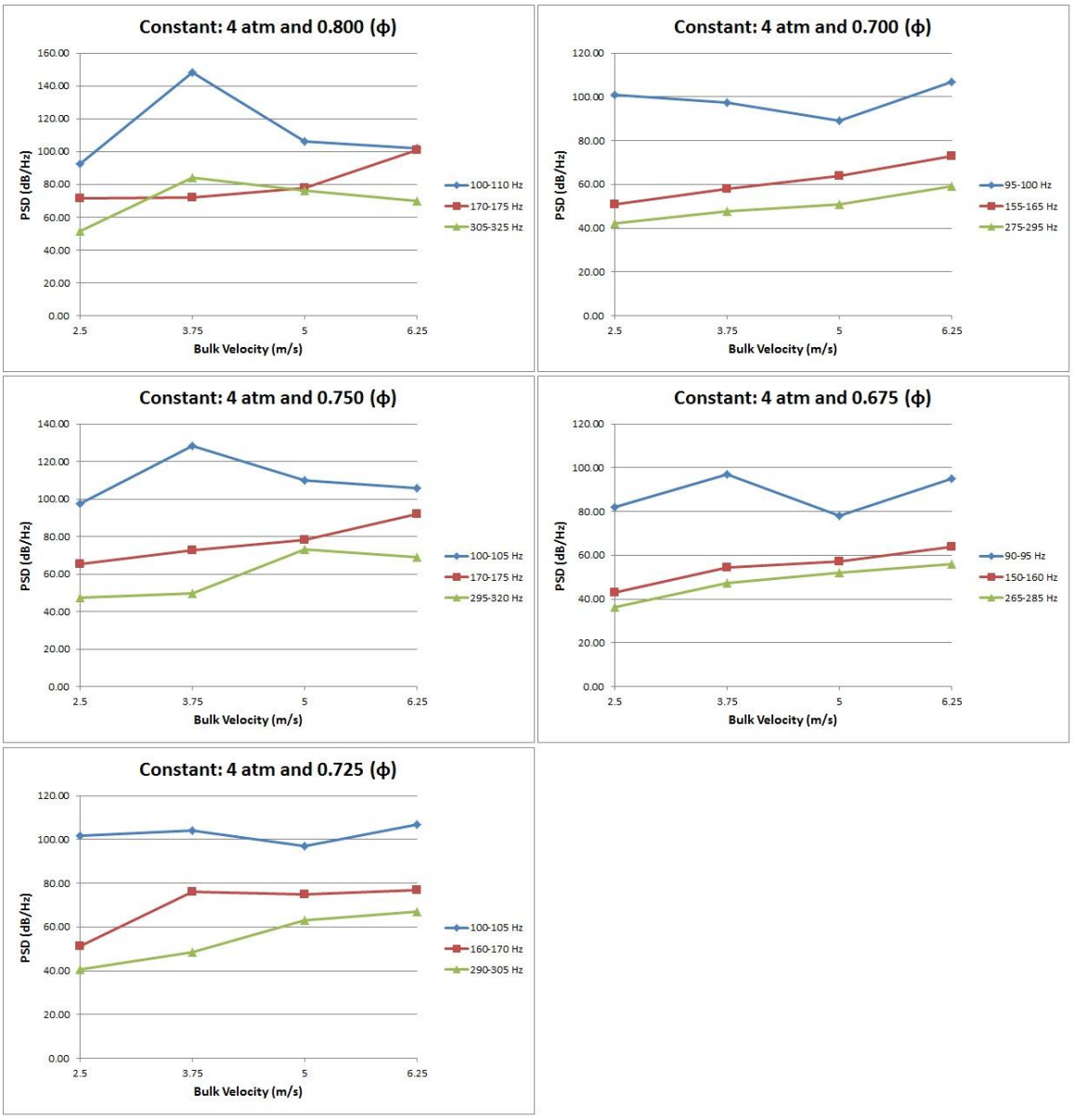

Figure A.18 PSD vs. Bulk Velocity at 4 atm

APPENDIX B - 20% HYDROGEN (80% METHANE) DATA

B.1 Frequency vs. Equivalence Ratio

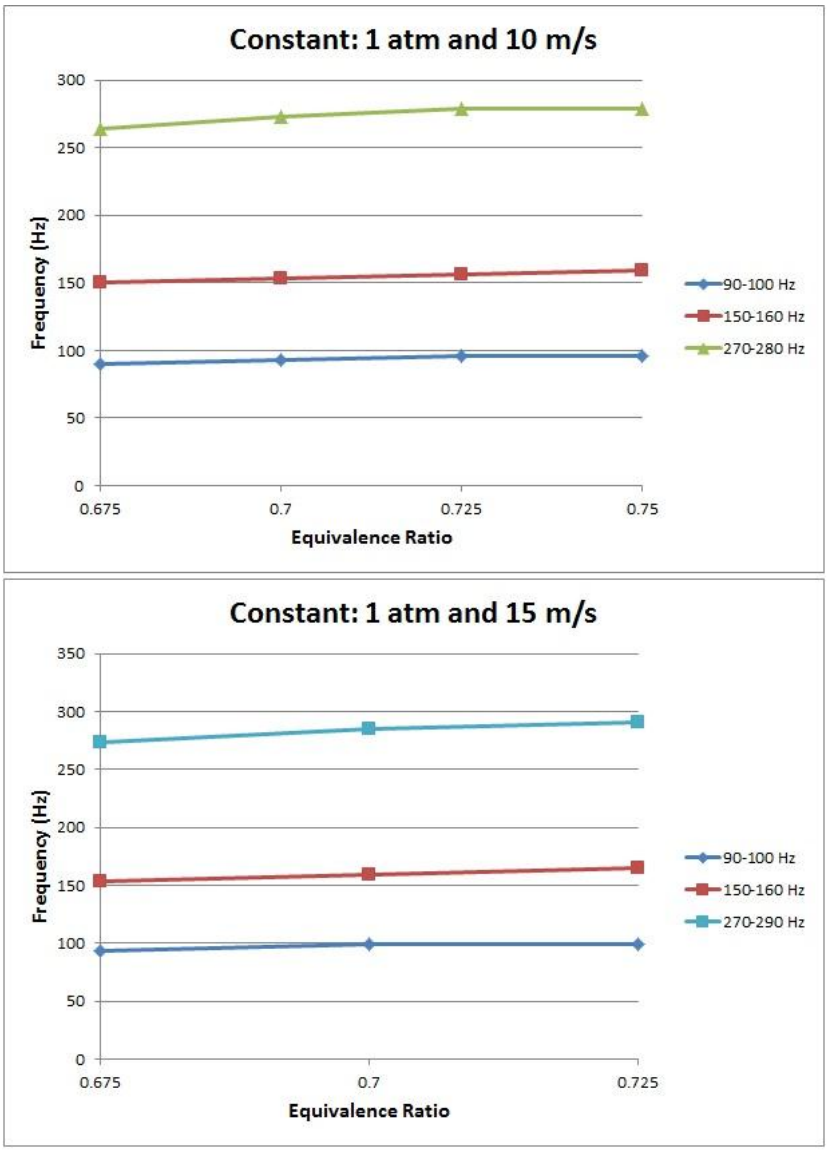

Figure B.1 Frequency vs. Equivalence Ratio at 1 atm

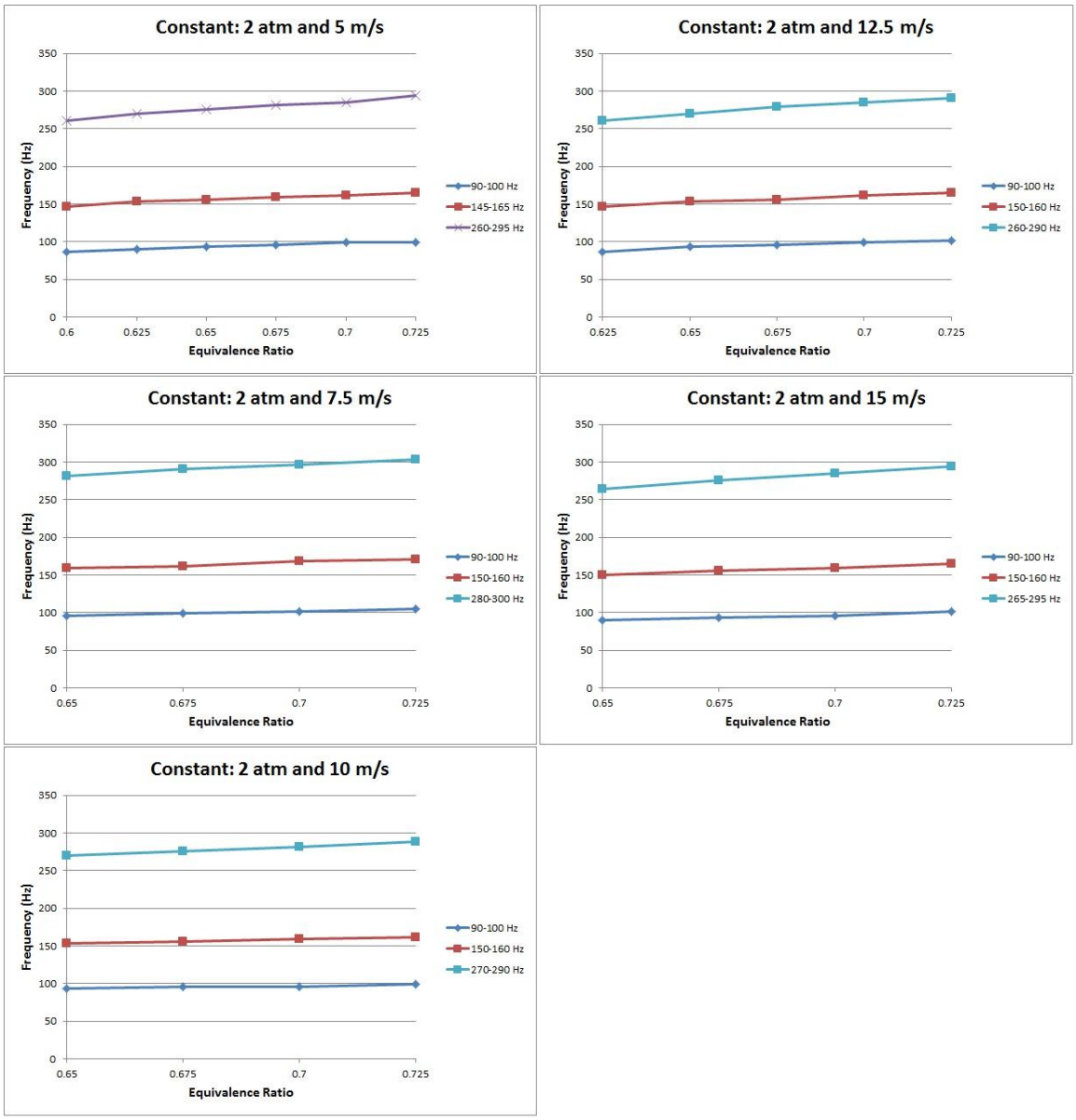

Figure B.2 Frequency vs. Equivalence Ratio at 2 atm

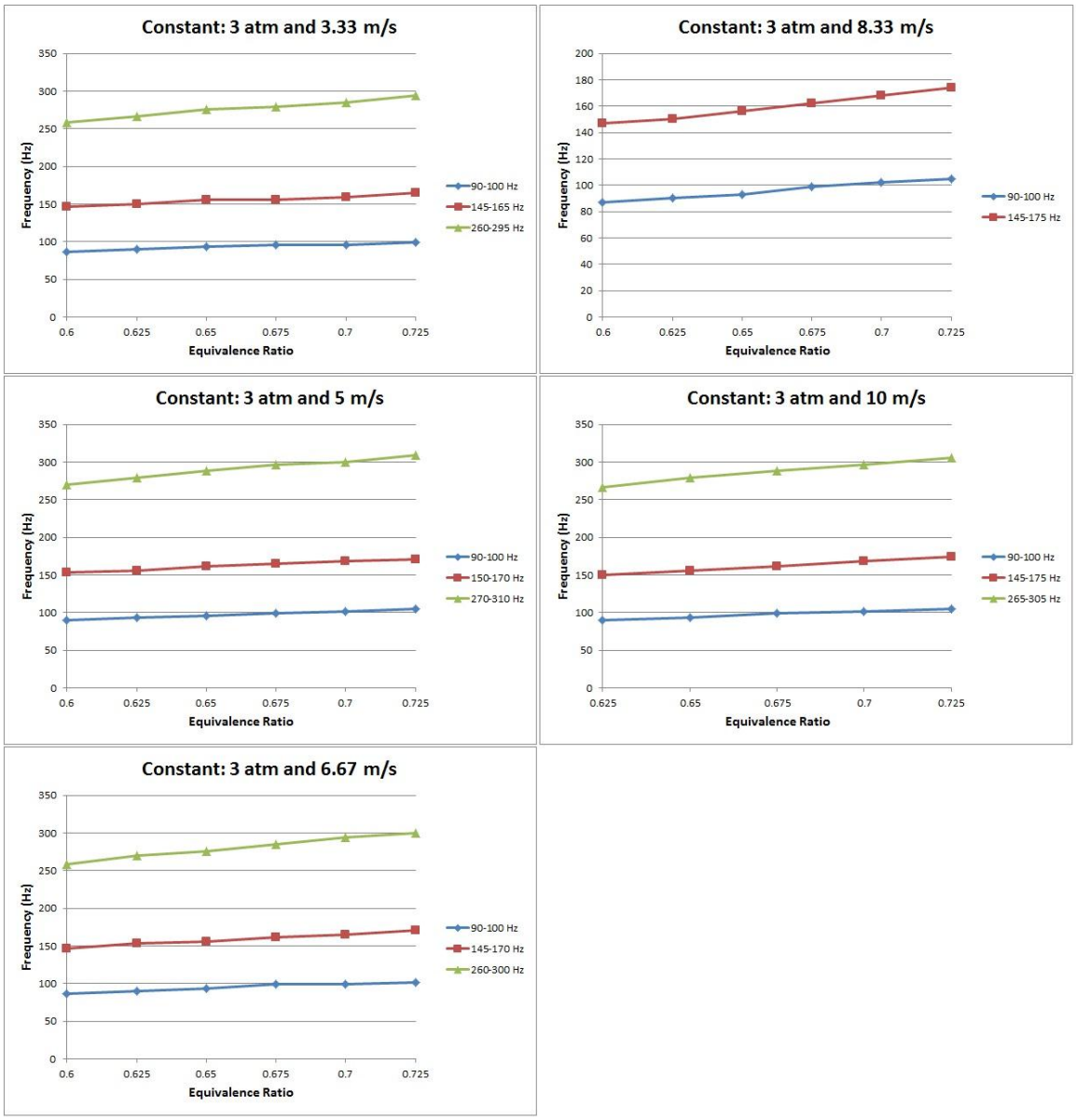

Figure B.3 Frequency vs. Equivalence Ratio at 3 atm

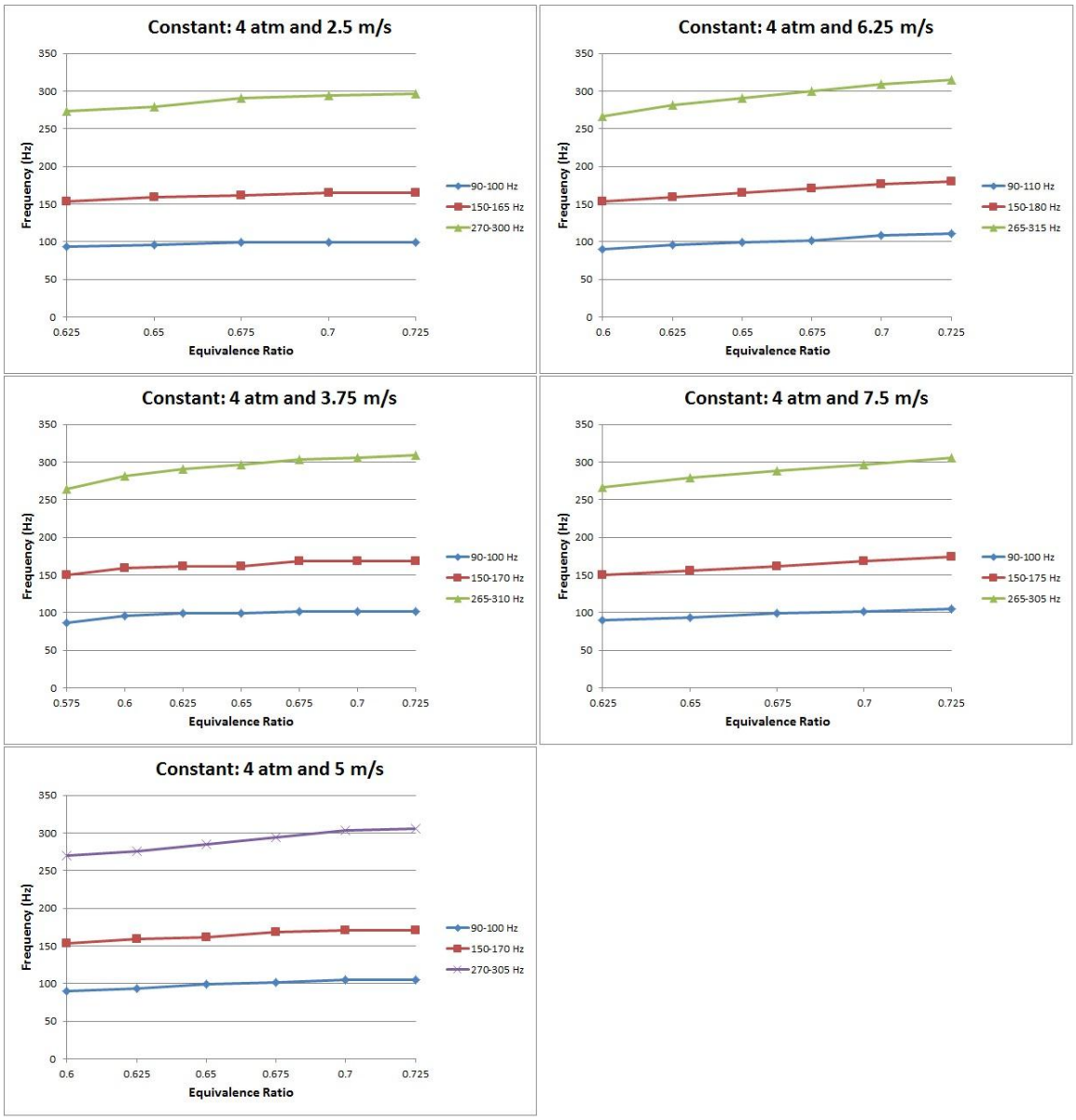

Figure B.4 Frequency vs. Equivalence Ratio at 4 atm

B.2 Frequency Shift vs. Equivalence Ratio

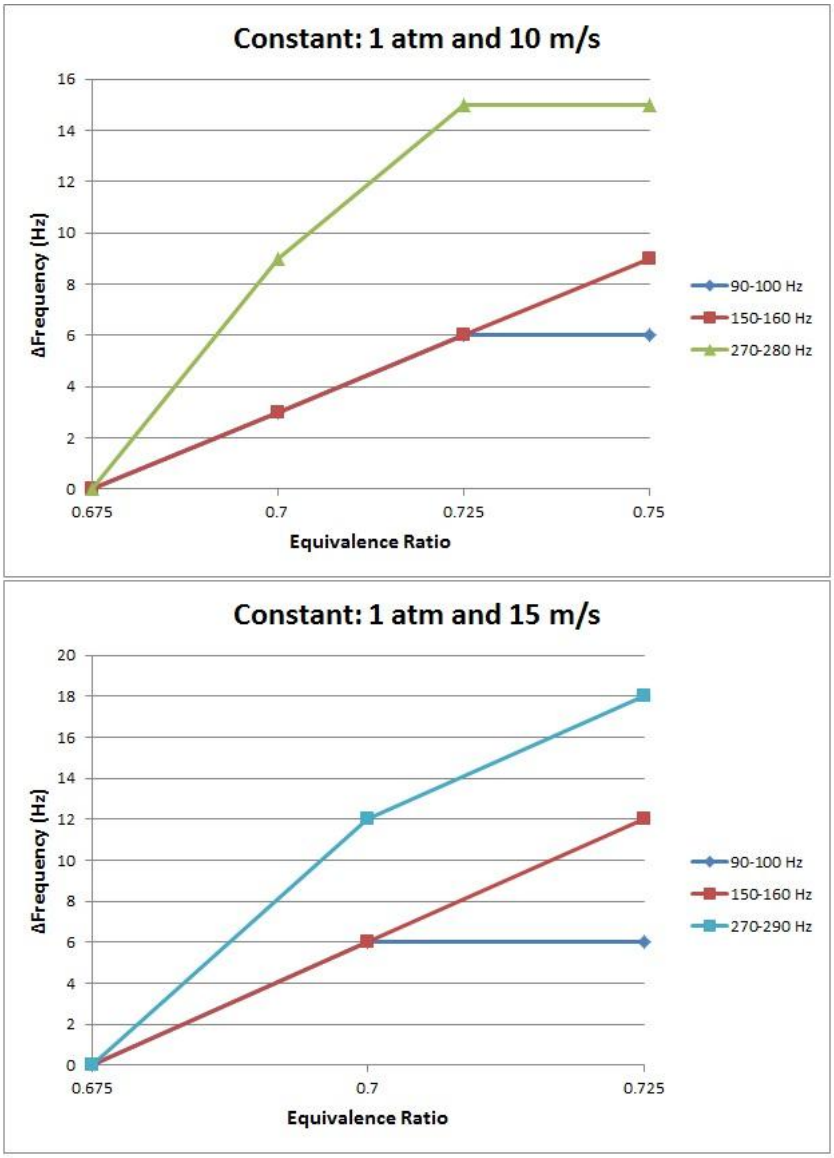

Figure B.5 Frequency Shift vs. Equivalence Ratio at 1 atm

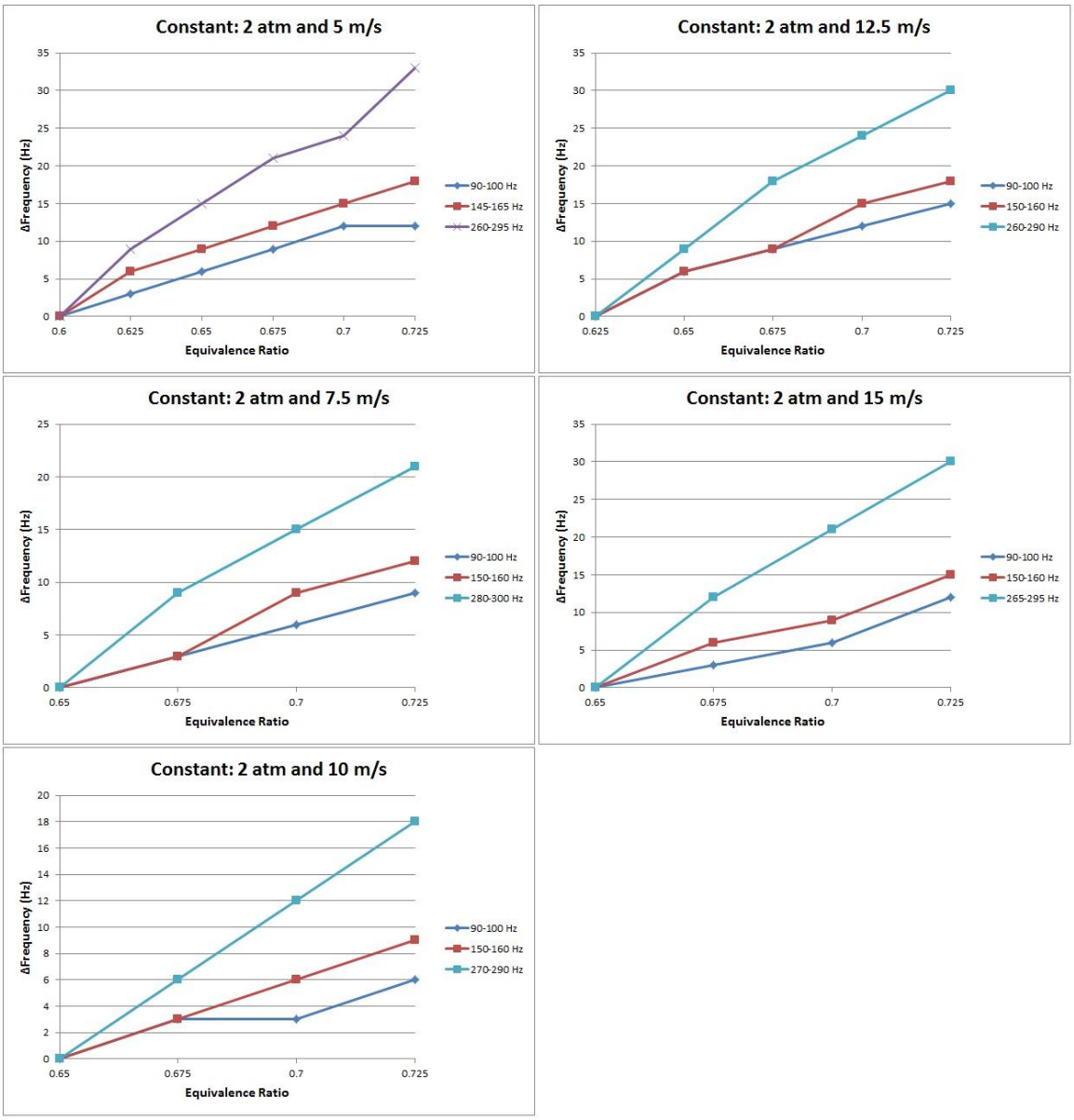

Figure B.6 Frequency Shift vs. Equivalence Ratio at 2 atm

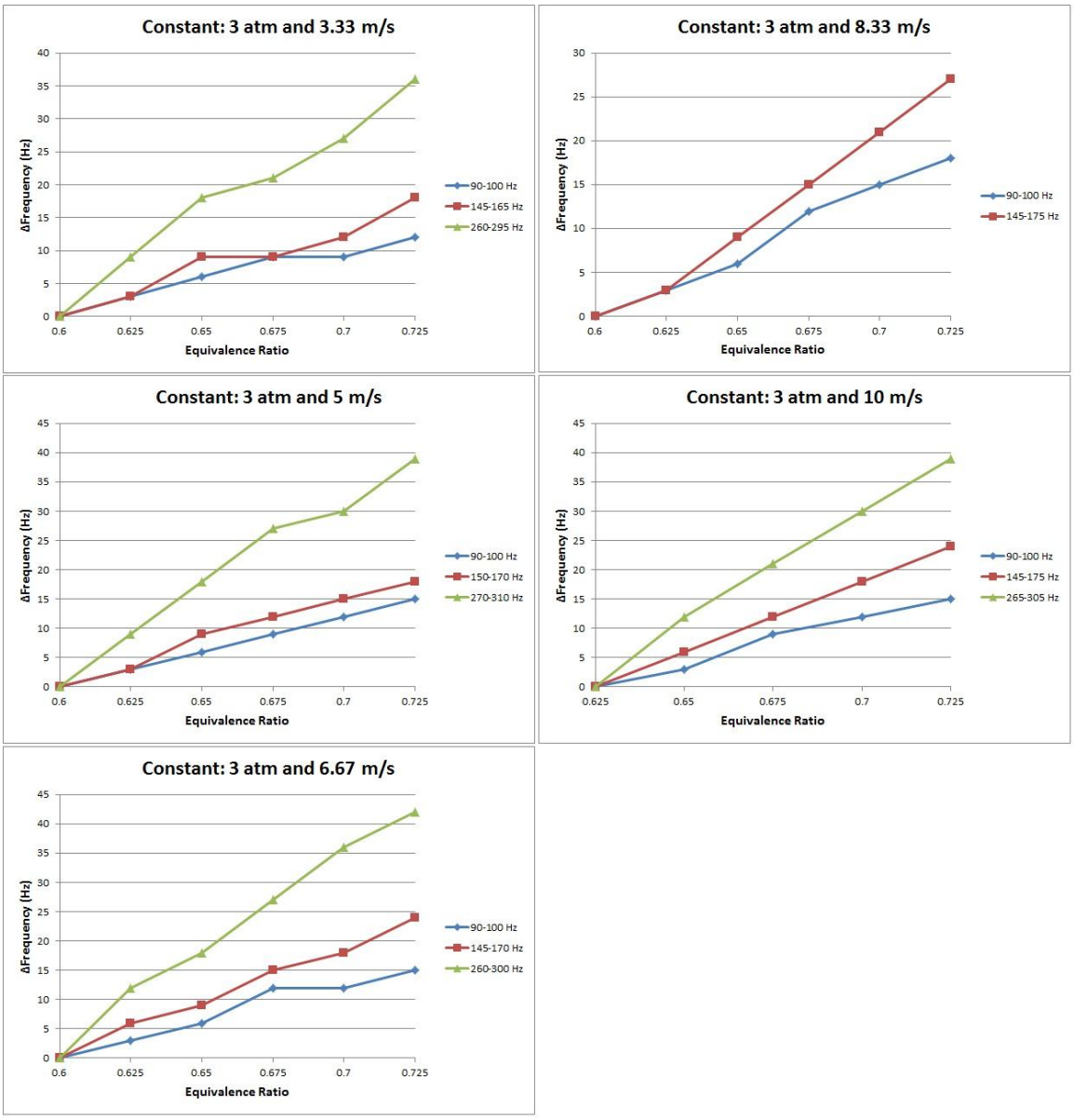

Figure B.7 Frequency Shift vs. Equivalence Ratio at 3 atm

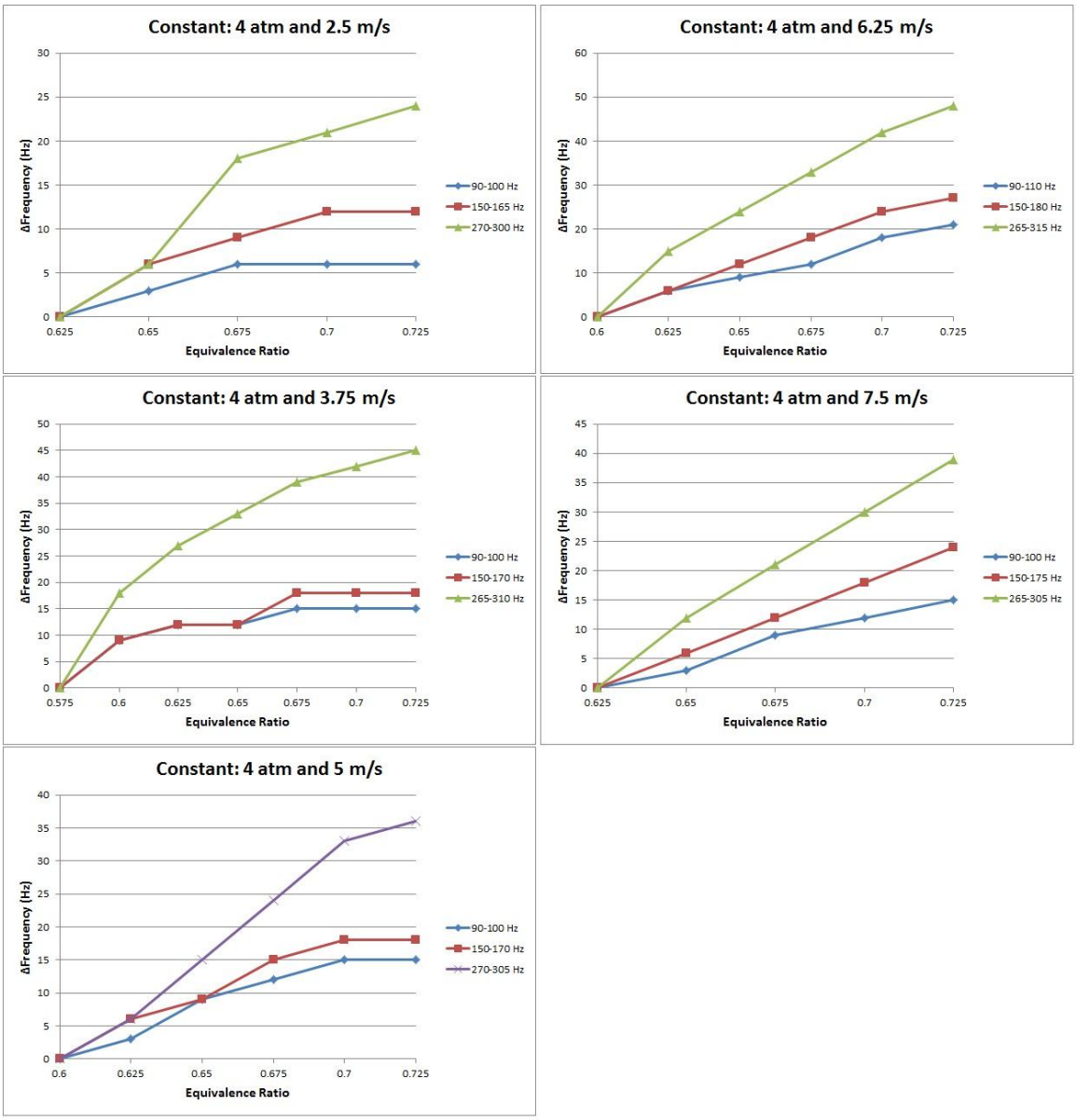

Figure B.8 Frequency Shift vs. Equivalence Ratio at 4 atm

B.3 PSD vs. Equivalence Ratio

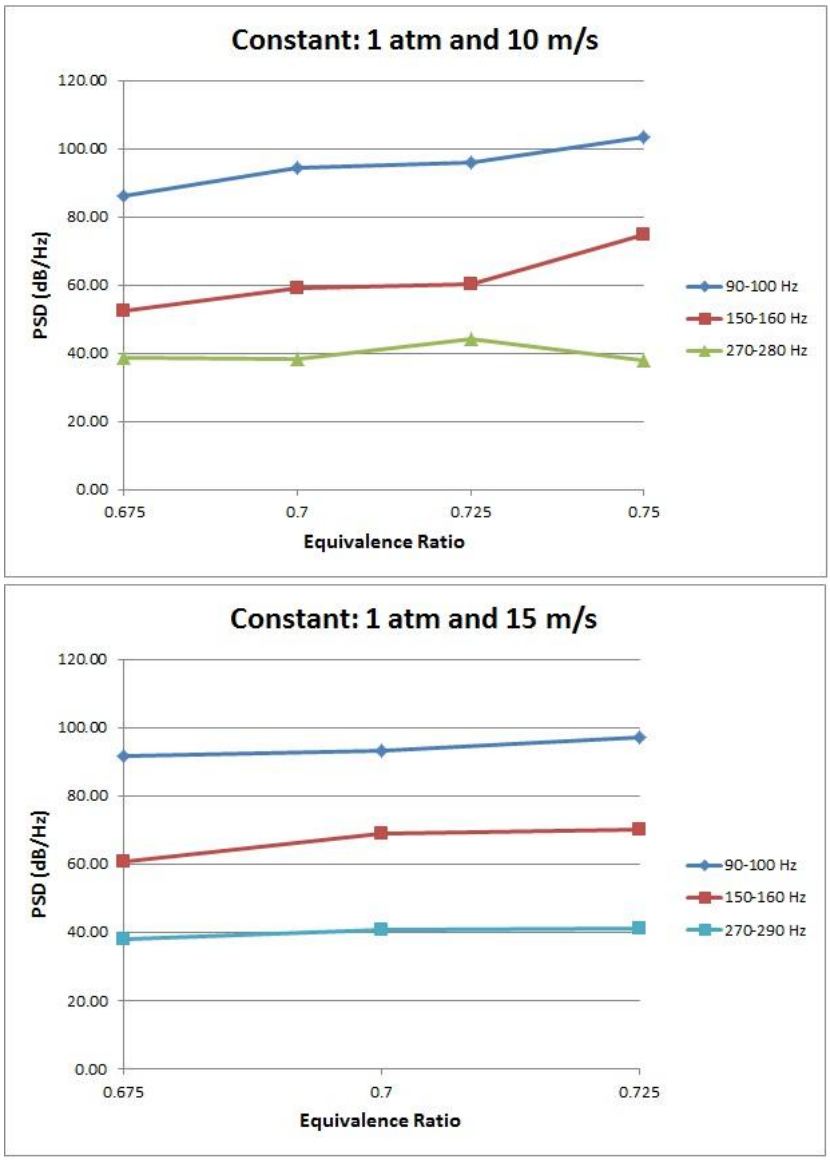

Figure B.9 PSD vs. Equivalence Ratio at 1 atm

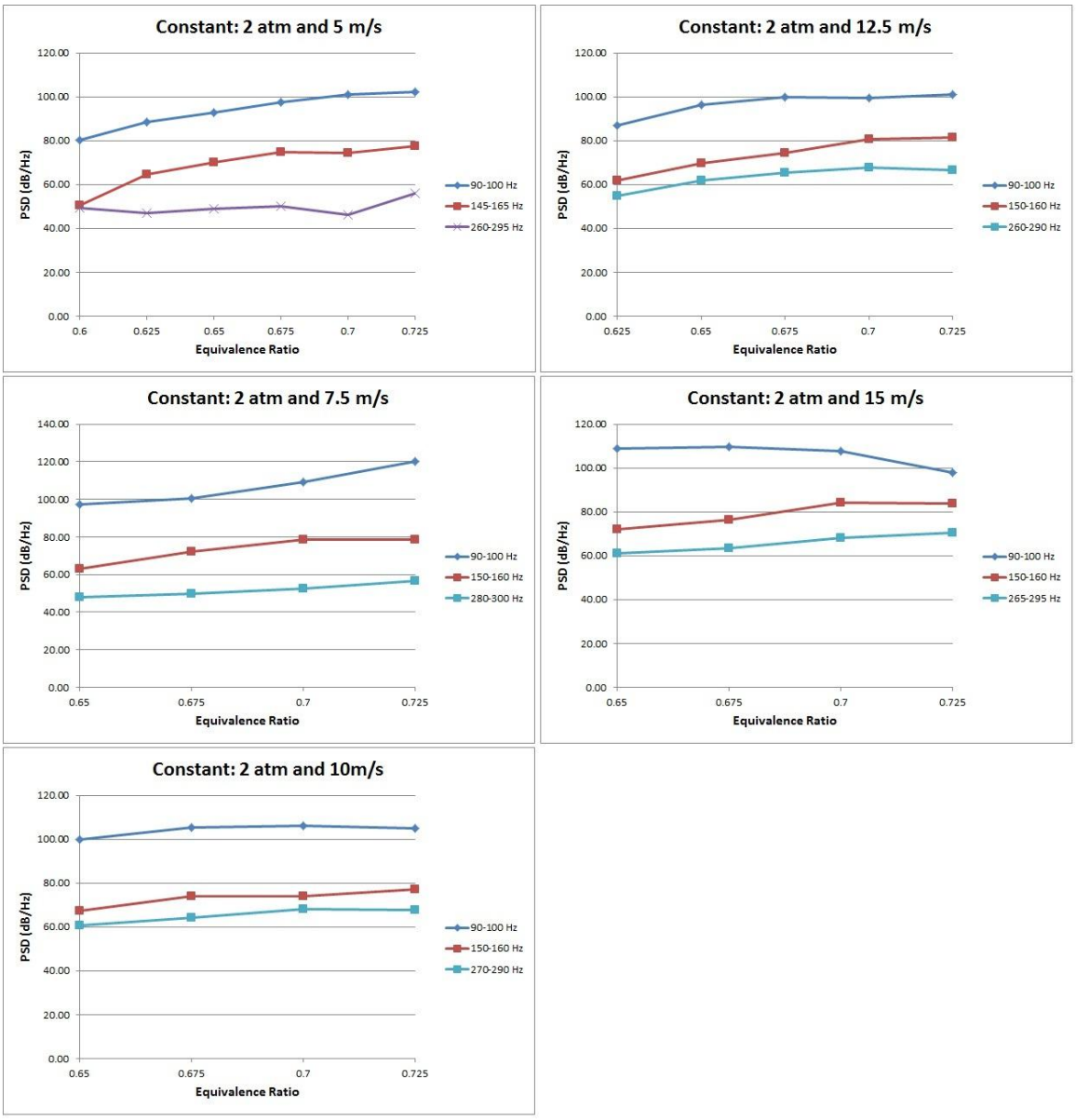

Figure B.10 PSD vs. Equivalence Ratio at 2 atm

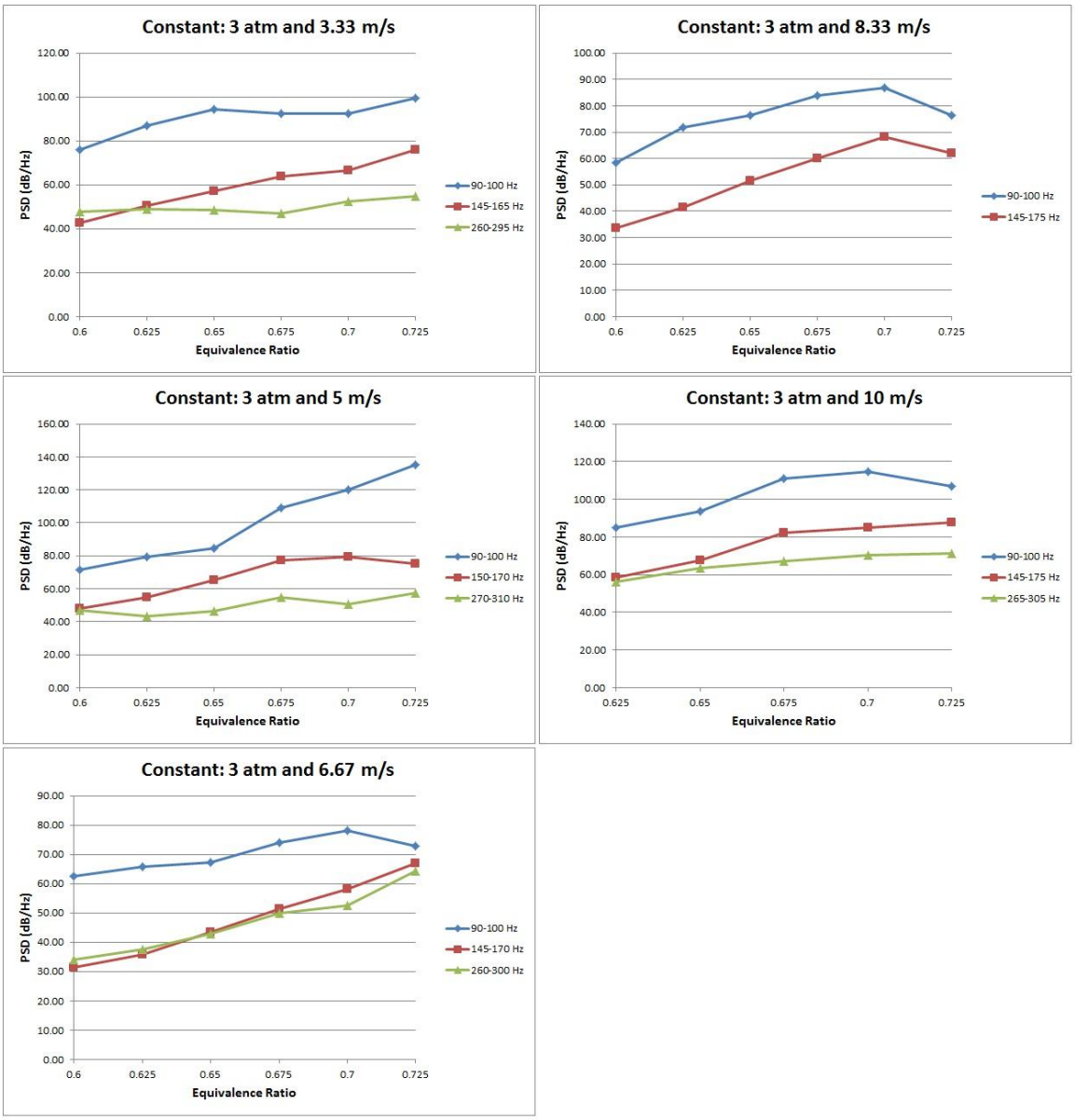

Figure B.11 PSD vs. Equivalence Ratio at 3 atm

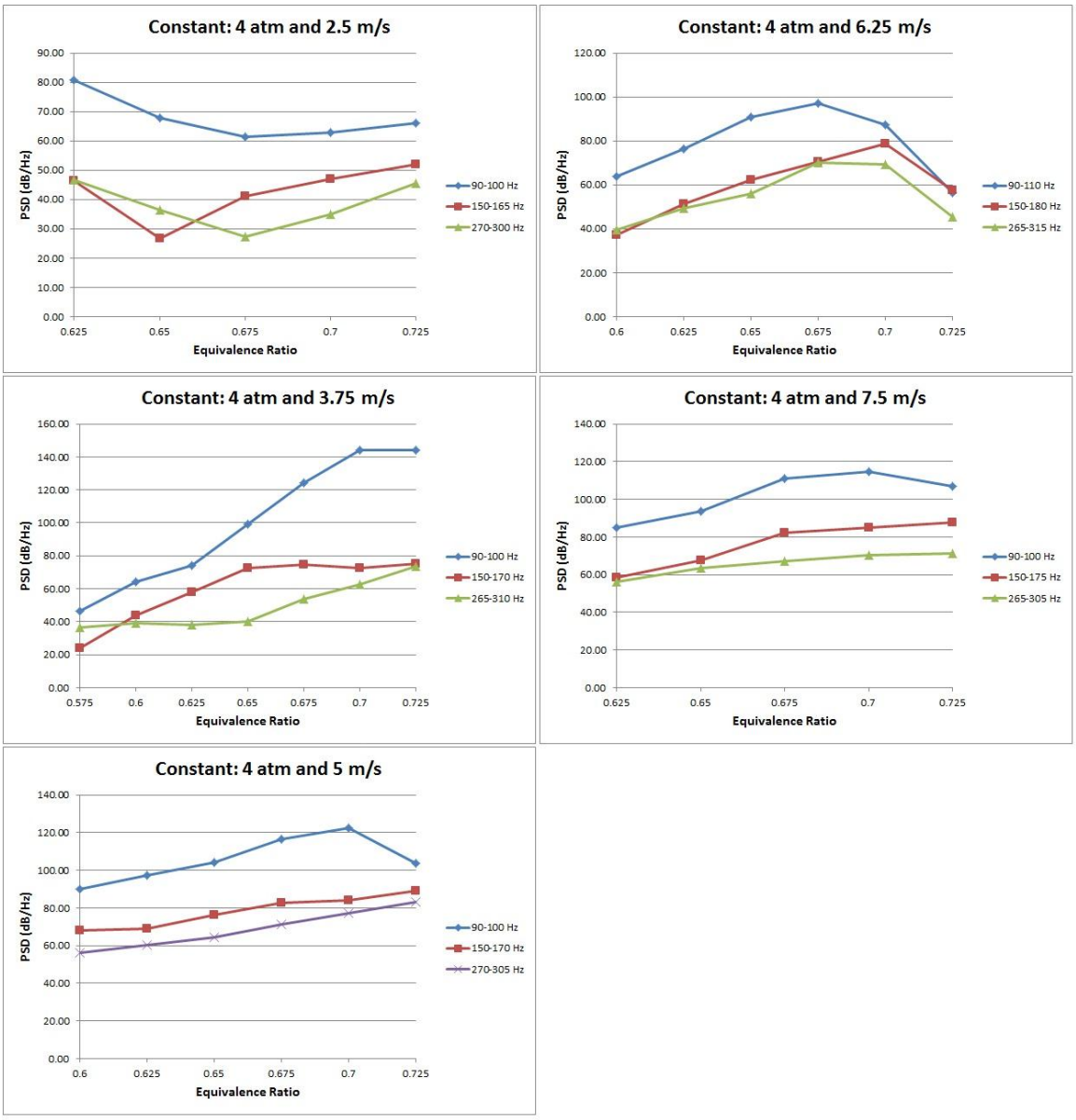

Figure B.12 PSD vs. Equivalence Ratio at 4 atm

B.4 Frequency vs. Bulk Velocity

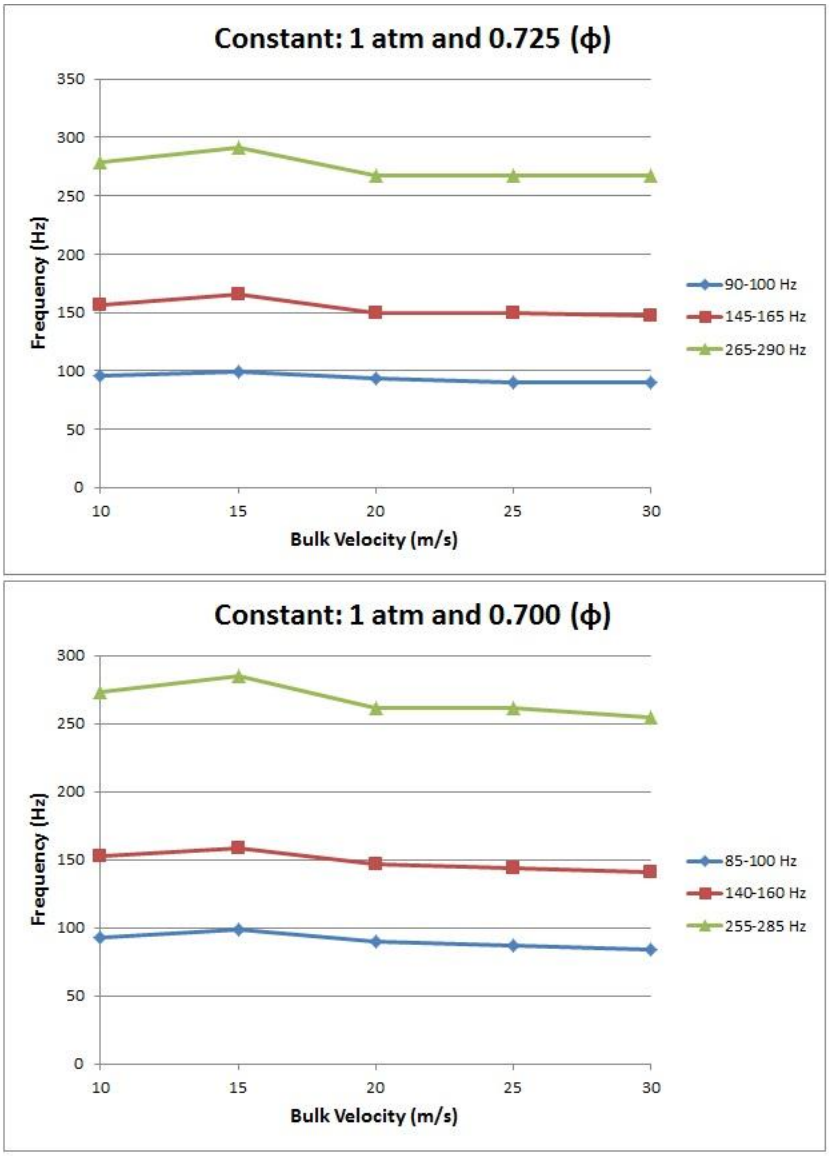

Figure B.13 Frequency vs. Bulk Velocity at 1 atm

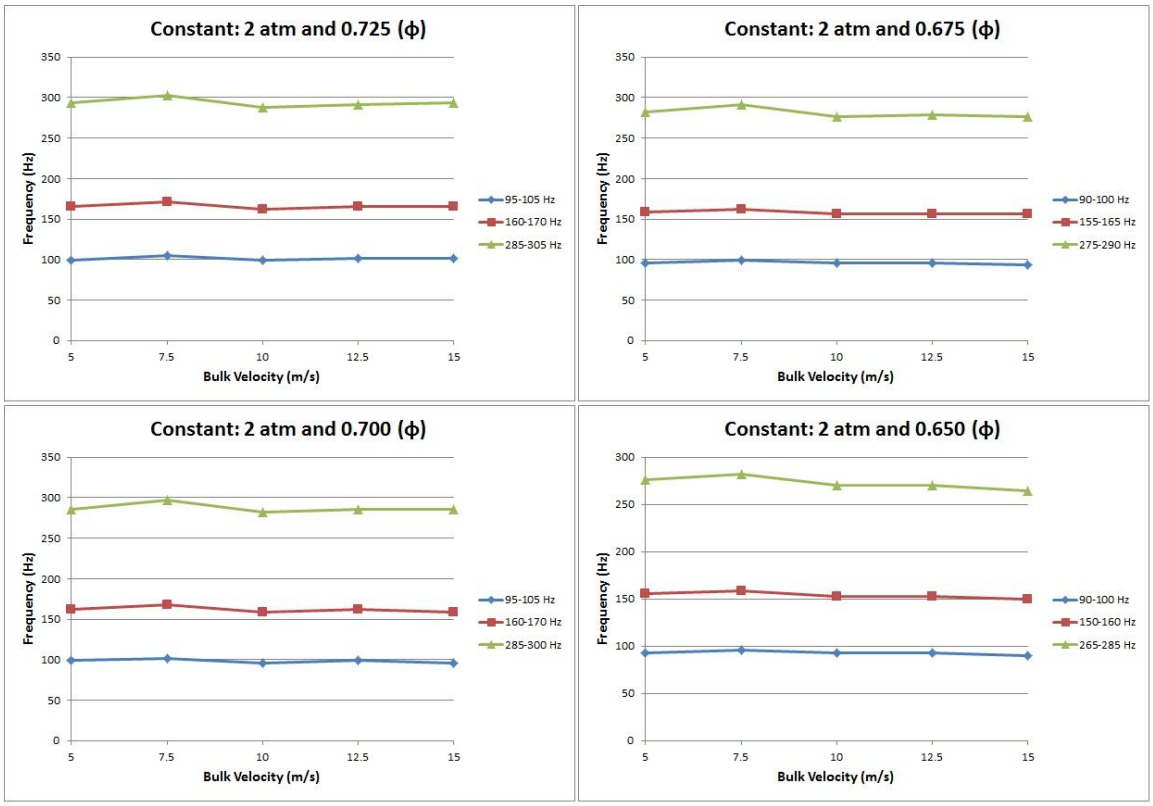

Figure B.14 Frequency vs. Bulk Velocity at 2 atm

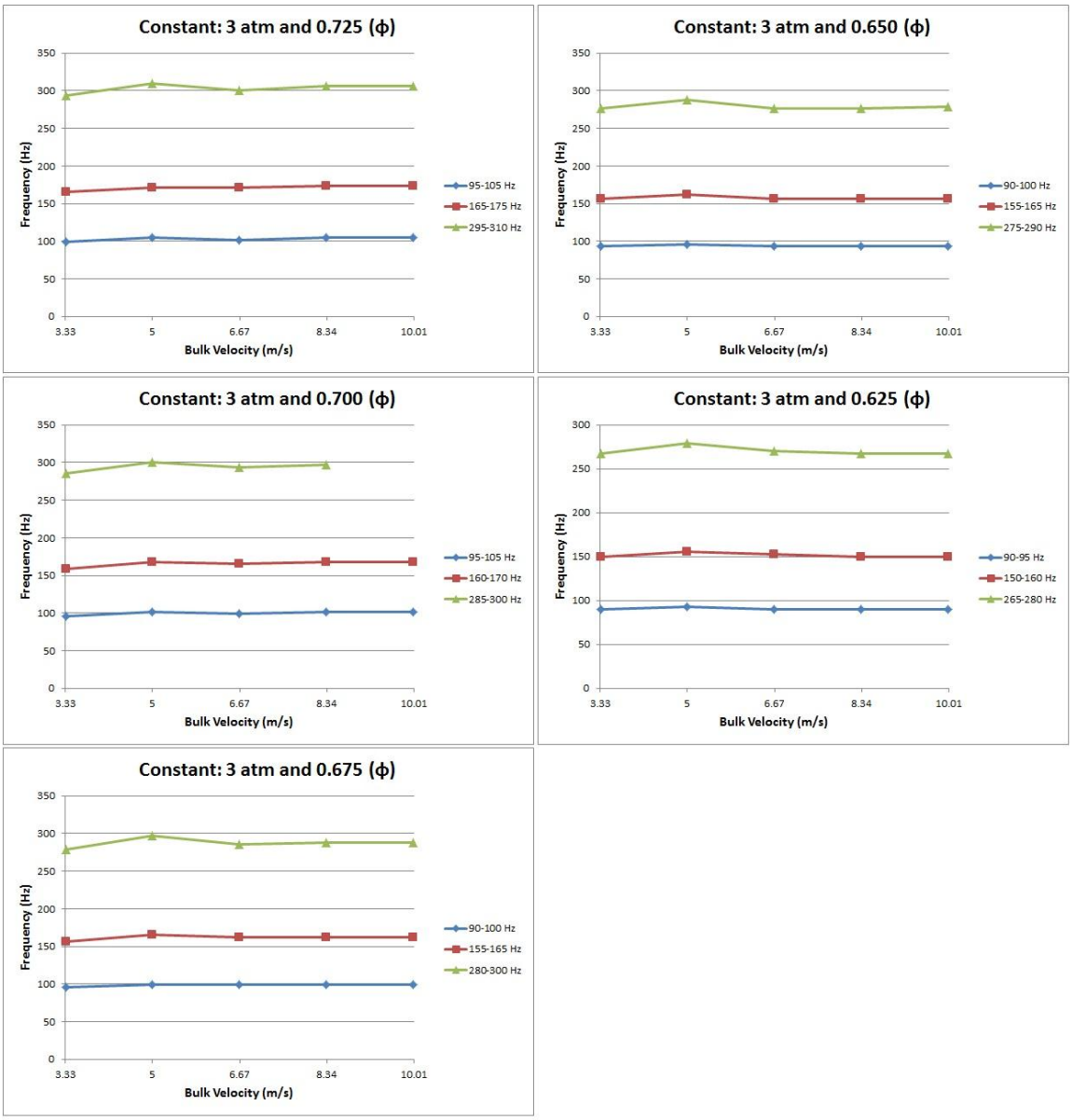

Figure B.15 Frequency vs. Bulk Velocity at 3 atm

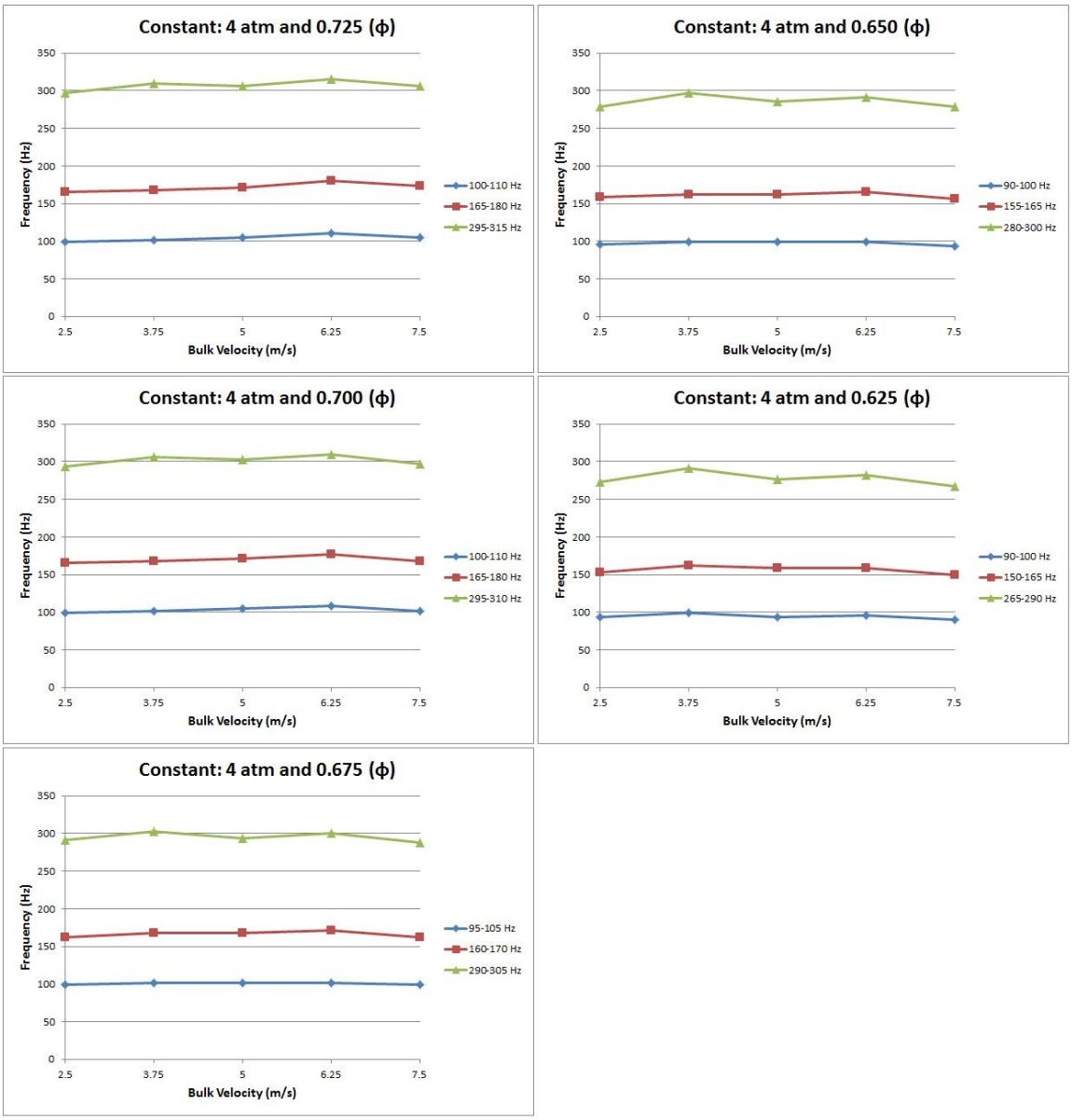

Figure B.16 Frequency vs. Bulk Velocity at 4 atm

B.5 Frequency Shift vs. Bulk Velocity

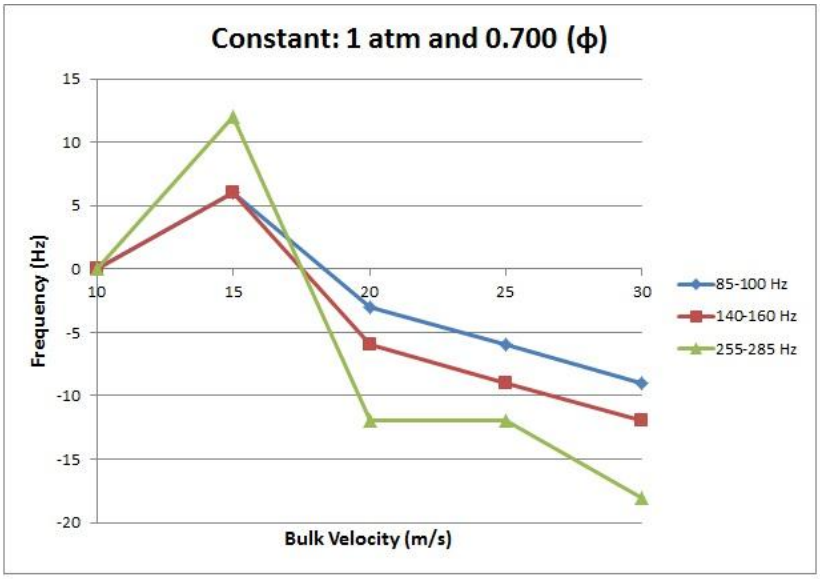

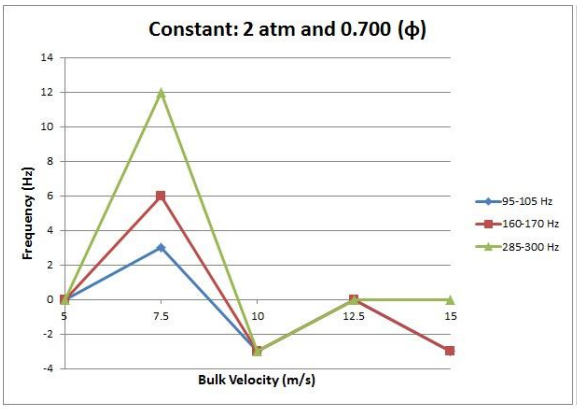

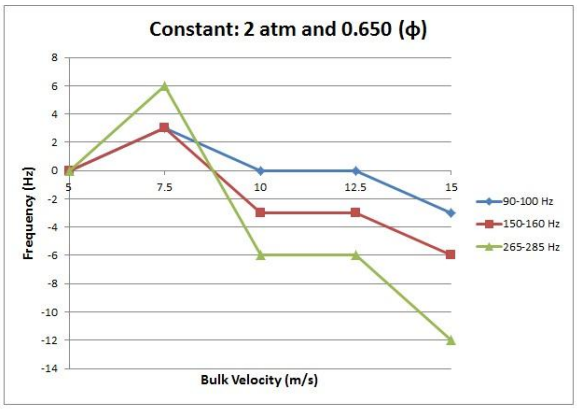

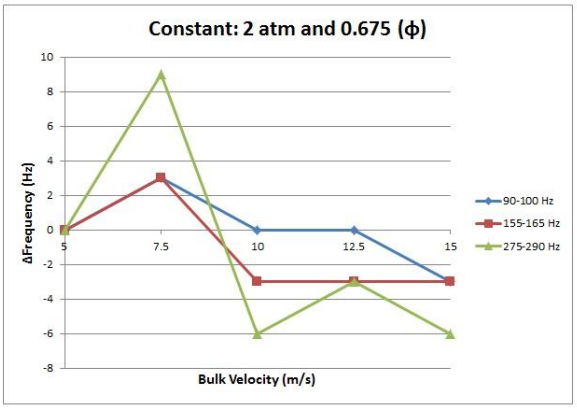

Figure B.17 Frequency Shift vs. Bulk Velocity at 1 and 2 atm

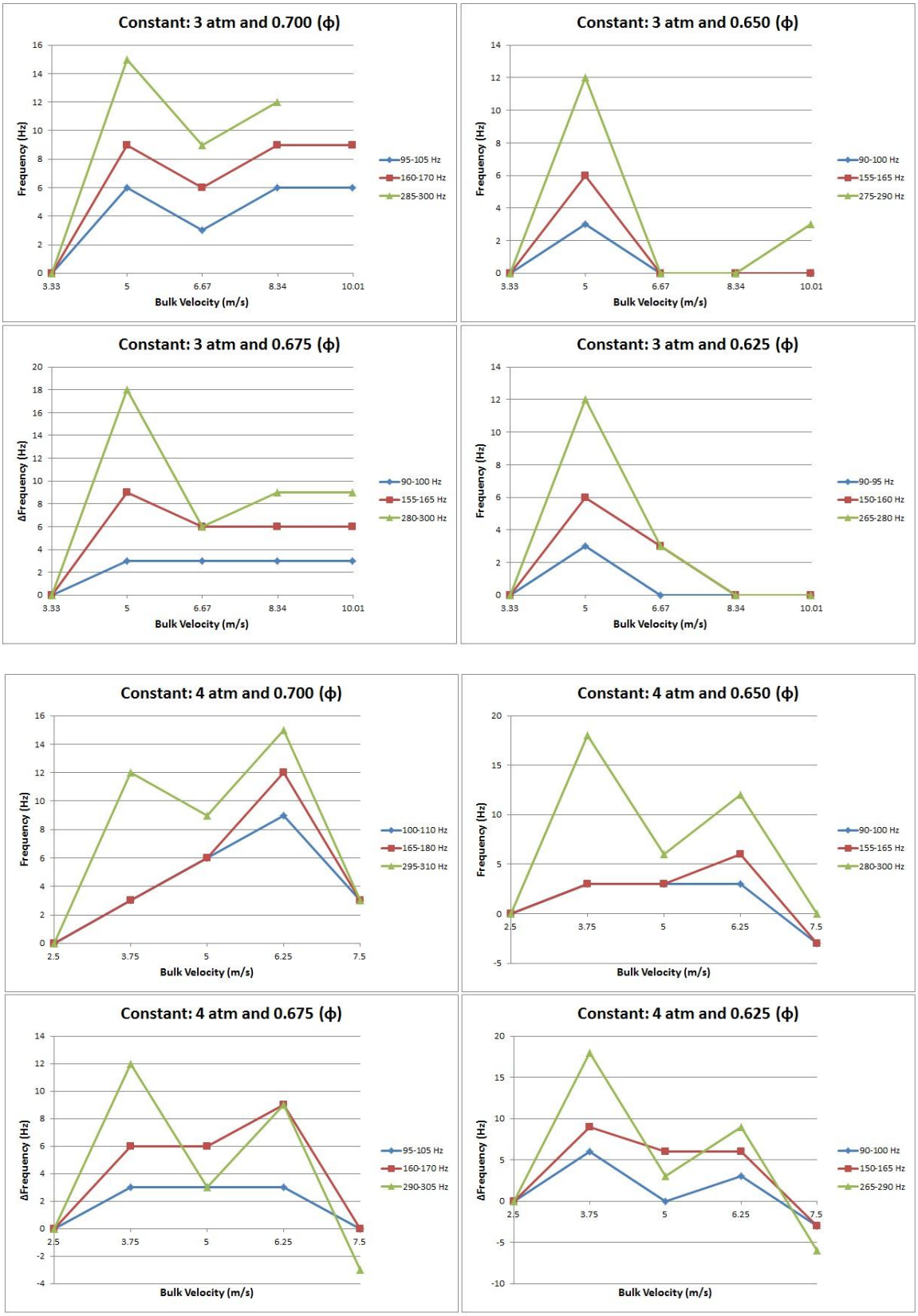

Figure B.18 Frequency Shift vs. Bulk Velocity at 3 and 4 atm

B.6 PSD vs. Bulk Velocity

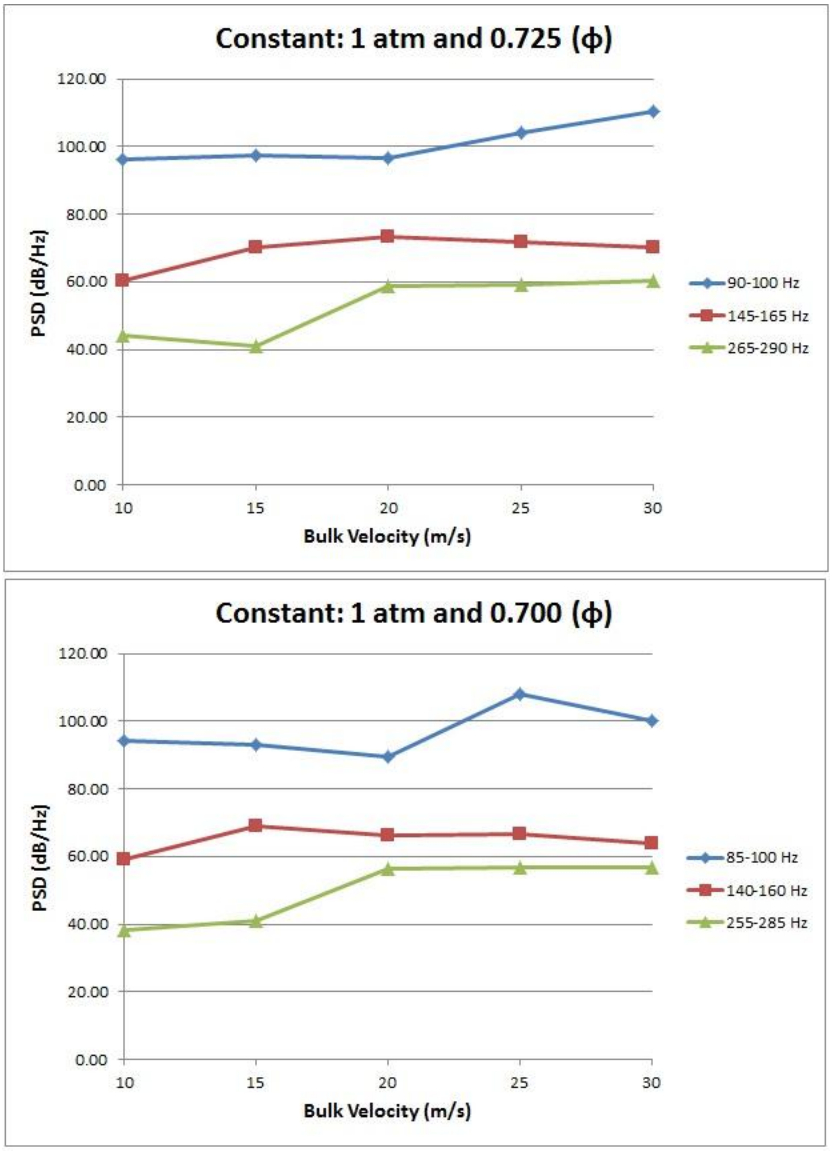

Figure B.19 PSD vs. Bulk Velocity at 1 atm

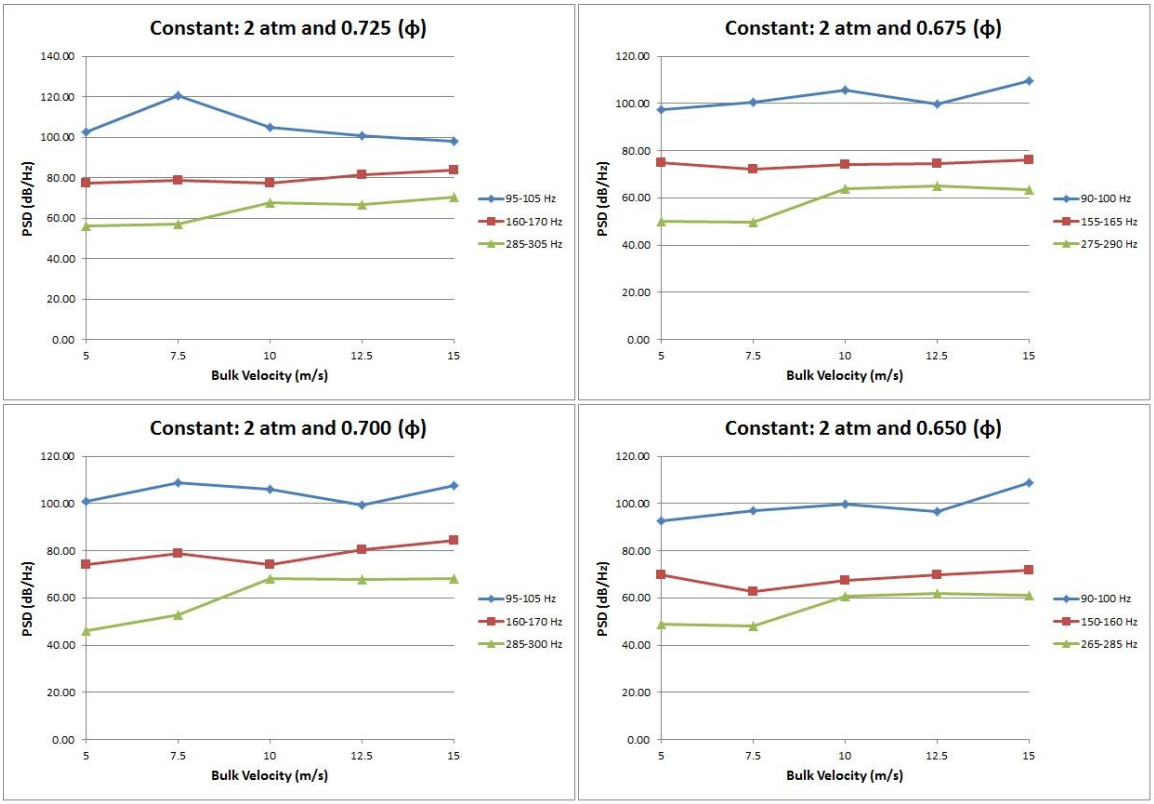

Figure B.20 PSD vs. Bulk Velocity at 2 atm

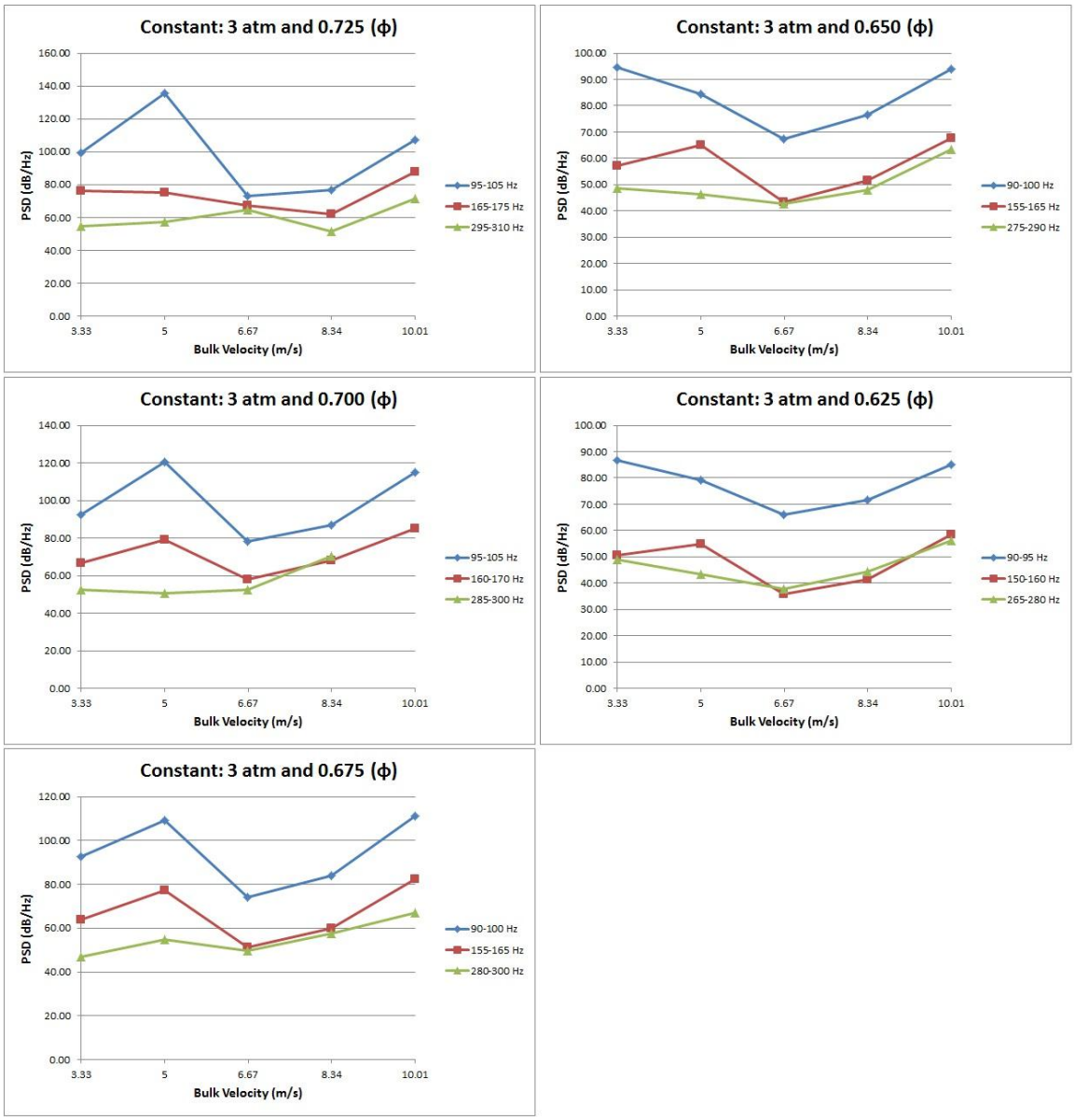

Figure B.21 PSD vs. Bulk Velocity at 3 atm

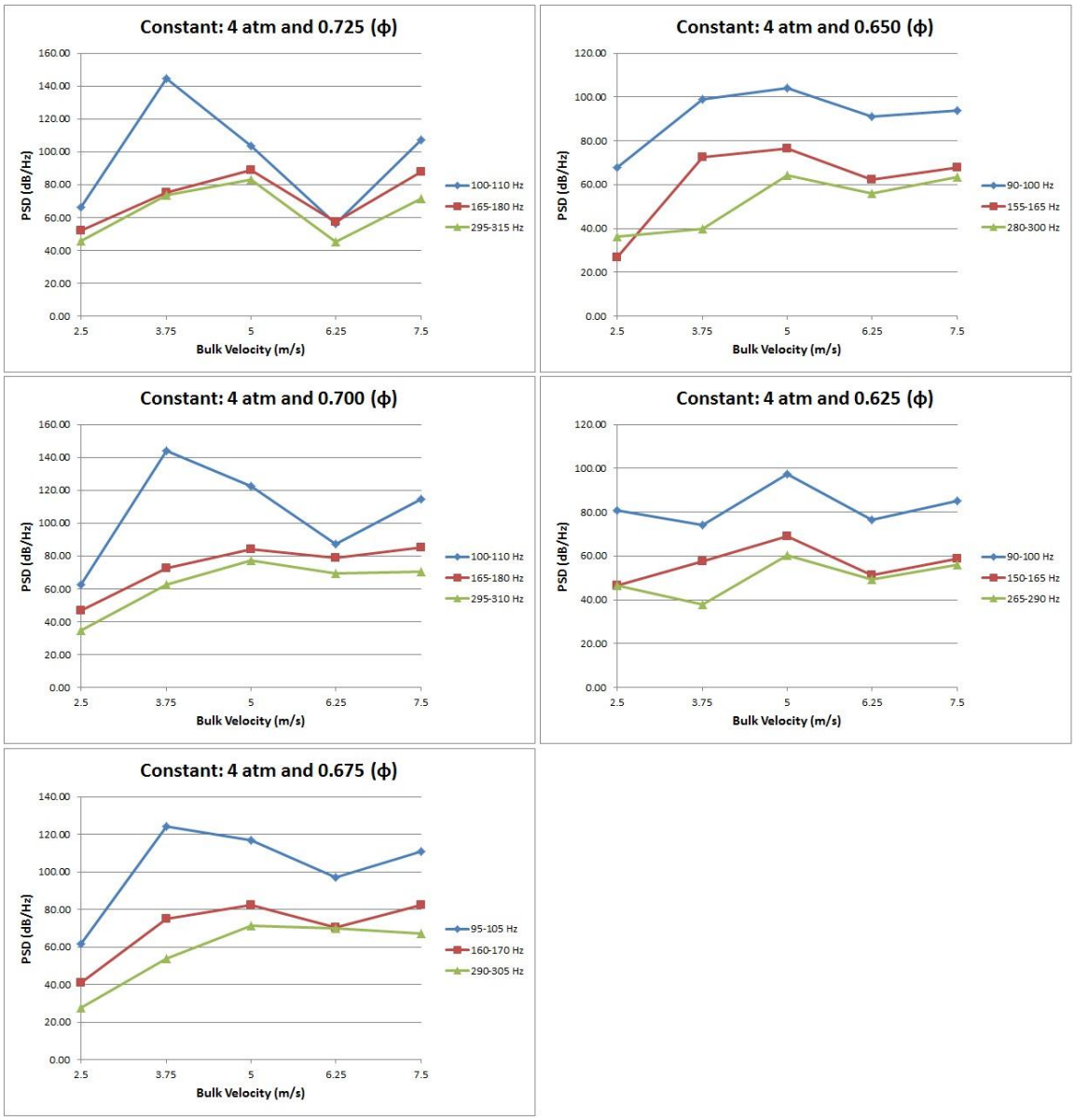

Figure B.22 PSD vs. Bulk Velocity at 4 atm